



INVESTMENTS IN EDUCATION DEVELOPMENT

MODAL TESTING

CONTENTS

Foreword.....	7
List of Symbols.....	8
List of Abbreviations.....	10
1. Introduction.....	11
1.1 Application of Modal Tests.....	11
1.2 Summary of Theory.....	13
1.3 Various Types of Frequency Response Functions.....	14
1.4 Summary of Measurement Methods.....	15
1.5 Summary of Modal Analysis.....	17
2. Dual-channel Analysis.....	18
2.1 Autospectrum.....	18
2.2 Cross Spectrum.....	19
2.3 Coherence.....	20
2.4 System descriptors.....	22
2.4.1 Frequency Response Function (FRF).....	23
2.4.2 Impulse Response Function - IRF.....	25
2.5 Effect of Noise on the FRF.....	26
2.6 Digital Signal Processing.....	29
2.6.1 Aliasing.....	30
2.6.2 Leakage.....	32
2.6.3 Frequency Zoom.....	35
2.6.4 Averaging.....	36
3. Theoretical Basis of Modal Analysis.....	38
3.1 Single Degree-of-freedom System (SDOF).....	38
3.1.1 Undamped Single Degree-of-freedom System.....	38
3.1.2 Viscously damped SDOF system.....	39
3.1.2.1 Free vibration.....	39
3.1.2.2 Forced vibration.....	41
3.1.2.3 Determination of Resonance Tuning.....	46
3.1.2.4 Determination of Damping from FRF Plots.....	46
3.1.3 Single Degree-of-freedom System with Hysteretic (Structural) Damping...	49
3.1.3.1 Forced Vibration.....	49

3.1.3.2	Determination of Damping from FRF Plots	52
3.1.4	Various Forms of FRF for Single Degree-of-freedom System.....	52
3.2	Multi Degree-of-freedom System (MDOF).....	53
3.2.1	Undamped MDOF System	54
3.2.1.1	Free vibration.....	54
3.2.1.2	Orthogonal Properties of Eigenvectors.....	57
3.2.1.3	Normalization of Mode Shapes	58
3.2.1.4	Forced Response Analysis of Multi Degree-of-freedom System	59
3.2.2	Characteristics and Presentation of Multi Degree-of-Freedom FRF Data....	62
3.2.3	Damped Multi Degree-of-Freedom System	67
3.2.3.1	Proportional Viscous Damping	67
3.2.3.2	Proportional Hysteretic Damping	69
3.2.3.3	Hysteretic Damping - General Case	69
3.2.3.4	MDOF System with General Hysteretic Damping - Forced Response Solution	70
3.2.3.5	MDOF Systems - Summary for Various Types of Damping.....	71
3.2.3.6	Excitation by a General Force Vector.....	72
3.2.3.7	Excitation by a Vector of Mono-Phased Forces	73
4.	Modal Test.....	75
4.1	Preparation.....	75
4.1.1	Preparation of the Measured Structure	75
4.1.1.1	Free Support	75
4.1.1.2	Grounded (Fixed) Support.....	76
4.1.1.3	Support in-situ	76
4.1.2	Preparation of Experimental Model	76
4.2	Measurement Techniques	78
4.2.1	Basic Measurement Setup	79
4.2.1.1	Excitation Techniques	80
4.2.1.2	Transducers Used for Excitation Force and Response Measurements	89
4.2.1.3	Analyzer.....	90
4.2.2	Preparation of Measurement.....	91
4.2.2.1	Reference Point Measurement.....	92
4.3	Experimental Modal Analysis - Modal Parameters Identification	93
4.3.1	Single Degree-of-Freedom Approach.....	94
4.3.1.1	Peak-picking method	94
4.3.1.2	Circle-fit Method	95

4.3.2	MDOF System Approximation Methods	99
4.4	Modal Model	100
4.4.1	Presentation of the Obtained Modal Model.....	100
4.4.2	Verification of the Obtained Modal Model	102
4.4.3	Comparison of the Experimentally and Computationally Derived Models	104
4.4.3.1	Comparison of Natural Frequencies	104
4.4.3.2	Graphical Comparison of Modal Shapes.....	106
4.4.3.3	Numerical Comparison of Mode Shapes.....	107
5.	Operational Deflection Shapes (ODS).....	110
6.	Operational Modal Analysis (OMA).....	114
6.1	Identification Methods.....	117
6.2	Presentation of Results	118
	References.....	120

Foreword

The area of modal testing is quite extensive and to master it perfectly, it is necessary to integrate knowledge from different fields: vibration measurements, signal processing, post-processing, mathematical background, issues of vibrating multi degree-of-freedom systems with different models of damping, etc. This text does not aim to discuss in detail all aspects of modal testing, but only to familiarize students with this issue enough to be able to perform a modal test independently and be aware of problems that may occur during measurements and data processing. Most of the readers will be students of Applied Mechanics specialization. My main goal is to create awareness in their minds of what a modal test is about, what it is used for and when they should consider its implementation in their engineering practice. I have noticed during the years of working with students that their confidence of the results obtained using finite element method is sometimes too high and that they often do not realize that even the results obtained using very sophisticated finite element programs can be far from reality - usually due to the fact that when using these programs, they neglected or overly simplified something. Therefore, verifying and updating the computational model with the use of experimentally derived data is highly advisable and in some branches (e.g. aircraft) even mandatory.

The basic source for writing this text was the book "Modal Analysis – theory, practice and application" written by prof. David J. Ewins from Imperial College of Science, Technology and Medicine in London, who can be regarded as a leading figure in the modal analysis in Europe. I hope he would appreciate that I left his words unchanged wherever it was appropriate.

The second relevant source I used were materials provided by Brüel&Kjær company - articles, application notes, presentations and pictures. This company produces all the equipment used for modal testing and also provides a technical support to their customers by publishing a lot of technical papers and organizing technical training.

Of course, I added my own experience and tried to create a text that would be useful and well readable for students. I wish to all of you that the time spent by reading this text will not be a loss but contribute to your effort to become a competent and well educated mechanical engineer.

author

List of Symbols

*	complex conjugate
$[]^T$	matrix transpose
$a(t)$	time record in channel A
$A(f)$	instantaneous spectrum of channel A
$A(\omega)$	inertance (accelerance) $[\text{kg}^{-1}]$
b	viscous damping constant $[\text{kg}\cdot\text{s}^{-1}]$
$b(t)$	time record in channel B
$B(f)$	instantaneous spectrum of channel B
$[B]$	viscous damping matrix $[\text{kg}\cdot\text{s}^{-1}]$
F_b	damping force $[\text{kg}\cdot\text{m}\cdot\text{s}^{-2}]$
$\{F\}$	vector of complex magnitudes of excitation forces $[\text{kg}\cdot\text{m}\cdot\text{s}^{-2}]$
$\{f(t)\}$	excitation forces vector $[\text{kg}\cdot\text{m}\cdot\text{s}^{-2}]$
f	natural frequency of damped vibration [Hz]
f_0	natural frequency of undamped vibration [Hz]
f_s	sampling frequency [Hz]
$G_{AA}(f)$	autospectrum of channel A of an analyzer (one-sided)
$G_{BB}(f)$	autospectrum of channel B of an analyzer (one-sided)
$G_{AB}(f)$	cross spectrum from channel A to channel B of an analyzer (one-sided)
$G_{BA}(f)$	cross spectrum from channel B to channel A of an analyzer (one-sided)
$h(t)$	impulse response function
$[H]$	hysteretic damping matrix $[\text{kg}\cdot\text{s}^{-2}]$
$H(\omega)$	frequency response function (receptance, mobility or inertance)
$H(s)$	transfer function
$H_1(f)$	estimate of frequency response function
$H_2(f)$	estimate of frequency response function
i	imaginary unit
$[I]$	unity matrix (diagonal)
k	stiffness $[\text{kg}\cdot\text{s}^{-2}]$
$[K]$	stiffness matrix $[\text{kg}\cdot\text{s}^{-2}]$
m	mass [kg]
$[M]$	mass matrix [kg]
N	number of degrees of freedom

p	pole [s^{-1}]
$\{p\}$	vector of modal coordinates
R	residuum [kg^{-1}]
$S_{AA}(f)$	autospectrum of channel A of an analyzer (two-sided)
$S_{BB}(f)$	autospectrum of channel B of an analyzer (two-sided)
$S_{AB}(f)$	cross spectrum from channel A to channel B of an analyzer (two-sided)
$S_{BA}(f)$	cross spectrum from channel B to channel A of an analyzer (two-sided)
t	time [s]
T	period [s]
$T(f)$	transmissibility [-]
$\{X\}$	vector of complex magnitudes of displacements [m]
$\{x(t)\}$	vector of displacements [m]
$\{\dot{x}(t)\}, \{v(t)\}$	velocity vector [$m \cdot s^{-1}$]
$\{\ddot{x}(t)\}, \{a(t)\}$	acceleration vector [$m \cdot s^{-2}$]
$Y(\omega)$	mobility [$kg^{-1} \cdot s^1$]
$\alpha(\omega)$	receptance [$kg^{-1} \cdot s^2$]
δ	decay constant [s^{-1}]
Φ_j^r	j^{th} element of the r^{th} eigenvector [-]
$\{\Phi\}^r$	r^{th} eigenvector [-]
$[\Phi]$	modal matrix (mass-normalized) [-]
γ	structural damping loss factor [-]
η	tuning coefficient [-]
λ_r	eigenvalue of the r^{th} mode [s^{-1}]
τ	time constant of exponential weighting window [s]
ν	logarithmic decrement [-]
ω	angular frequency of excitation [s^{-1}]
Ω	angular natural frequency of damped vibration [s^{-1}]
Ω_0	angular natural frequency of undamped vibration [s^{-1}]
$[\Psi]$	modal matrix (general form) [-]
ζ	damping ratio [-]
$\gamma^2(f)$	coherence function [-]

List of Abbreviations

COP	Coherence Output Power
DFT	Discrete Fourier Transform
DOF	Degree of Freedom
FDD	Frequency Domain Decomposition
FRF	Frequency Response Function
FFT	Fast Fourier Transform
IRF	Impulse Response Function
MAC	Modal Assurance Criterion
MDOF	Multi Degree of Freedom System
MIMO	Multiple Input Multiple Output
MSF	Modal Scale Factor
ODS	Operational Deflection Shape
OMA	Operational Modal Analysis
PSD	Power Spectral Density
SDOF	Single Degree of Freedom System
SISO	Single Input Single Output
SIMO	Single Input Multiple Output
SSI	Stochastic Subspace Identification
SVD	Singular Value Decomposition

1. Introduction

Before speaking about the area of modal testing itself, it is worth to know something about different approaches to vibration measurements. From both methodical and practical points of view, it is useful to distinguish the two experimental approaches dealing with vibrations:

- 1) Assessment of the nature and level of vibration responses - *signal analysis*
- 2) Deriving theoretical models and presumptions and their evaluation - *system analysis*

Two types of measurements correspond to these two approaches:

- ad 1) Vibration responses of the machine or the structure under investigation are measured during operation conditions. Vibration diagnostics deals with this area.
- ad 2) Structure or a machine part is put into vibration by means of known excitation forces, often out of its working environment. This process is substantial for modal tests. It is obvious that we are able to get more accurate and detailed information about the measured system under controlled conditions rather than by simple response measurements.

This material deals with the latter approach thoroughly. By performing a modal test, we are able to determine modal parameters of the system, thus having a base for solving many problems caused by structural vibrations. Problems with structural vibrations pose significant risks and limitations for design of a wide range of machinery products. They could be a cause of a structural integrity failure (for instance breaking of a turbine blade) or they could reduce machinery performance. At least, excessive vibrations always cause excessive noise and discomfort during operation.

Modal test :

"Processes applied to the tested parts or structures with the aim to get mathematical description of their dynamic behaviour."

1.1 Application of Modal Tests

There are several reasons for performing modal tests. Here they are sorted by accuracy requirements and by the degree of relationship to theoretical analysis:

- a) Identification of modal parameters (natural frequencies, modal shapes and modal damping respectively) without relationship to theoretical model. Doing this, we can discover e.g. whether excessive vibrations during operation are caused by resonance and what the excited modal shape looks like.

- b) Identification of modal parameters to compare the experimentally obtained data with corresponding data obtained by FEM or other theoretical methods. The goal is to verify the theoretical model before other calculations such as responses to different loads are carried out. For this we need:
- precise determination of natural frequencies
 - identification of modal shapes with such precision that their comparison with computed modal shapes is possible - matching the corresponding modal shapes together
- c) The same as b) plus correction of the theoretical model so that it better matches the measured values. This is done by trial-and-error method usually, e.g. by a slight change in material parameters or inclusion of modal damping in the theoretical model.
- d) Correlation of experimental and theoretical results - two sets of data are numerically compared in order to precisely identify the causes of discrepancy between the calculated and measured properties. This requires a much more accurate measurement of modal shapes than when we only want to animate them (as it is in the previous cases).
- e) Using modal testing to obtain a mathematical model of a component that can be included in a complex one. This approach is often used for theoretical analysis of complex structures. It requires accurate values of natural frequencies, modal damping and modal shapes. All modes must be included, it is not possible to fit the model to a few individual natural frequencies. Excluded modes affect dynamic behaviour of the entire structure in the observed frequency range. This application is more demanding than all previous ones.
- f) Creating a model that can be used to predict the impact of structural modifications to the original test structure. It is a smaller change than in the case of the substructures, so here are a little lower accuracy requirements than in the previous case. Yet, in both of these cases complications usually occur with non-measured rotational degrees of freedom.
- g) Using the model obtained through modal testing to determine the excitation forces. It is possible to compare responses caused by excitation forces with the mathematical description of transfer functions of the structure and, on the base of this comparison, to estimate the excitation forces.

Successful modal testing requires a combination of the three skills and knowledge:

- theoretical framework
- accurate measurement of vibration
- realistic and detailed data processing

In this introductory chapter, only the basis of these three requirements are presented. They will further be explained in details.

1.2 Summary of Theory

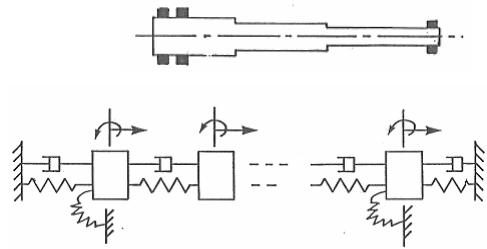
The system under investigation can be described by three different types of models. Each of them is defined by system matrices.

- **spatial model**

- [M] ... mass matrix
- [K] ... stiffness matrix
- [B] or [H] ... viscous damping or structural (hysteretic) damping matrix

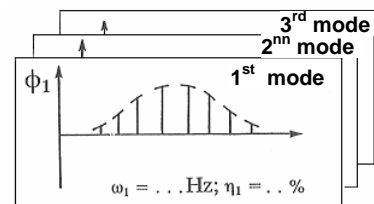
Matrices are of dimensions $N \times N$.

(N = number of degrees of freedom = number of equations of motion)



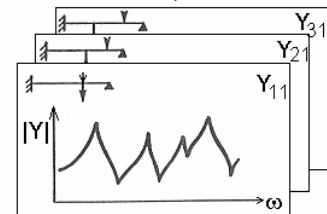
- **modal model**

- $[\lambda^2]$... spectral matrix, diagonal, eigenvalues are on the diagonal
- $[\Phi]$... modal matrix, columns are modal shapes



- **response model**

- $[H(\omega)]$... FRF matrix (matrix of FRFs - frequency response functions, e.g. mobilities $Y(\omega)$ or IRFs - impulse response functions, symmetrical)



Performing **theoretical** vibration analysis, we advance from a spatial model to a response model in the following steps:

1. establish equations of motion \Rightarrow *spatial model*
2. free vibration analysis \Rightarrow *modal model*
3. analysis of forced vibration using harmonic excitation \Rightarrow *response model*

Performing **experimental** vibration analysis, we advance in opposite direction in the following steps:

1. measurements of the appropriate set of FRFs \Rightarrow *response model*
2. curve-fitting of the measured data \Rightarrow *modal model*
3. further calculations \Rightarrow *spatial model* (it is not common to perform this step)

Frequency Response Function - FRF, which is the basis of the response model, can be expressed as:

$$H(\omega) = \frac{\text{output}}{\text{input}} = \frac{\text{movement}}{\text{force}} = \frac{\text{response}}{\text{excitation}}$$

There are three basic types of FRFs according to the type of response parameter, which can be either displacement, velocity or acceleration - see Table 1.1.

One element of the receptance matrix $\alpha_{jk}(\omega)$ represents harmonic response x_j at point j caused by a single harmonic force F_k acting at the different point k .

Precise definition of one element of frequency response function (for receptance matrix $[\alpha(\omega)]$):

$$\alpha_{jk}(\omega) = \frac{x_j}{F_k} = \sum_{r=1}^N \frac{\Phi_j^r \cdot \Phi_k^r}{\lambda_r^2 - \omega^2} \quad (1.1)$$

where:

λ_r - eigenvalue of the r^{th} mode (natural frequency + modal damping)

Φ_j^r - the j^{th} element of the r^{th} natural shapes' vector $\{\Phi\}$, i.e. relative displacement at the j^{th} point as vibrating with the r^{th} shape

N - number of modes

Note: With the experimental procedure, the number of extracted modes N is usually smaller than the number of degrees of freedom (DOF), which is caused by limited frequency range of measurements. An experimentally obtained model is a so called incomplete model, in contrast to a complete model obtained by computation; we can theoretically obtain a number of modes of vibration equal to a number of DOFs in a computational model.

The expression (1.1) is the basis of modal tests - it reflects a direct connection between modal properties of the system and its response characteristics. From a purely theoretical point of view it provides an effective means to calculate responses, whereas from a practical point of view it allows to determine modal properties from mobility measurements.

If we apply the theoretical knowledge of the relationship between receptance functions and modal parameters, it is possible to prove that the "appropriate" set of measured receptances must only contain one row or one column of the mobility matrix $[\alpha(\omega)]$. In practice, this means that we either excite the structure at one point and measure responses at all points or we measure the response at one point and excite the structure at all points. The first option applies when a dynamic exciter is used, the second when an impact hammer or other contactless device is used.

dynamic exciter \Rightarrow one column of FRF matrix is measured
 impact hammer excitation \Rightarrow one row of FRF matrix is measured

1.3 Various Types of Frequency Response Functions

When a frequency response function is referred to without response parameter specification, it is usually denoted as $H(\omega)$. When a response parameter is specified, individual FRFs have their own denotation (see Table 1.1).

Response parameter r	Frequency response function	
	Standard $\frac{r}{F}$	Inverse $\frac{F}{r}$
displacement X	receptance admittance dynamic compliance dynamic flexibility $\alpha(\omega)$	dynamic stiffness
velocity V	mobility $Y(\omega)$	mechanical impedance
acceleration A	inertance accelerance $A(\omega)$	apparent mass

Tab 1.1 Various Types of FRFs According to Response Parameter

Displacement as a function of time is in complex notation expressed as:

$$x(t) = X e^{i\omega t} \quad (1.2)$$

Expressions for velocity and acceleration can be obtain by simple derivative:

$$v(t) = \dot{x}(t) = i\omega X e^{i\omega t} \quad (1.3)$$

$$a(t) = \ddot{x}(t) = -\omega^2 X e^{i\omega t} \quad (1.4)$$

FRF of type receptance with displacement as a response parameter is defined:

$$\alpha(\omega) = \frac{X}{F} \quad (1.5)$$

And again, using derivatives we obtain another types of FRF:

$$Y(\omega) = \frac{V}{F} = i\omega \frac{X}{F} = i\omega \alpha(\omega) \quad \dots \text{mobility} \quad (1.6)$$

$$A(\omega) = \frac{A}{F} = -\omega^2 \alpha(\omega) \quad \dots \text{inertance} \quad (1.7)$$

1.4 Summary of Measurement Methods

The following aspects demand special attention in order to ensure acquisition of high-quality data:

- a) mechanical aspects of supporting and correctly exciting the structure
- b) correct transduction of the quantities to be measured - force input and motion response
- c) signal processing which is appropriate to the type of the test used

Various Ways of Supporting the Testpiece

Before a modal test, we have to consider various ways of supporting the measured structure. Generally, we choose one of the following three options of support corresponding to the aim of the modal test and to the limitations caused by operating conditions, respectively:

- **free (unrestrained)** - It is the simplest way how to support the testpiece and it is preferably used each time we want to correlate experimental model with a theoretical one. It is usually implemented by suspending the testpiece on very soft springs (rubber ropes or foam pad).
- **grounded (clamped)** - It requires rigid clamping of the testpiece at certain points. It is more complicated, because ideal fixation is impossible in real. Then, discrepancies between an experimental and theoretical model could largely originate from unequal boundary conditions. However, this support needs to be used occasionally (e.g. for determination modal parameters of turbine blades).
- **in situ** (under operational conditions) - It is used when modal parameters under real operational conditions are needed and no correlation with a theoretical model is required.

Excitation of the Structure

The way of how to excite vibrations of the measured structure is again given mostly by the aim of the modal test, precision requirements and frequency range in which the modal parameters are to be determined. There are basically two ways of excitation:

- **excitation by means of dynamic exciter**
 - by harmonic signal
 - by random signal
 - by other types of signals (see chapter 4.2.1.1.3)
- **impulse excitation**
 - by means of impact hammer
 - step release (from deformed position)

Transducers

Transducers used for sensing force and response should affect the measured structure as little as possible and their effectiveness should be adequate to measurement frequency range and to displacements under consideration. Nowadays, piezoelectric transducers of both force and acceleration are used; response is mostly picked in the form of acceleration. Chapter 4.5.1.2 deals with transducers in more detail.

1.5 Summary of Modal Analysis

An analysis of measured data is a process in which the measured frequency response functions are analyzed in order to find a theoretical model that most closely resembles the dynamic behaviour of the structure under test. This part of the modal test is called experimental modal analysis, although this term is often incorrectly used for the entire modal test. The process of data analysis proceeds in two stages:

1. Identifying the appropriate type of model (with viscous or structural damping). This choice is often in practice limited by software used for the modal analysis. Most of software packages work with one type of damping and give no choice to the user.
2. Determining appropriate parameters of the chosen model. This stage, also called modal parameters extraction, is done by curve-fitting of the measured frequency response functions to the theoretical expressions. This stage is discussed in detail in chapter 4.3.

2. Dual-channel Analysis

In this chapter we will introduce some terms that concern modal tests and that fall within signal processing area. Whilst we use a single-channel analysis for vibration diagnostics tasks (even if there could be more channels processed simultaneously), system analysis tasks work on the principle of a dual-channel analysis. The basic scheme of dual-channel FFT (Fast Fourier Transform) analyzer is in Fig. 2.1.

During a simultaneous analysis of signals in at least two channels, the signals themselves are not in the forefront any more, but rather properties of the physical system responsible for the differences between those signals. The methods can be theoretically expanded to any number of channels, but basically two of them are processed simultaneously each time. In the following text, individual functions that occur in system analysis will be described.

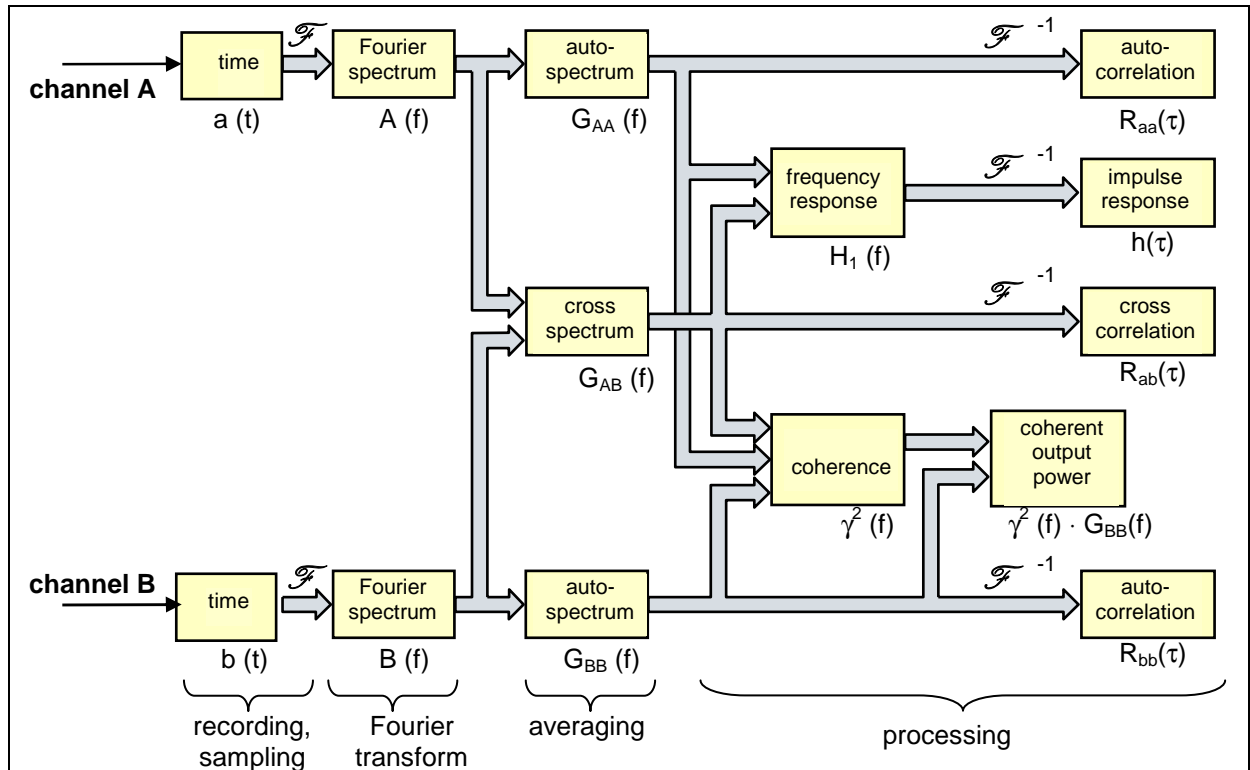
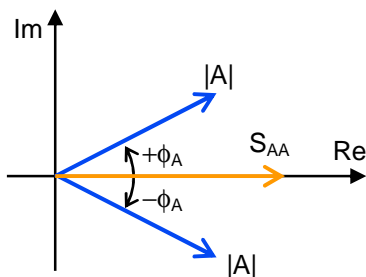


Fig. 2.1 Scheme of Dual-channel Analyzer

2.1 Autospectrum

Autospectrum is a function commonly explored both in signal and system analysis. It is computed from the instantaneous (Fourier) spectrum as:

$$S_{AA}(f) = E[A(f) \cdot A^*(f)] = \mathcal{F} E[a(t) * a(-t)] = \mathcal{F} [R_{aa}(\tau)] \quad (2.1)$$



$$A(f) = |A(f)| \cdot e^{i\phi_A(f)} \quad (2.2)$$

$$A^*(f) = |A(f)| \cdot e^{-i\phi_A(f)} \quad (2.3)$$

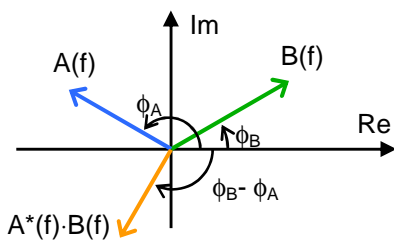
$$S_{AA}(f) = E[A(f) \cdot |A^*(f)| \cdot e^{i0}] = E[|A|^2(f)] \quad (2.4)$$

There is a new, fundamental function - cross spectrum - in the dual channel processing. It is computed from instantaneous spectra of both channels. All other functions in the scheme in Fig. 2.1 are computed during post-processing from the cross spectrum and the two autospectra. Of course, all functions are the functions of frequency.

2.2 Cross Spectrum

Based on complex instantaneous spectra $A(f)$ and $B(f)$, the cross spectrum S_{AB} (from A to B) is defined as:

$$S_{AB}(f) = E[A^*(f) \cdot B(f)] = \mathcal{F} E[a(-t) * b(t)] = \mathcal{F} [R_{ab}(\tau)] \quad (2.5)$$



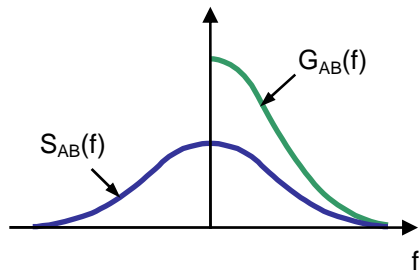
$$A(f) = |A(f)| \cdot e^{i\phi_A(f)} \quad (2.6)$$

$$B(f) = |B(f)| \cdot e^{i\phi_B(f)} \quad (2.7)$$

$$S_{AB}(f) = E[|A(f)| \cdot |B(f)| \cdot e^{i(\phi_B(f) - \phi_A(f))}] \quad (2.8)$$

Amplitude of the cross spectrum S_{AB} is the product of amplitudes, its phase is the difference of both phases (from A to B). Cross spectrum S_{BA} (from B to A) has the same amplitude, but opposite phase. The phase of the cross spectrum is the phase of the system as well.

Both autospectra and cross spectrum can be defined either as two-sided (notation S_{AA} , S_{BB} , S_{AB} , S_{BA}) or as one-sided (notation G_{AA} , G_{BB} , G_{AB} , G_{BA}). One-sided spectrum is obtained from the two-sided one as:



$$G_{AB}(f) = \begin{cases} 0 & \text{for } f < 0 \\ S_{AB}(f) & \text{for } f = 0 \\ 2 \cdot S_{AB}(f) & \text{for } f > 0 \end{cases} \quad (2.9)$$

The cross spectrum itself has little importance, but it is used to compute other functions. Its amplitude $|G_{AB}|$ indicates the extent to which the two signals correlate as the function of frequency, phase angle $\angle G_{AB}$ indicates the phase shift between the two signals as the function of frequency. The advantage of the cross spectrum is that influence of noise can be reduced by averaging. That is because the phase angle of the noise spectrum takes random values so that the sum of those several random spectra tends to zero (see Fig. 2.2). It can be seen that the measured autospectrum is a sum of the true autospectrum and autospectrum of noise, whilst the measured cross spectrum is equal to the true cross spectrum.

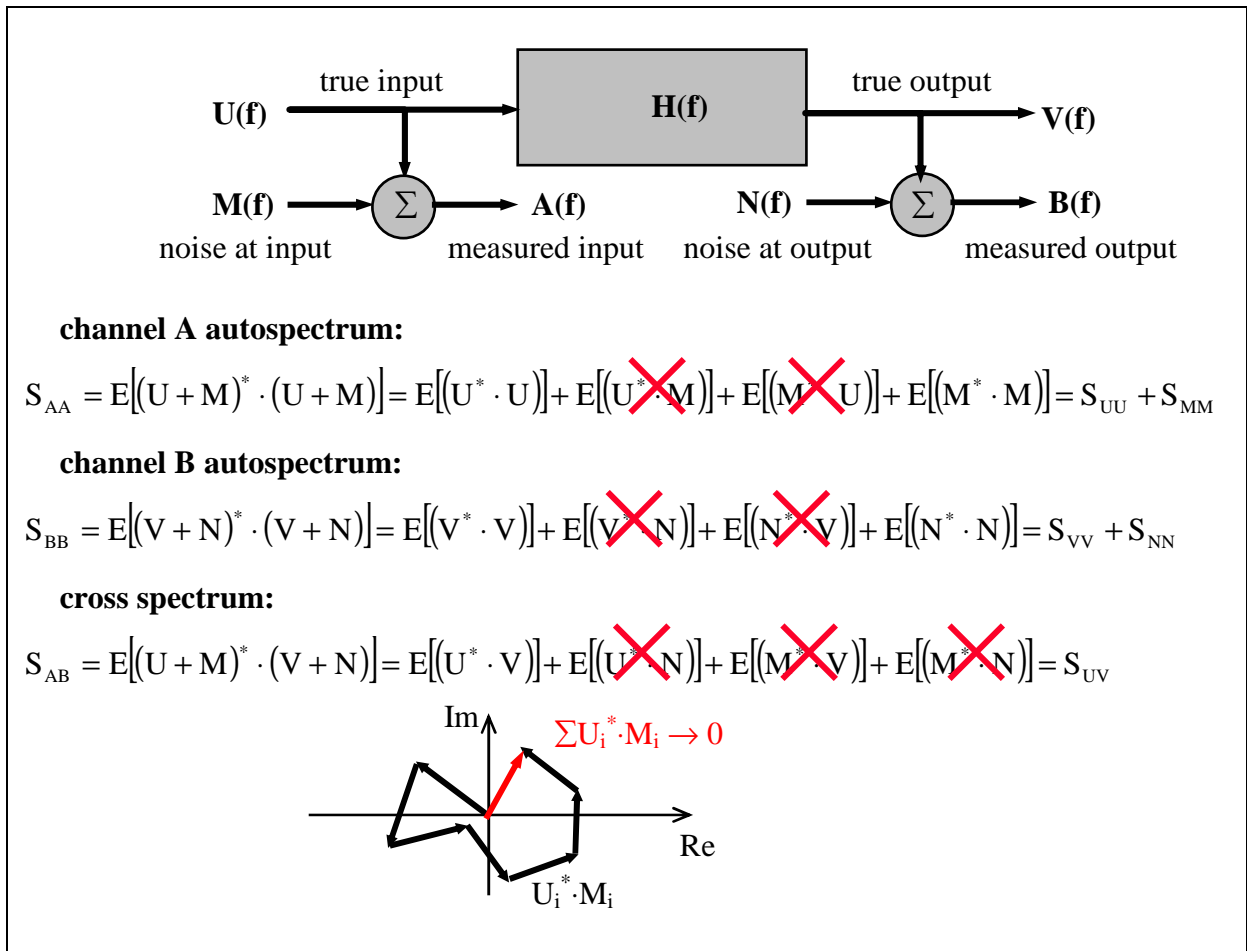


Fig. 2.2 Reduction of Noise at the Cross Spectrum by Averaging

2.3 Coherence

Coherence function indicates the degree of linear relationship between two signals as a function of frequency. It is defined by two autospectra and a cross spectrum as:

$$\gamma^2(f) = \frac{|G_{AB}(f)|^2}{G_{AA}(f) \cdot G_{BB}(f)} \quad (2.10)$$

At each frequency coherence can be taken as a correlation coefficient (squared) which expresses the degree of linear relationship between two variables, where the magnitudes of autospectra correspond to variances of those two variables and the magnitude of cross spectrum corresponds to covariance.

Coherence value varies from zero to one. Zero means no relationship between the input **A** and output **B**, whilst one means a perfectly linear relationship (see Fig. 2.3).

$$0 \leq \gamma^2(f) \leq 1 \quad (2.11)$$

There are four possible relationships between input **A** and output **B** in Fig. 2.3 :

- perfectly linear relationship
- sufficiently linear relationship with a slight scatter caused by noise
- non-linear relationship
- no relationship

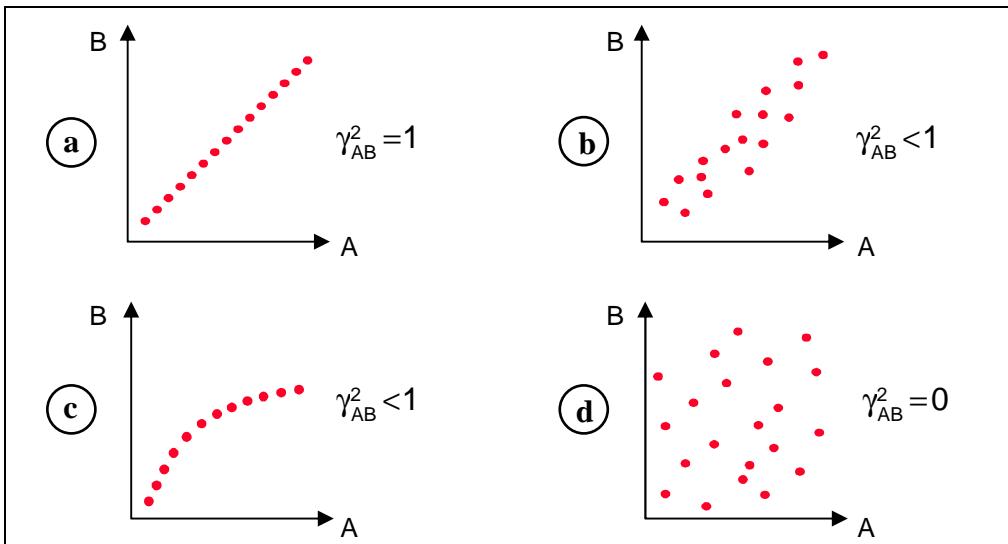


Fig. 2.3 Analogy Between Coherence and Correlation Coefficient

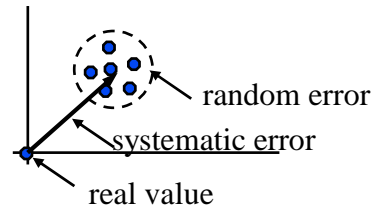
Coherence function provides useful information only when spectra $G_{AA}(f)$, $G_{BB}(f)$ and $G_{AB}(f)$ are estimates, i.e. spectra averaged from more records. For only one sample (without averaging) applies:

$$|G_{AB}(f)| = |A(f)|^2 \cdot |B(f)|^2 = G_{AA}(f) \cdot G_{BB}(f) \quad \wedge \quad \gamma^2(f) = 1 \quad (2.12)$$

In the case of no averaging, coherence is always equal to 1. In the case of averaging and samples G_{AB} influenced by noise, deviations in the phase angles cause that the resulting magnitude $|G_{AB}|$ is lower than it would be without presence of noise (see Fig. 2.4). Presence of non-linearities has similar influence.

If signals are random or if they include some noise, a more reliable estimate could be obtained with the help of averaging. Generally, the result may be loaded with two types of errors:

- systematic (bias) errors
- random errors



For linear systems, a systematic error doesn't occur in the cross spectrum if the analysis is performed with sufficient resolution (see chapter 2.6.2).

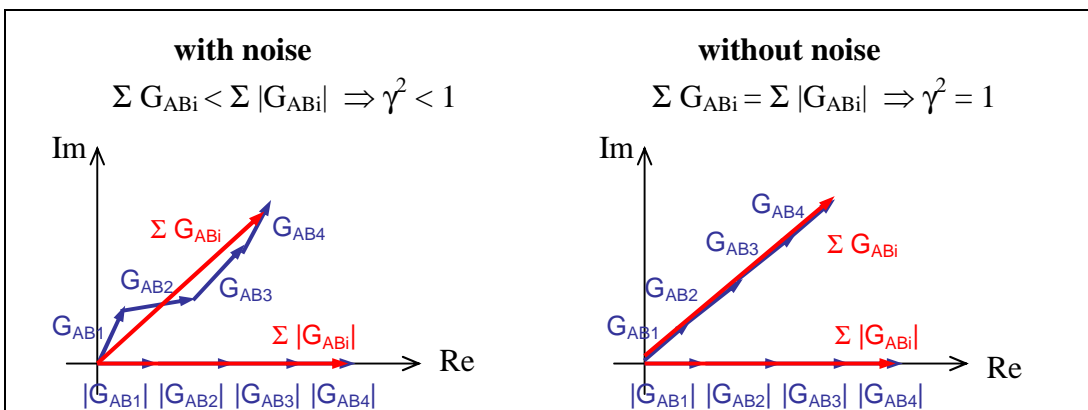


Fig. 2.4 Influence of Noise to the Coherence

The most important application of the coherence function is verification of other functions and determination whether they are affected by noise or by the presence of nonlinearities. Low coherence does not automatically mean that the measurement was invalid, but sometimes it is a sign that a lot of averages should be performed to get a valid result. The reasons for reduced coherence may be:

- difficult measurements:
 - noise in measured output signal
 - noise in measured input signal
 - other inputs not correlated with measured input signal
 - system nonlinearities
- bad measurements:
 - leakage
 - time varying systems
 - DOF jitter (while impact excitation, when we do not hit exactly the same position in all of the hits)

Coherence is also used to obtain some of the derived functions that have various applications. One of these functions is *Coherent Output Power*:

$$\text{COP} = \gamma^2 \cdot G_{\text{BB}}(f) \quad (2.13)$$

COP gives a measure of what part of the measured output autospectrum, $G_{\text{BB}}(f)$, is fully coherent with a particular input signal represented by autospectrum $G_{\text{AA}}(f)$.

COP can be used when low coherence is caused by noise in the measured output signal. It has no sense when there is noise in the input signal or when there are nonlinearities in the system.

Another function derived from the coherence function is Signal-to-Noise Ratio:

$$\text{S/N} = \frac{\gamma^2}{1 - \gamma^2} \quad (2.14)$$

Here, noise in the measured output signal is considered as the only factor affecting the coherence. Then, coherent output (proportional to γ^2) gives the measure of signal contained in the output and the non-coherent output (proportional to $1 - \gamma^2$) gives the measure of noise in the output.

2.4 System descriptors

When the signals A and B represent input and output of the physical system, frequency response function $H(f)$ in the frequency domain and impulse response function $h(\tau)$ in the time domain are used to describe the relationship between these two signals (see Fig. 2.5). Frequency response function and impulse response function are so-called system descriptors. They are independent of the signals involved.

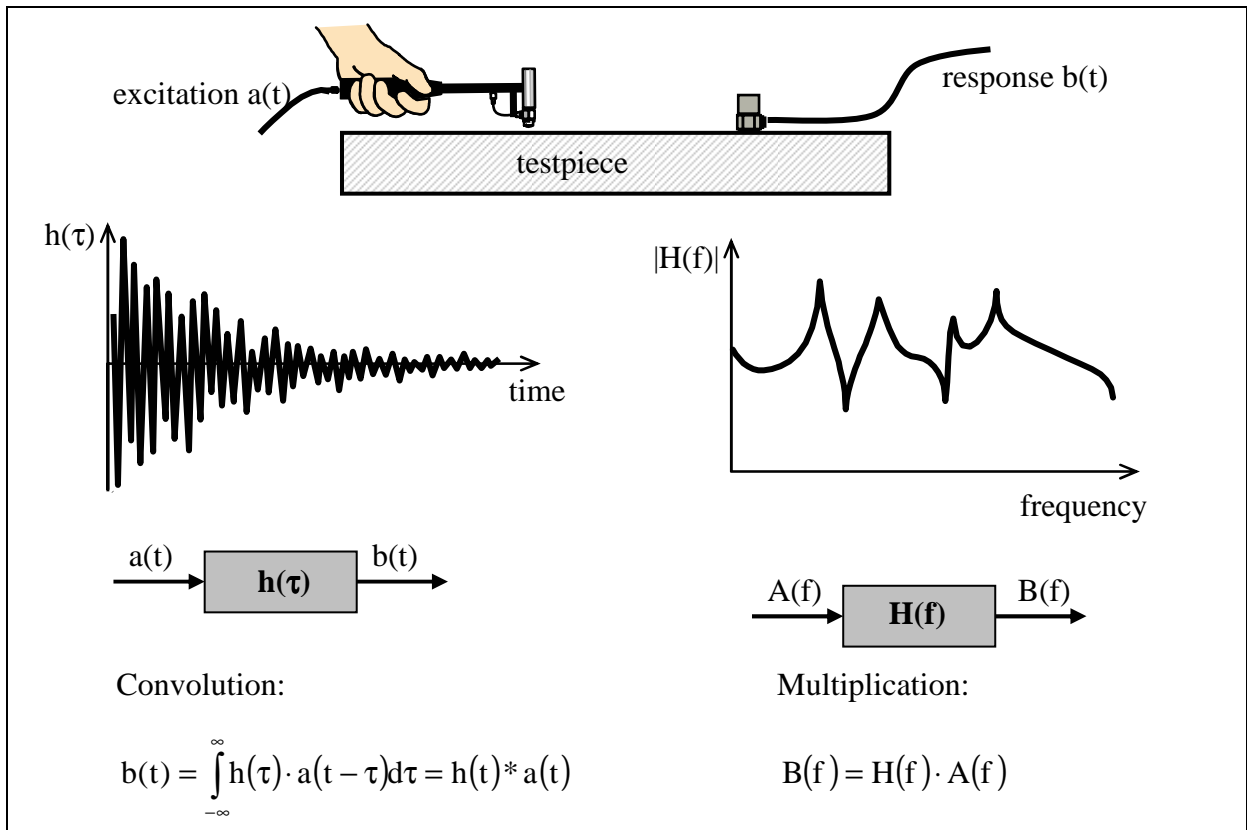


Fig. 2.5 System Descriptors

2.4.1 Frequency Response Function (FRF)

The main reason for using FRFs is the simplicity with which the response of the real system can be described. A detailed derivation of FRF of a single degree of freedom system (SDOF, see Fig. 2.6) will be carried out in chapter 3.1. Here, we will mention only the fact that for an ideal physical system, the properties of which could be described by system of linear differential 2nd order equations, using Laplace transform leads to conversion of these differential equations to algebraic equations of the Laplace variable s . Solution of these equations can be expressed in the form of transfer functions $\mathbf{H}_{ij}(s)$ that represent the ratio of the response in the point i to the input in the point j . The typical transfer function of the n degree-of-freedom system (Multi-Degree-of-Freedom system - MDOF) can be expressed as:

$$H_{ij}(s) = \sum_{k=1}^n \left[\frac{R_{ijk}}{s - p_k} + \frac{R_{ijk}^*}{s - p_k^*} \right] \tag{2.15}$$

where:

- $p_k \dots$ poles - global property for all the transfer functions of a system
- $R_{ijk} \dots$ residues - specific for each of the transfer functions

Each member in the sum represents the response of single degree of freedom system with the pole

$$p_k = -\delta_k + i\Omega_k \tag{2.16}$$

The real part represents damping and the imaginary part represents natural angular frequency of the damped vibration of the k^{th} mode.

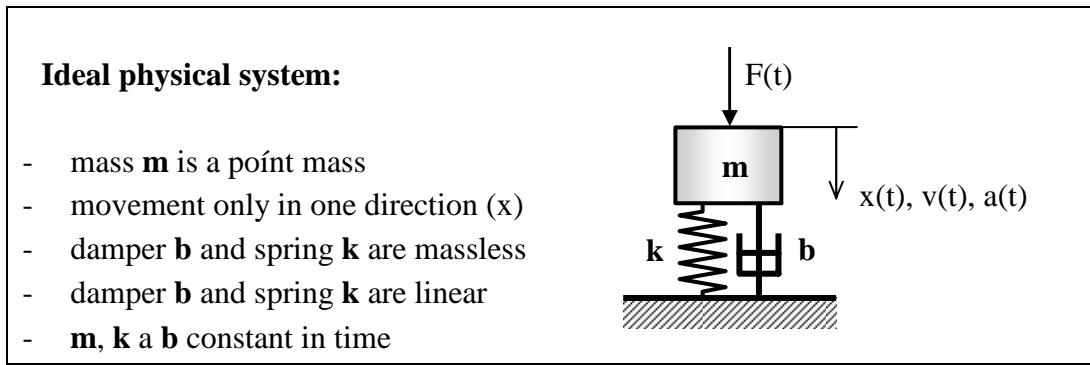


Fig. 2.6 Ideal SDOF System

A transfer function is three-dimensional; for an SDOF system it is shown in Fig. 2.7. If $i\omega$ is put for s (i.e. transfer function is evaluated along the imaginary axis), frequency response function $\mathbf{H}_{ij}(i\omega)$ is obtained, that is in fact a slice of the transfer function along the imaginary axis. The same as with the transfer function, FRF also could be treated as a sum of components, each of which corresponds to the response of an SDOF system. Global properties δ_k a Ω_k could be basically obtained from any of the measured functions \mathbf{H}_{ij} , whereas residues \mathbf{R}_{ijk} define the eigenvector Φ_k and are specific for each of the \mathbf{H}_{ij} functions.

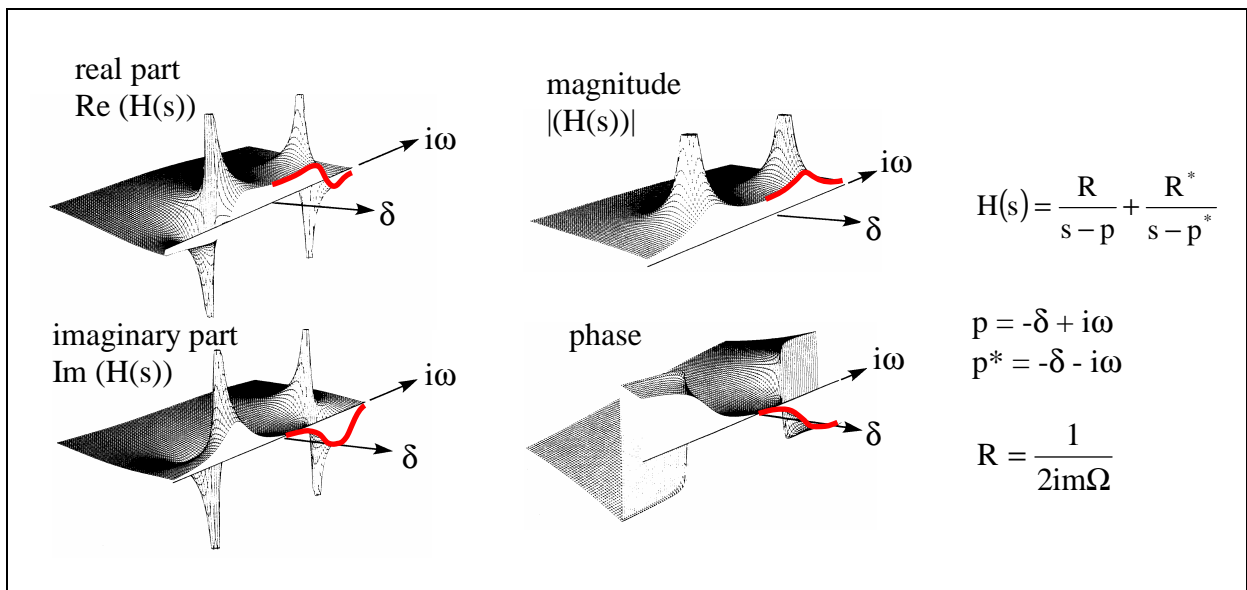


Fig. 2.7 Transfer Function

FRF for a single degree of freedom system from Fig. 2.6 is shown in Fig. 2.8. Various forms of displaying FRF are discussed in detail in chapters 3.1.2.2 and 3.1.3.1.

An SDOF system (or one mode of MDOF system) is described by means of 3 parameters:

- undamped natural frequency $\Omega_0 = \sqrt{\frac{k}{m}}$ (2.17)

- damping ratio $\zeta = \frac{b}{2\sqrt{km}} = \frac{\delta}{\Omega_0}$ (2.18)

- residuum $R = \frac{1}{2im\omega}$ (2.19)

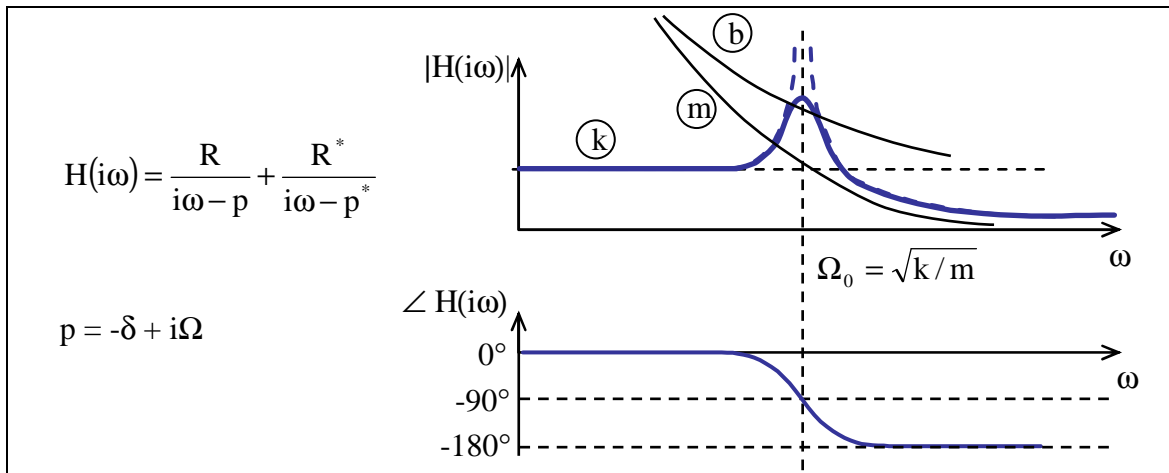


Fig. 2.8 FRF of Single Degree-of-Freedom System

2.4.2 Impulse Response Function - IRF

An impulse response of a system is an output signal when the Dirac impulse (unit impulse, delta function) is applied at the input. It is an inverse Fourier transform of the frequency response function, and this is the procedure used to calculate it in an FFT analyzer:

$$h(t) = \mathcal{F}^{-1} \{H(f)\} \quad (2.20)$$

An impulse response of an SDOF system is one-sided damped sinusoid (see Fig. 2.9) given by the formula:

$$h(t) = 2 \cdot |R| \cdot e^{-\delta t} \cdot \sin(\Omega t) \quad (2.21)$$

Just like the FRF, also IRF of an MDOF system is a sum of n IRFs of n SDOF systems. Summing all the n modes, more general formula is obtained:

$$h_{ij}(t) = \sum_{k=1}^n 2 \cdot |R_{ijk}| \cdot e^{-\delta_k t} \cdot \sin(\Omega_k t) \quad (2.22)$$

The average decay constant of this summarized impulse response can be used to estimate average damping properties of the system.

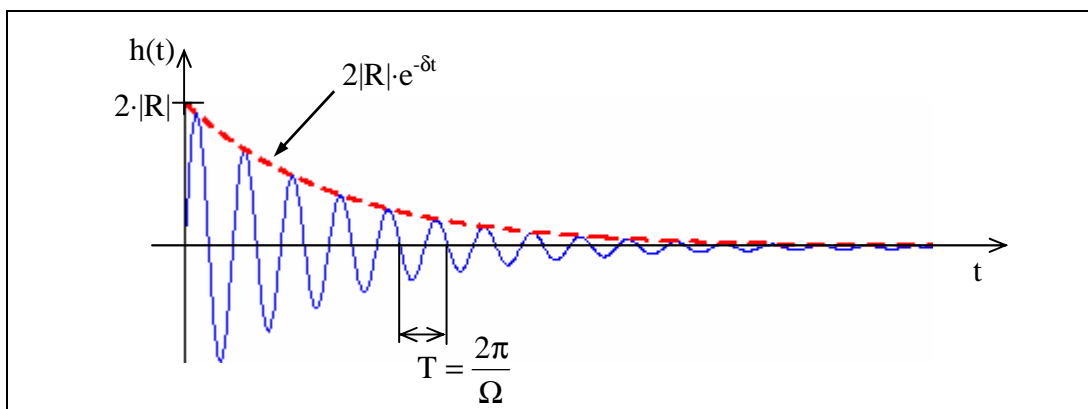


Fig. 2.9 IRF of Single Degree-of-Freedom System

If the magnitude of IRF is displayed in logarithmic scale, the envelope of the function is a line, and its slope indicates damping of the system. Come out of the definition of logarithmic decrement ν :

$$\nu = \ln \frac{x(t)}{x(t+T)} = \delta T \quad (2.23)$$

Magnitude decreases e -times in the time τ (τ is so-called systems's time constant):

$$\ln e = \delta \cdot \tau$$

$$1 = \delta \cdot \tau$$

$$\delta = 1/\tau$$

Written in dB: $20 \log e = 8.7 \text{ dB}$

If there is logarithmic scale for the magnitude of IRF on the vertical axis, time τ , during which magnitude drops by 8.7 dB can be read out and decay constant δ can be calculated (see Fig. 2.10). This procedure is the same for both estimating the decay constant of the SDOF system and estimating the average decay constant of the MDOF system.

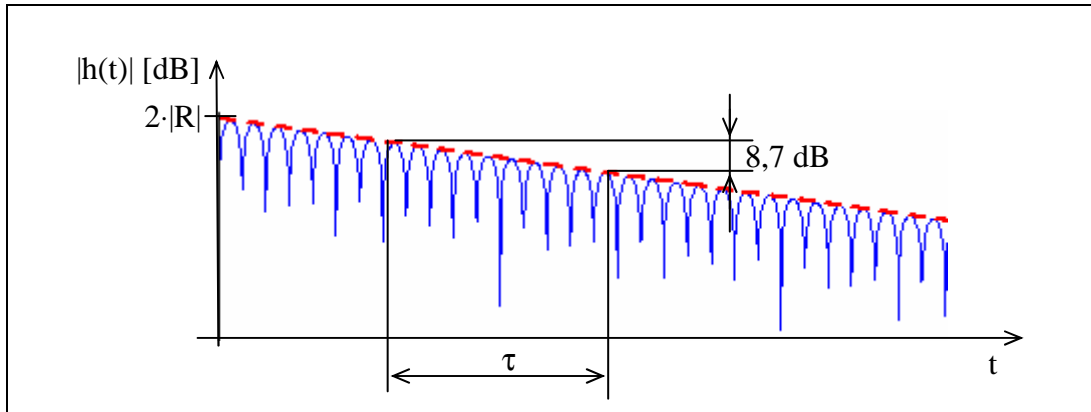


Fig. 2.10 Estimating Damping from Impulse Response Function

2.5 Effect of Noise on the FRF

A frequency response function could be also defined as a slope of the line which, for linear systems, defines output as a function of input. If the system is not linear, its linear approximation is obtained using Fourier transform. The influence of random noise is eliminated by linear approximation as well (see Fig. 2.11).

A frequency response function is defined as the ratio of output to input. Three alternative estimates are at disposal using a dual channel analyzer. They are defined using autospectra and cross spectrum:

$$H_1(f) = \frac{G_{AB}(f)}{G_{AA}(f)} \quad (2.24)$$

$$H_2(f) = \frac{G_{BB}(f)}{G_{BA}(f)} \quad (2.25)$$

$$H_3(f) = \sqrt{\frac{G_{BB}(f)}{G_{AA}(f)}} \cdot \frac{G_{AB}(f)}{|G_{AB}(f)|} = \sqrt{H_1(f) \cdot H_2(f)} \quad (2.26)$$

Coherence function could be defined as:

$$\gamma^2(f) = \frac{|G_{AB}(f)|^2}{G_{AA}(f) \cdot G_{BB}(f)} = \frac{H_1(f)}{H_2(f)} \quad (2.27)$$

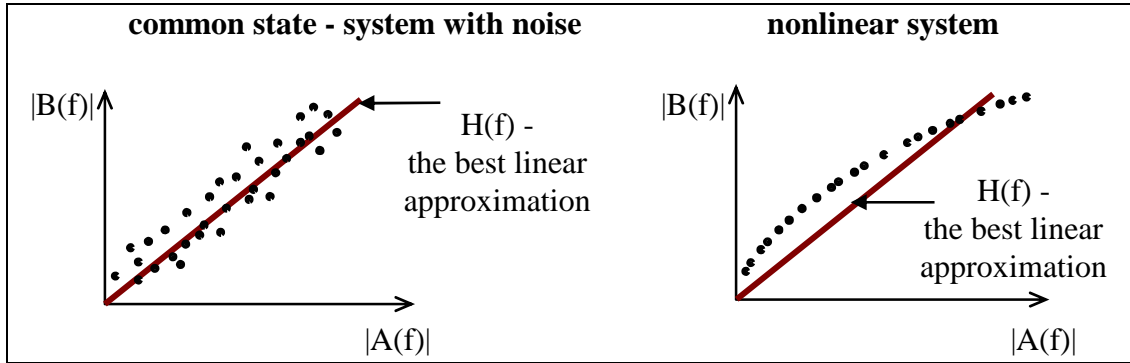


Fig. 2.11 Linearization

Which of these three estimates is better to use depends on whether there is noise on the input or output. When FRF is measured using impact excitation, the input signal is clean, without noise, whilst the output signal is modified by system response and deteriorated by noise, particularly in antiresonances. On the contrary, when FRF is measured using dynamic exciter, the input signal is deteriorated by noise in the vicinity of resonances, particularly for slightly damped structures. The structure behaves as a short circuit in the vicinity of resonances and the input power spectrum has low values even if the signal entering the exciter is white noise. The output signal is relatively clean. If there is a need for having as accurate values of FRF magnitudes as possible, the best solution is to read magnitudes of resonant peaks from H_2 function and the rest from H_1 function.

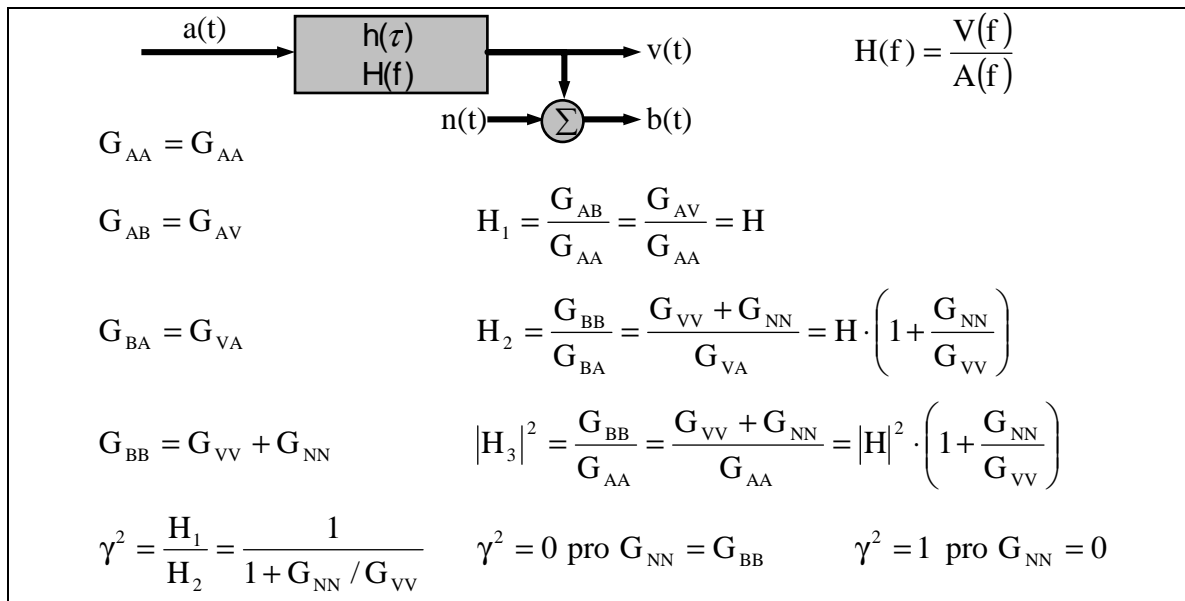


Fig. 2.12 Influence of Noise at the Output

The influence of noise at the output is shown in detail in Fig. 2.12, the influence of noise at the input in Fig. 2.13 and the influence of noise at both input and output, which is a common case, is shown in Fig. 2.14.

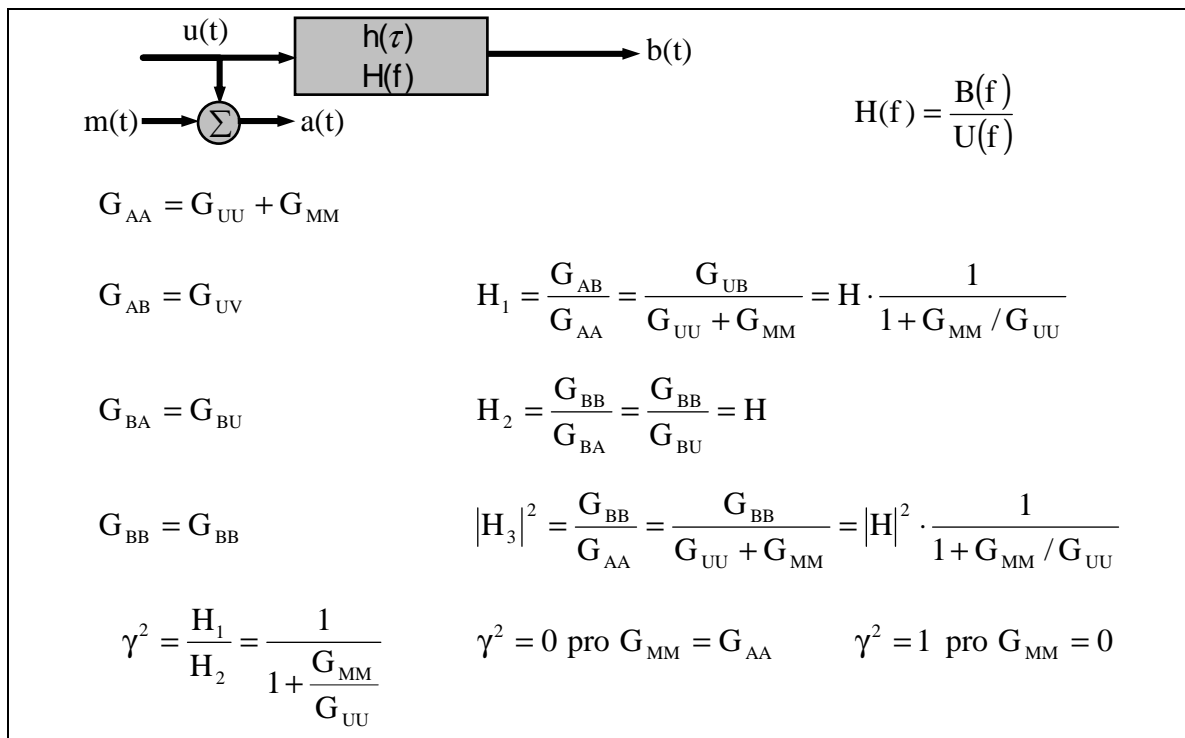


Fig. 2.13 Influence of Noise at the Input

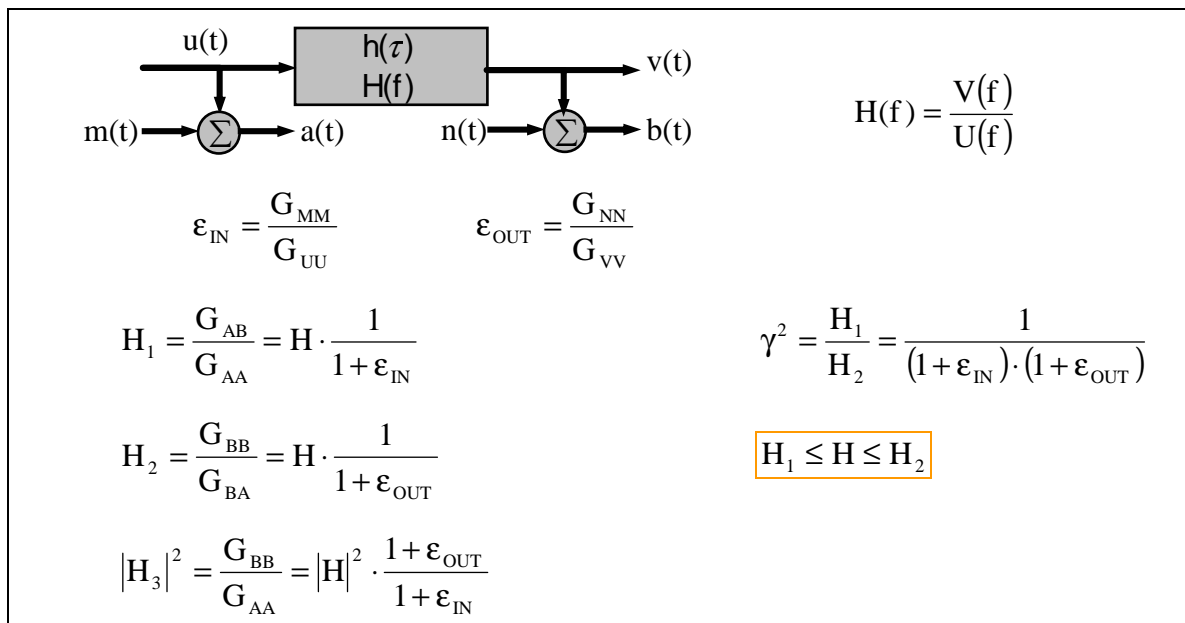


Fig. 2.14 Influence of Noise at Both Input and Output

2.6 Digital Signal Processing

The main function of a spectral analyzer is to perform Fourier transform of signals that are coming to the input. It is useful to recall the relationship between two major versions of basic Fourier transform, between time and frequency domain. In its simplest form it means that the function $\mathbf{x}(t)$, periodic in time \mathbf{T} , can be expressed as an infinite sequence:

$$\mathbf{x}(t) = \frac{a_0}{2} + \sum_{n=1}^{\infty} \left(a_n \cdot \cos\left(\frac{2\pi n t}{T}\right) + b_n \cdot \sin\left(\frac{2\pi n t}{T}\right) \right) \quad (2.28)$$

where \mathbf{a}_n and \mathbf{b}_n can be computed from $\mathbf{x}(t)$ using formulas (2.29) a (2.30):

$$a_n = \frac{2}{T} \cdot \int_0^T \mathbf{x}(t) \cdot \cos\left(\frac{2\pi n t}{T}\right) dt \quad (2.29)$$

$$b_n = \frac{2}{T} \cdot \int_0^T \mathbf{x}(t) \cdot \sin\left(\frac{2\pi n t}{T}\right) dt \quad (2.30)$$

When $\mathbf{x}(t)$ is discretized and takes finite time, so it is only defined on the set of \mathbf{N} individual time moments \mathbf{t}_k ($k = 1, N$), we can write the finite Fourier series:

$$\mathbf{x}_k (= \mathbf{x}(t_k)) = \frac{a_0}{2} + \sum_{n=1}^{N/2} \left(a_n \cdot \cos\left(\frac{2\pi n t_k}{T}\right) + b_n \cdot \sin\left(\frac{2\pi n t_k}{T}\right) \right) ; k = 1, N \quad (2.31)$$

Coefficients \mathbf{a}_n and \mathbf{b}_n are Fourier or spectral coefficients of the function $\mathbf{x}(t)$ and they are often denoted in the form of amplitude \mathbf{c}_n and phase ϕ_n :

$$c_n (= X_n) = \sqrt{a_n^2 + b_n^2} \quad a \quad \phi_n = \arctg\left(-\frac{b_n}{a_n}\right) \quad (2.32)$$

This is the form of Fourier transform concerned in practical applications of theory used in modal test area. Due to discretization of the input signals (from force transducers and accelerometers) it is called discrete Fourier transform (DFT).

The input signal is then digitized by an A/D converter and recorded as a set of \mathbf{N} discrete values with regular spacing in the time interval \mathbf{T} during which the measurement was made. Then, assuming that the sample is periodic in time \mathbf{T} , finite Fourier series (transform) is calculated according to the relation (2.31), as an estimate of the desired Fourier transform. There is a basic relationship between the length of the sample \mathbf{T} , number of discrete values \mathbf{N} , sample (or capture) frequency \mathbf{f}_s and range and resolution of the frequency spectrum. The range of the spectrum is $0\text{-}f_{\max}$, where \mathbf{f}_{\max} is *Nyquist frequency* and the resolution between frequency lines is $\Delta\mathbf{f}$, where:

$$f_{\max} = \frac{f_s}{2} = \frac{1}{2} \cdot \frac{N}{T} \quad (2.33)$$

$$\Delta f = \frac{f_s}{N} = \frac{1}{T} \quad (2.34)$$

Since the transformation size (\mathbf{N}) is usually fixed for the given type of analyzer, and it is usually (even though not always) the power of 2, i.e. 512, 1024 etc., the frequency range and spectral resolution is determined only by duration of each sample.

The fundamental equation, that is solved for determination of spectral content is derived from the equation (2.35):

$$\begin{Bmatrix} x_1 \\ x_2 \\ x_3 \\ \vdots \\ x_N \end{Bmatrix} = \begin{bmatrix} 0.5 & \cos(2\pi/T) & \dots \\ 0.5 & \cos(4\pi/T) & \dots \\ 0.5 & \cos(6\pi/T) & \dots \\ \vdots & \vdots & \dots \\ 0.5 & \cos(2N\pi/T) & \dots \end{bmatrix} \cdot \begin{Bmatrix} a_0 \\ a_1 \\ b_1 \\ \vdots \\ \vdots \end{Bmatrix} \quad \text{or} \quad \{x_k\} = [C] \cdot \{a_n\} \quad (2.35)$$

To solve unknown spectral or Fourier coefficients contained in $\{a_n\}$ following equation is used:

$$\{a_n\} = [C]^{-1} \{x_k\} \quad (2.36)$$

An optimized algorithm of solving the equation (2.36) was derived, that is called *Fast Fourier Transform* (FFT). This algorithm requires N to be an integral power of 2. Usually, values between 256 and 4096 are used.

Digital Fourier analysis has many features which, if not properly treated, can lead to erroneous results. Generally speaking, they result from discretization and from the need to reduce the length of time signal. In the following sections, specific features of aliasing, leakage, weighting windows, frequency zoom and averaging will be discussed.

2.6.1 Aliasing

There is a problem called "aliasing", which is associated with a digital spectral analysis and results from discretisation of the originally continuous time signal. If the sampling frequency in relation to the frequency content of the signal is too small, the presence of high frequencies in the original signal could be misinterpreted in the discretisation process. In fact, such high frequencies will appear as low frequencies, or, they will be rather indistinguishable from genuine low frequency components. Fig. 2.15 shows that digitising a low frequency signal (above) produces exactly the same set of discrete values as a result from the same process applied to a higher frequency signal (below).

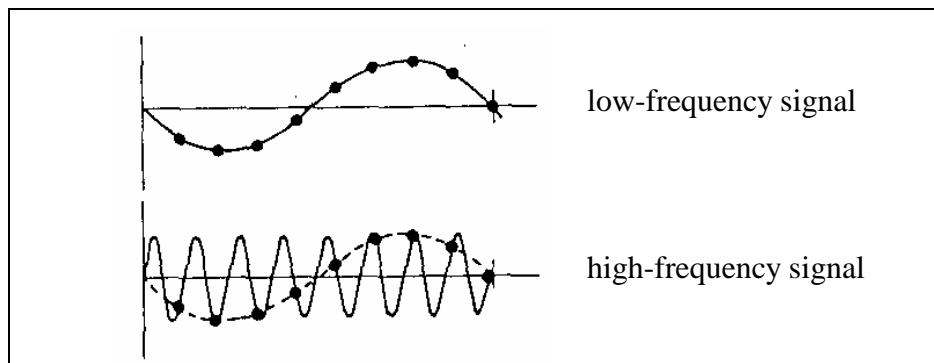


Fig. 2.15 Aliasing - High Frequency Manifested as Low Frequency

If the sampling frequency is f_s , then the signal of frequency f and signal of frequency $(f_s - f)$ are indistinguishable after discretization, and this causes distortion of the measured spectra using DFT, although the calculation is performed accurately. In the description of the DFT, it

was stated that the highest frequency that can be included in the spectrum (transform) is $f_s/2$, and the spectrum should stop at this frequency, regardless of the number of discrete values.

The signal, which has the actual frequency content displayed in Fig. 2.16, appears in DFT as a distorted form. Distortion towards the upper end of the applicable frequency range can be explained by the fact that the portion of the signal which has frequency components above $f_s/2$ will be reflected in the range $0-f_s/2$. These high frequency components then put on the appearance of being low frequency ones and create an indistinguishable mixture with the real low frequency components.

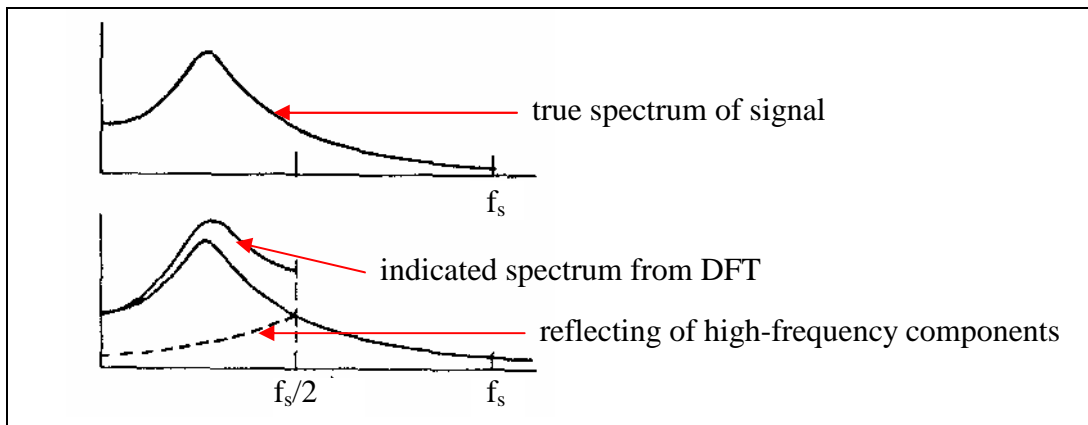


Fig. 2.16 Alias Distortion of Spectrum by DFT

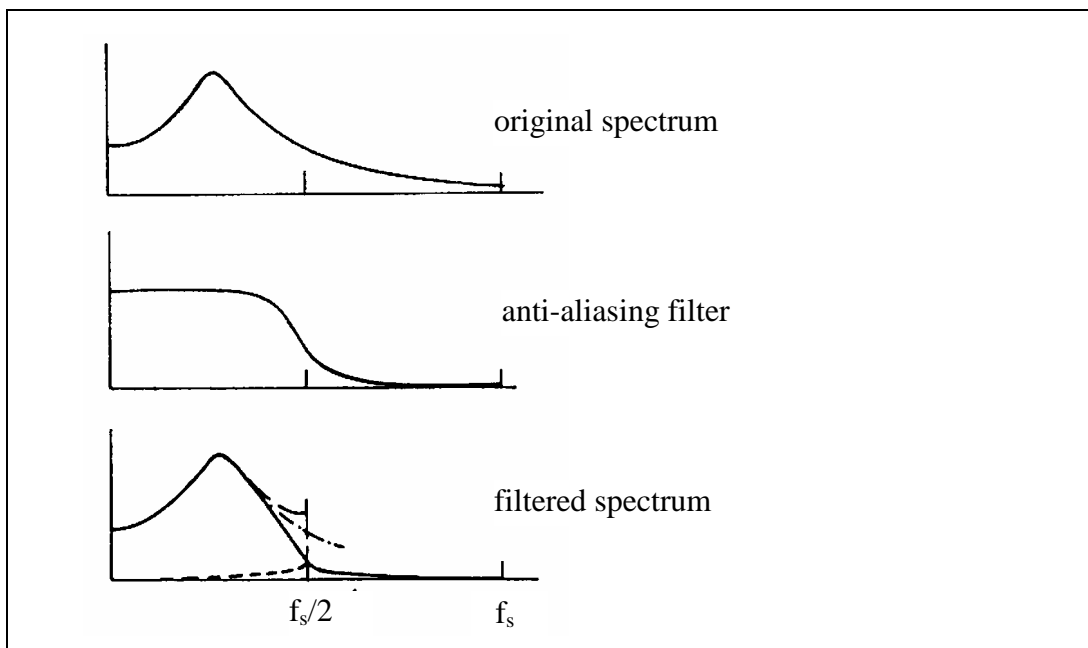


Fig. 2.17 Anti-aliasing Filter Process

The solution to the problem is to use an anti-aliasing filter which subjects the original time signal to a low-pass, sharp cut-off filter with a characteristic of the form shown in Fig. 2.17. This results in submitting a modified time history to the analyzer. Because the filters used are inevitably less than perfect and have a finite cut-off rate, it remains necessary to reject the spectral measurements in a frequency range approaching the Nyquist frequency, $f_s/2$. Typically, the range from $0.8 \cdot f_s/2$ to $f_s/2$ is rejected. It is for this reason that a 2048-point

transform does not result in a complete 1024-line spectrum being given on the analyzer display. Typically, only the first 800 lines will be shown because the higher ones are liable to be contaminated by imperfect anti-aliasing.

It can be concluded that time signal should be submitted to an anti-aliasing filter prior it enters an A/D converter, and therefore these filters are an integral part of each analyzer.

2.6.2 Leakage

Leakage is a problem which is a direct consequence of the need to take only a finite length of time history coupled with the assumption of periodicity. The problem is best illustrated by the two examples shown in Fig. 2.18, where two sinusoidal signals of slightly different frequencies are subjected to the same analysis process. On the left side, the signal is perfectly periodic in the time window T , and the resulting spectrum is simply a single line at the frequency of the sine wave. On the right side, the periodicity assumption is not satisfied and there is a discontinuity at the end of the sample. As a result, the spectrum does not indicate the single frequency which the original time signal possessed, and this frequency is not even prevailing in the spectral lines. The energy has "leaked" into a number of spectral lines close to the true frequency and the spectrum is spread over several lines. The two examples represent the best case and the worst case. The problem is more serious for low frequency signals.

Leakage is a serious problem in many application of digital signal processing, including FRF measurements. There are several ways of avoiding or at least minimizing its effects:

- Changing the duration of the measurement sample length to match any underlying periodicity in the signal, e.g. by changing measurement time T so that to capture an exact number of cycles of the signal. Although such a solution can remove the leakage effect altogether, it can only do so if the signal being analyzed is periodic - which is not always the case - and if the period of that signal can be determined - which is often difficult and it could be the first objective of the analysis. Moreover, measurement time T can not be changed fully arbitrary in FFT analyzers, but only by some steps according to frequency range of measurement (see formula 2.33).
- Increasing the duration of measurement time T , so that the separation between the spectral lines - the frequency resolution - is finer (see formula 2.34). This does not remove but does reduce the severity of the leakage effect.
- Modifying the signal sample obtained in such a way as to reduce the severity of the leakage effect. This process is referred to as *windowing* or *window transformation* and is widely employed in signal processing and modal testing. Windowing involves the imposition of a prescribed profile $w(t)$ on the time signal prior to performing Fourier transform. The analyzed signal is then product of original signal and window profile (see Fig. 2.19). The influence of often used Hanning window to Fourier transform of a signal is shown in Fig. 2.18 (below). Other types of windows often used in modal testing (transient and exponential) are discussed in the chapter 4.2.1.1.1. Other well known type is flat-top window, which is used for transducers' calibration.

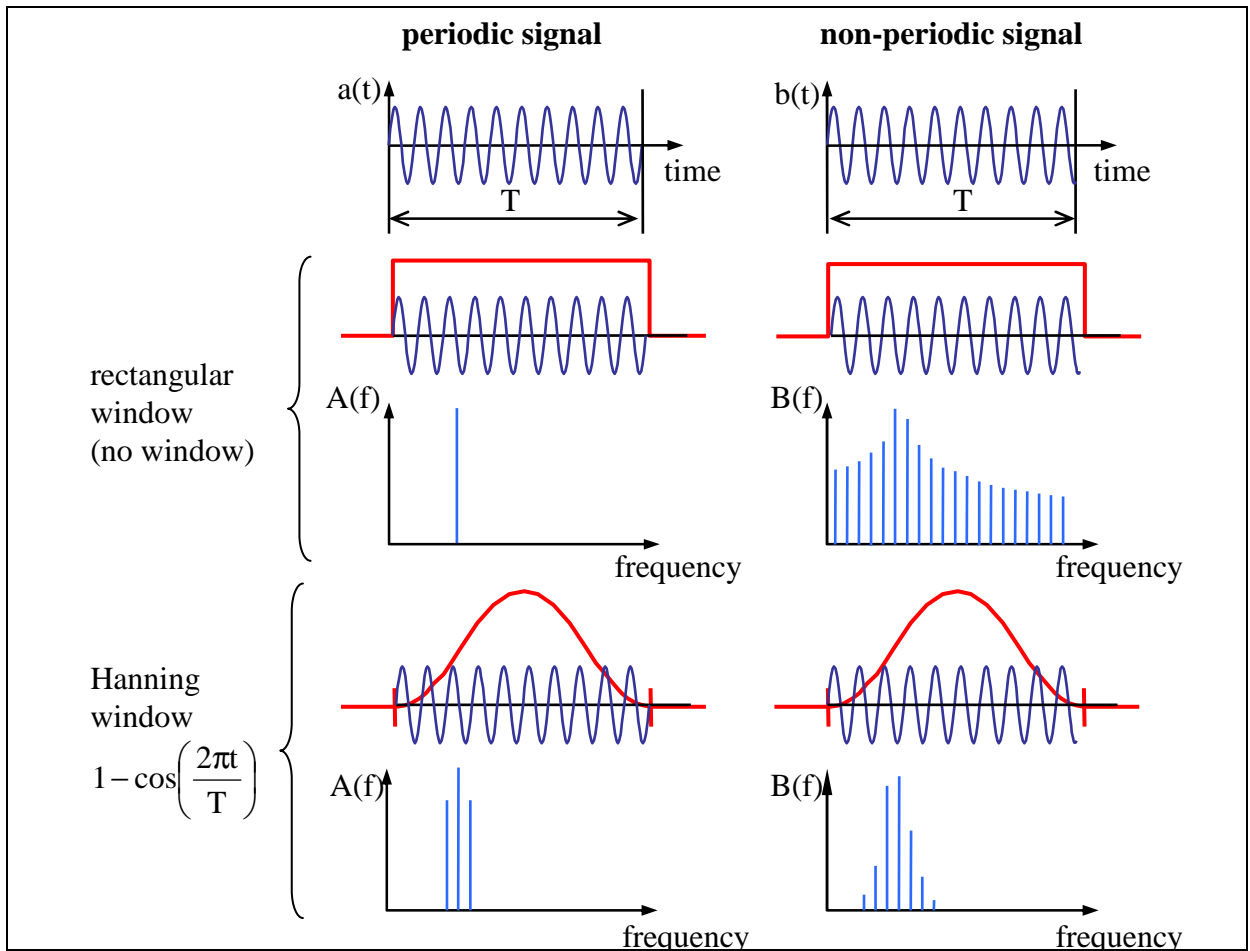


Fig. 2.18 Influence of Weighting Windows and Periodicity of the Signal on Leakage Error

Fig. 2.19 shows what influence has truncation of time signal on frequency spectrum. For digital signal processing, spectral frequency resolution Δf is equal to the inverse time length of the sample T (according to formula 2.34). It means that the better frequency resolution is required (with the same frequency range), the longer the measurement time should be. And vice versa: the longer measurement time is, the more time the transient signal has to decay to zero and, consequently, the less is the leakage error (and better frequency resolution at the same time). Thus, the leakage error can be eliminated by extending the measurement time.

Similarly to spectrum, a leakage error also occurs in frequency response function as *resolution bias error*. Due to this error, magnitude of the measured FRF could be, compared with the true value, lower in resonances and higher in antiresonances (see Fig. 2.20). This error occurs if the frequency resolution of measurement Δf is much coarser than the frequency resolution of the system Δf_s , i.e. than the frequency resolution that would capture the function accurately. It corresponds to time truncation of the signal, i.e. to the fact that the measurement time T is much shorter than the true response of the system T_s :

$$T \ll T_s \Leftrightarrow \Delta f \gg \Delta f_s$$

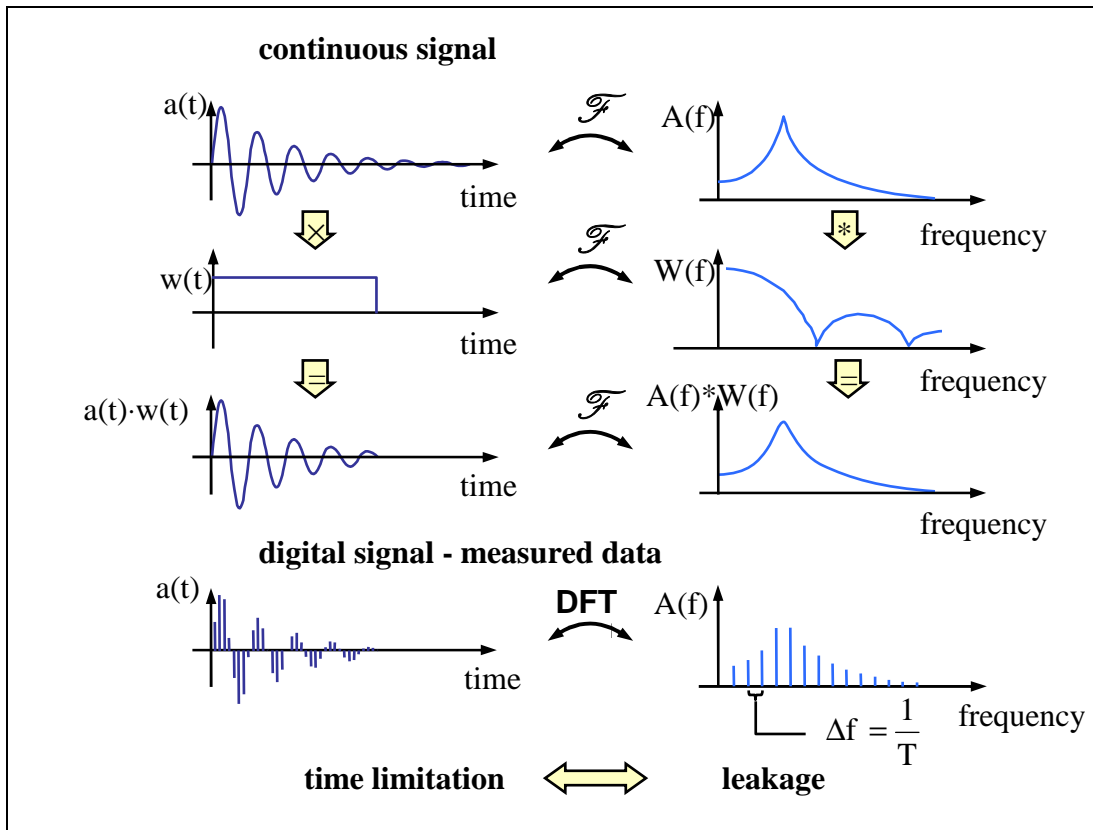


Fig. 2.19 Relation Between Time Limitation of the Signal and Leakage Error in Spectrum

Measurement time can be extended by increasing the number of frequency lines of Fourier transform when using FFT analyzer (see chapter 2.6). This way, the frequency resolution increases without changing the frequency range of the measurement. When using an analyzer with a fixed number of frequency lines, there is another way how to improve frequency resolution - to reduce the frequency range of the measurement. When measurements are done in baseband (from 0 to f_{\max} Hz), it means to limit the frequency range from above. If resonances of interest are of higher frequencies, another approach - frequency zoom - should be applied. The frequency range is then from f_{\min} to f_{\max} (see chapter 2.6.3).

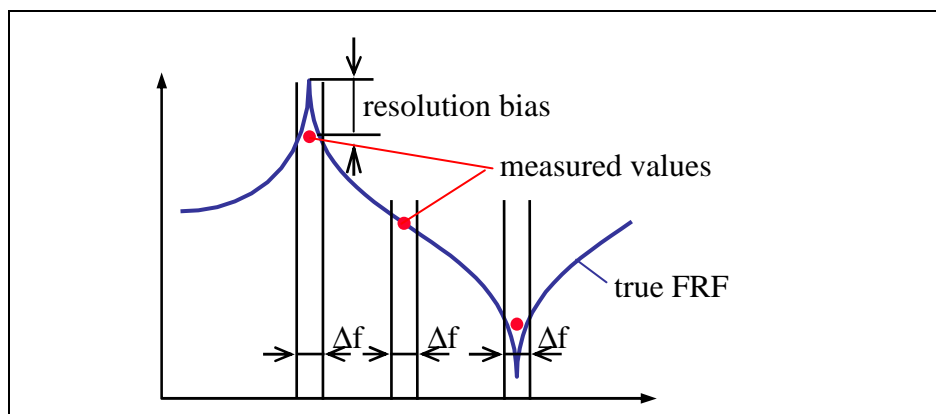


Fig. 2.20 Influence of Leakage in FRF - Resolution Bias Error

The relationship between the true FRF and its alternative estimates H_1 and H_2 when leakage occurs is shown in Fig. 2.21. The magnitude of the true FRF is always higher in resonances

and always lower in antiresonances than both estimates. Nevertheless, closer to the true values is H_2 in resonances and H_1 in antiresonances.

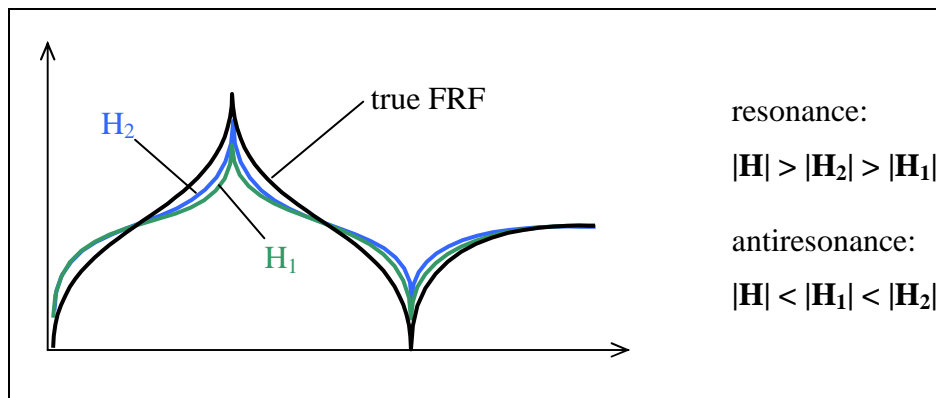


Fig. 2.21 Influence of Leakage in Alternative FRF Estimates

2.6.3 Frequency Zoom

The common solution to the need for a finer frequency resolution is to "zoom in" on the frequency range of interest and to concentrate all the spectral lines to the narrow band between f_{\min} and f_{\max} (instead of between 0 and f_{\max}). There are various ways of achieving this result but perhaps the one which is easiest to understand physically is that which uses a frequency shifting process coupled with a controlled aliasing device.

Suppose the signal to be analysed, $\mathbf{x}(t)$, has a spectrum, $\mathbf{X}(\omega)$, of the type shown in Fig.2.22 and that a detailed (zoom) analysis around the second peak, between f_1 and f_2 , is of interest. If a band-pass filter to the signal is applied (see Fig. 2.22 below), and DFT is performed between 0 and f_2-f_1 , then because of the aliasing phenomenon described in chapter 2.7, the frequency components between f_1 and f_2 will appear aliased in the analysis range 0 to f_2-f_1 with the advantage of a finer resolution.

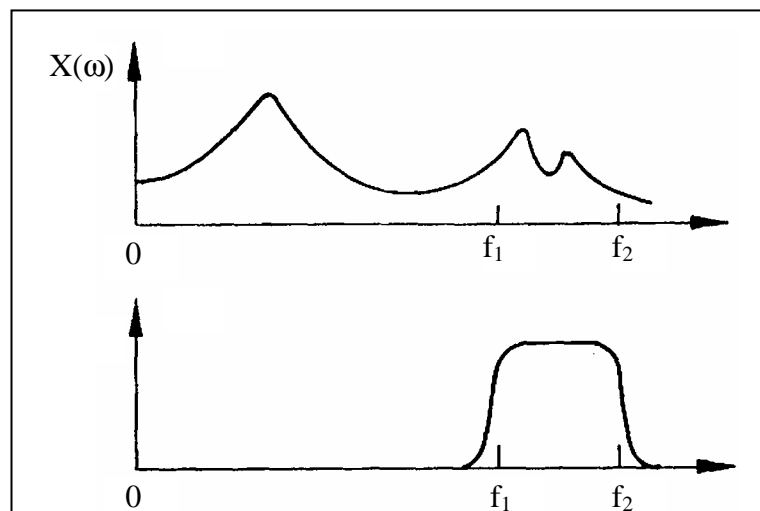


Fig. 2.22 Frequency Zoom Realized by Band-Pass Filter

This is not the only way of achieving a zoom measurement, but it serves to illustrate the concept. Other methods are based on effectively shifting the frequency origin of the spectrum

by multiplying the original time history by a $\cos(\mathbf{f}_1\mathbf{t})$ function and then filtering out the higher of the two components thus produced. For example, suppose the signal to be analysed is:

$$x(t) = A \cdot \sin(2\pi ft)$$

Multiplying this by $\cos(2\pi f_1 t)$ yields:

$$x'(t) = A \cdot \sin(2\pi f t) \cdot \cos(2\pi f_1 t) = \frac{A}{2} (\sin 2\pi(f - f_1)t + \sin 2\pi(f + f_1)t) \quad (2.37)$$

and if the second component is then filtered out, the original signal translated down the frequency range by f_1 is left. The modified signal is then analysed in the range 0 to $f_2 - f_1$, yielding a zoom measurement of the original signal between f_1 and f_2 . In this method, sample times are multiplied by the zoom magnification factor ($2\times$, $4\times$ etc.) but the sampling is carried out at a slower rate (also $2\times$, $4\times$, etc.) dictated by the new effective frequency range.

When using a frequency zoom for measuring FRF in a narrow frequency band, it is important to ensure that as low vibrational energy as possible is out of the frequency band of interest. It means that whenever possible, excitation of the structure should be restricted to the frequency band of analysis. This problem is discussed in more detail in chapter 4.2.1.1.

2.6.4 Averaging

This chapter deals with another feature of a digital spectral analysis that concerns particular requirements for processing random signals. When analyzing random vibration signals, it is not sufficient to compute the Fourier transform (strictly, it does not exist for a random process), and instead estimates for spectral densities and correlation functions which are used to characterize this type of signal must be obtained. Although these properties are computed from the Fourier transform, there are additional considerations concerning their accuracy and statistical reliability which must be given due attention. Generally, it is necessary to perform an averaging process, involving several individual time records (samples) before a result which can be used with confidence is obtained. The two major considerations which determine the number of averages required are the statistical reliability and the removal of spurious random noise from the signals.

There are several possibilities or averaging modes provided by analyzers - common are:

- *peak hold* - it is used mostly in vibration diagnostics with displacement transducers
- *exponential* - latest samples are weighting more than older signals
- *linear* - all samples are weighting equally

In modal testing, linear averaging is used, either with or without *overlap*. When averaging without overlap is used, it means for m samples each of duration T that the overall measurement time would be $m \times T$ (see Fig.2.23 below). Nowadays, analyzers compute DFT in extremely short times, which enables to compute a new transformation prior to capturing a complete new data sample. In this case it is often better to perform a new transformation as soon as possible and use the last N data points, even if some of them could have already been used in the previous transform. This process is called overlapping (see Fig. 2.23 below). It is clear that 100 averages performed with overlapping do not have the same statistical parameters as if completely independent 100 samples are averaged. Nevertheless, the process

with overlapping is more efficient than without overlapping and provides smoother spectra. This is perhaps because of windowing - when using Hanning window, samples are suppressed to zero in their edges and consequently, when using averaging without overlap, parts of the signal are not utilized.

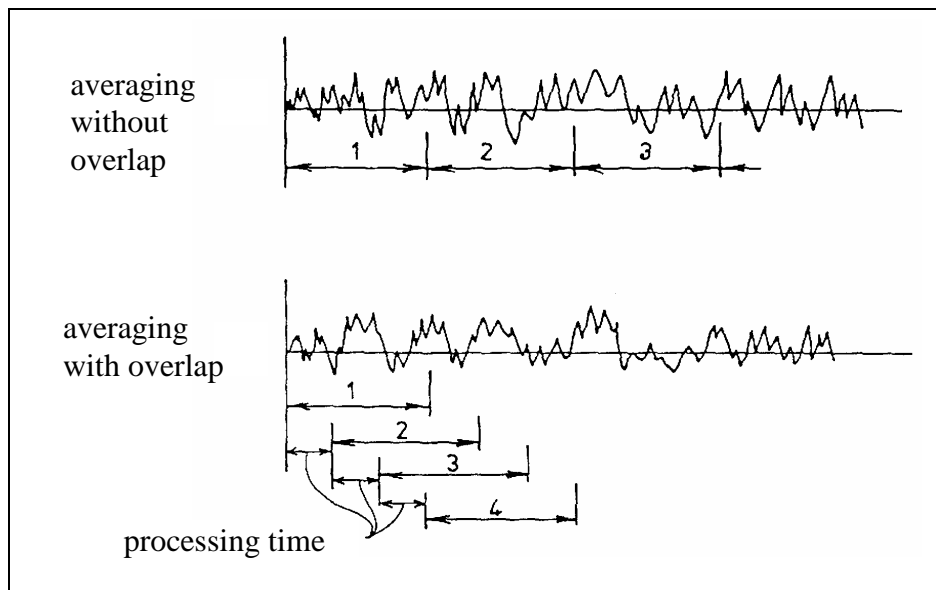


Fig. 2.23 Types of Averaging

3. Theoretical Basis of Modal Analysis

A complex structure can be considered as a number of masses interconnected by springs and damping elements. Since the damping forces in a real structure cannot be estimated with anything like the same accuracy as the elastic and inertia forces, a rigorous mathematic simulation of the damping effects is futile. Nevertheless, to account the dissipative forces in the structure, assumptions of the form of damping have to be made, to get as good estimate of the damping forces in practice as possible. The form has to be conducive to easy mathematical manipulation, specifically adaptable to linear equations of motion - implying that the damping forces are harmonic when excitation is harmonic. Two such suitable forms of damping are:

- viscous damping - damping effect is proportional to velocity $F_b = b \cdot v$
- hysteretic (structural) damping - damping coefficient is inversely proportional to angular velocity $F_b = \frac{k \cdot \gamma}{\omega} \cdot v$

3.1 Single Degree-of-freedom System (SDOF)

Although very few practical structures could realistically be modelled by a single degree-of-freedom system, properties of such a system are very important because those for a more complex multi degree-of-freedom system can always be represented as a linear superposition of a number of SDOF characteristics.

Basic spatial model of SDOF system (see Fig. 3.1) consists of mass **m** and a spring **k** and, in the case of damped system, of either viscous dashpot **b** or hysteretic damper **h**. In this model, **f(t)** is general time varying force and **x(t)** is response quantity.

In this chapter, three types of SDOF model will be described:

- undamped
- viscously damped
- hysteretically (or structurally) damped

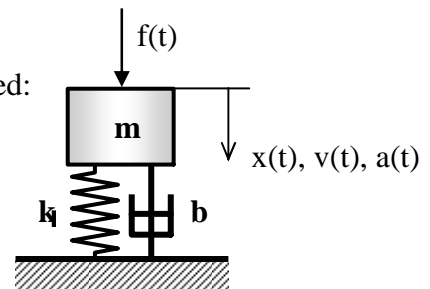


Fig. 3.1 Spatial model of SDOF system

3.1.1 Undamped Single Degree-of-freedom System

Spatial model of this system consists of mass **m** and spring **k**. For modal model, properties of the system without external force, i.e. $f(t)=0$ will be considered. In this case, equation of motion is:

$$ma + kx = 0 \tag{3.1}$$

when substitute for $a = \ddot{x}$

$$m\ddot{x} + kx = 0 \tag{3.2}$$

Expected solution of this equation is:

$$x(t) = X e^{i\omega t} \quad (3.3)$$

Putting into equation of motion leads to the requirement that

$$k - \omega^2 m = 0 \quad (3.4)$$

Modal model consists of a single solution (mode of vibration) with a natural frequency given by

$$\Omega_0 = \sqrt{\frac{k}{m}} \quad (3.5)$$

For frequency response analysis, excitation is considered of the form

$$f(t) = F e^{i\omega t} \quad (3.6)$$

and solution is assumed of the form

$$x(t) = X e^{i\omega t} \quad (3.7)$$

where \mathbf{X} and \mathbf{F} are complex to accommodate both the amplitude and phase information. Now the equation of motion is

$$(k - \omega^2 m) X e^{i\omega t} = F e^{i\omega t} \quad (3.8)$$

from which the required response model in the form of a frequency response function is extracted:

$$\frac{X}{F} = \frac{1}{k - \omega^2 m} = \alpha(\omega) \quad (3.9)$$

This particular form of frequency response function, $\alpha(\omega)$, with response parameter displacement, is called receptance. This function, along with other versions of FRF, is independent of the excitation.

3.1.2 Viscously damped SDOF system

3.1.2.1 Free vibration

Adding a viscous dashpot \mathbf{b} , the equation of motion for free vibration becomes

$$m \cdot a + b \cdot v + k \cdot x = 0 \quad (3.10)$$

$$m \cdot \ddot{x} + b \cdot \dot{x} + k \cdot x = 0 \quad (3.11)$$

Expected solution is of a more general form (s is complex, rather than imaginary, as with undamped system)

$$x(t) = X e^{st} \quad \text{Derivatives:} \quad \begin{aligned} \dot{x}(t) &= X s e^{st} \\ \ddot{x}(t) &= X s^2 e^{st} \end{aligned}$$

Having put these into equation of motion, characteristic equation is obtained:

$$m s^2 + b s + k = 0 \quad (3.12)$$

Solution of characteristic equation:

$$s_{1,2} = \frac{-b \pm \sqrt{b^2 - 4km}}{2m} \quad (3.13)$$

$$s_{1,2} = -\frac{b}{2m} \pm \sqrt{\left(\frac{b}{2m}\right)^2 - \frac{k}{m}} \quad (3.14)$$

$$s_{1,2} = -\delta \pm i\sqrt{\Omega_0^2 - \delta^2} = -\delta \pm i\Omega_0\sqrt{1 - \zeta^2} \quad (3.15)$$

$$s_{1,2} = -\delta \pm i\Omega \quad (3.16)$$

Where: $\Omega_0 = \sqrt{\frac{k}{m}}$... undamped natural frequency

$$\delta = \frac{b}{2m} \quad \dots \text{decay constant} \quad (3.17)$$

$$\zeta = \frac{\delta}{\Omega_0} = \frac{b}{2\sqrt{km}} = \frac{b}{b_{kr}} \quad \dots \text{damping ratio} \quad (3.18)$$

$$\Omega = \sqrt{\Omega_0^2 - \delta^2} = \Omega_0\sqrt{1 - \zeta^2} \quad \dots \text{damped natural frequency} \quad (3.19)$$

Roots of characteristic equation (poles) depend on the value of damping ratio ζ . For so called positive damping ($\zeta \geq 0$), there may be 3 cases, and therefore 3 different types of motion (see Fig.3.2):

- $\zeta = 0$ undamped vibration
 s_1 and s_2 are imaginary
- $\zeta < 1$ damped vibration
 s_1 and s_2 are complex conjugates (see Fig. 3.4)
- $\zeta \geq 1$ aperiodic movement
 s_1 and s_2 are real (for $\zeta=1$: $s_1 = s_2 = -\delta$)

If the real part of the pole is positive, which means that $\zeta < 0$ (negative damping), self-excited vibrations occur (see Fig. 3.3., right side).

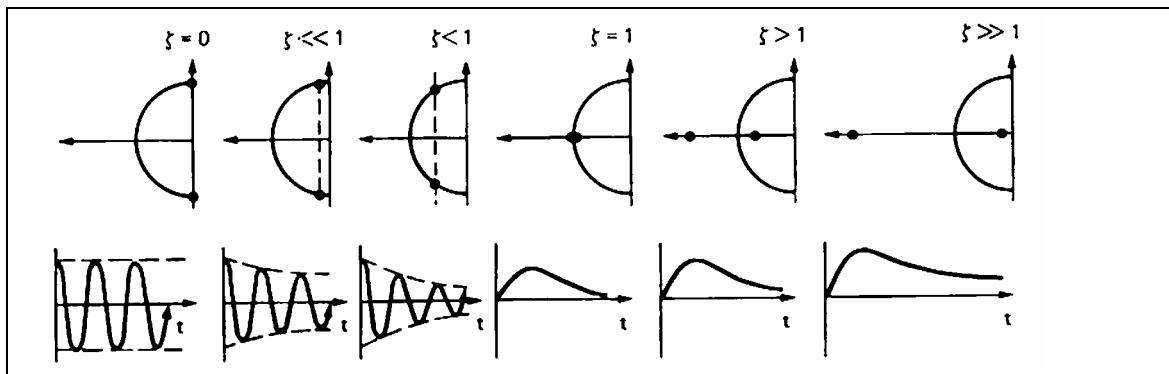


Fig. 3.2 Position of Poles According to Damping Ratio Values

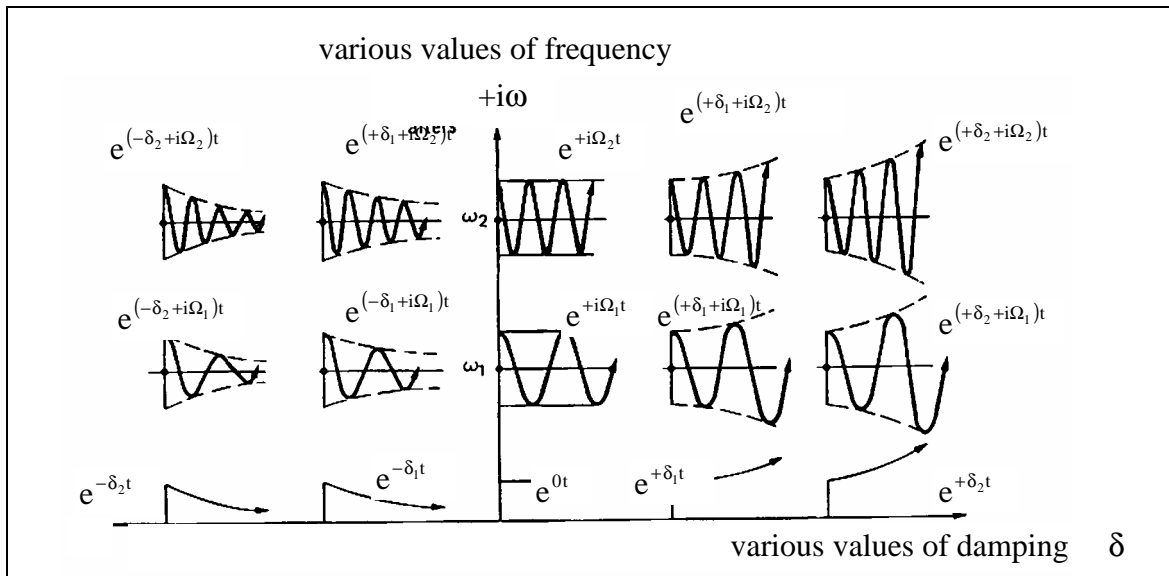


Fig. 3.3 Frequency Response as a Function of Natural Frequency and Damping Values

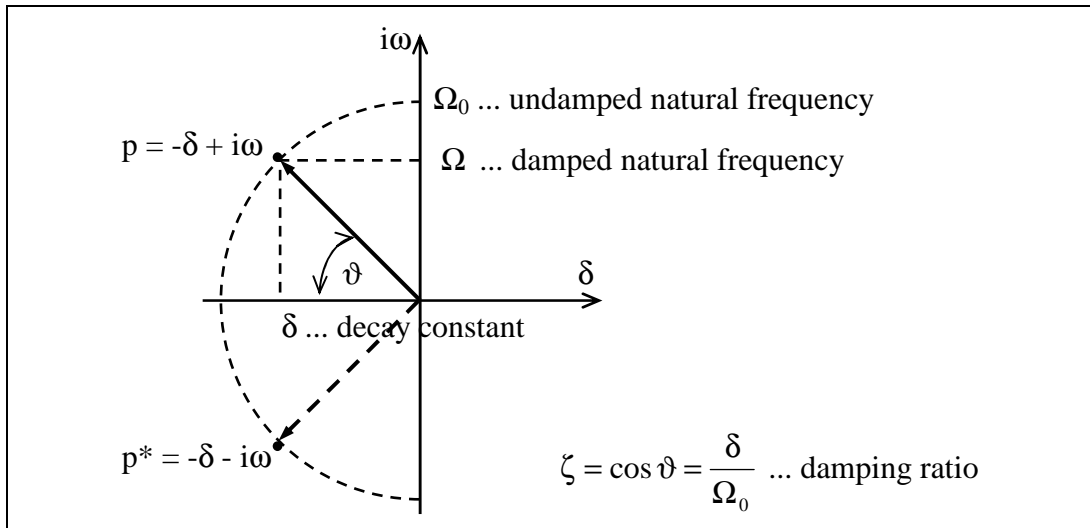


Fig. 3.4 Complex Conjugates - Poles - in Laplace Plane

3.1.2.2 Forced vibration

If movement is caused by acting of harmonic force, the equation of motion of viscously damped system has the form:

$$m\ddot{x}(t) + b\dot{x}(t) + kx(t) = f(t) \quad (3.20)$$

where $f(t) = Fe^{i\omega t}$... harmonic excitation force

$x(t) = Xe^{i\omega t}$... expected solution and its derivatives:

$$\dot{x}(t) = i\omega Xe^{i\omega t}$$

$$\ddot{x}(t) = -\omega^2 Xe^{i\omega t}$$

Dividing the equation (3.20) by mass \mathbf{m} and putting the expected solution together with equations (3.5) a (3.17) in it gives:

$$-\omega^2 \mathbf{X} + 2i\omega \cdot \zeta \Omega_0 \mathbf{X} + \Omega_0^2 \cdot \mathbf{X} = \Omega_0^2 \cdot \frac{\mathbf{F}}{\mathbf{k}} \quad (3.21)$$

Then, complex displacement amplitude is:

$$\mathbf{X} = \frac{\Omega_0^2 \cdot \frac{\mathbf{F}}{\mathbf{k}}}{\Omega_0^2 - \omega^2 + i2\zeta\omega\Omega_0} \quad \frac{\mathbf{F}}{\mathbf{k}} = \mathbf{X}_{st} \quad \dots \text{static displacement}$$

$$\mathbf{X} = \frac{\frac{\mathbf{F}}{\mathbf{k}}}{1 - \left(\frac{\omega}{\Omega_0}\right)^2 + i2\zeta \cdot \frac{\omega}{\Omega_0}} \quad \frac{\omega}{\Omega_0} = \eta \quad \dots \text{tuning factor}$$

$$\mathbf{X} = \frac{1}{1 - \eta^2 + i2\zeta\eta} \cdot \mathbf{X}_{st} \quad (3.22)$$

$$|\mathbf{X}| = \mathbf{X}_{st} \cdot \frac{1}{\sqrt{(1 - \eta^2)^2 + (2\zeta\eta)^2}} \quad \dots \text{amplitude of displacement} \quad (3.23)$$

Now, steady state solution of equation of motion will be derived:

$$\mathbf{X} = \frac{1}{1 - \eta^2 + i2\zeta\eta} \cdot \frac{\mathbf{F}}{\mathbf{k}} \quad \dots \text{amplitude of displacement (complex)}$$

$$\mathbf{x}(t) = \mathbf{X}e^{i\omega t} = \frac{1}{1 - \eta^2 + i2\zeta\eta} \cdot \frac{\mathbf{F}}{\mathbf{k}} e^{i\omega t} \quad \dots \text{displacement time history}$$

Displacement is proportional to the acting force, proportionality constant is:

$$\mathbf{H}(\eta) = \frac{1}{1 - \eta^2 + i2\zeta\eta} \quad (3.24)$$

what is so-called frequency response function receptance (dimensionless).

As the displacement is a complex number, it can be divided to the real part and imaginary part (by multiplying both numerator and denominator by denominator's complex conjugate):

$$\mathbf{x}(t) = \left(\frac{1 - \eta^2}{(1 - \eta^2)^2 + (2\zeta\eta)^2} - \frac{2\zeta\eta}{(1 - \eta^2)^2 + (2\zeta\eta)^2} i \right) \frac{\mathbf{F}}{\mathbf{k}} e^{i\omega t} \quad (3.25)$$

It can be seen, that the displacement has one part

$$\text{Re}(\mathbf{x}) = \frac{1 - \eta^2}{(1 - \eta^2)^2 + (2\zeta\eta)^2} \cdot \frac{\mathbf{F}}{\mathbf{k}} e^{i\omega t} \quad (3.26)$$

that is in-phase with the excitation force and the second part

$$\text{Im}(\mathbf{x}) = \frac{-2\zeta\eta}{(1 - \eta^2)^2 + (2\zeta\eta)^2} \cdot \frac{\mathbf{F}}{\mathbf{k}} e^{i\omega t} \quad (3.27)$$

that lags the excitation force at 90°. In Fig. 3.5, vectors OA and OB represent real and imaginary part of displacement. Vector OC represents the amplitude of displacement given by $\sqrt{\text{Re}^2(x) + \text{Im}^2(x)}$, thus:

$$|x(t)| = \frac{1}{\sqrt{(1-\eta^2)^2 + (2\zeta\eta)^2}} \cdot \frac{F}{k} e^{i\omega t} \quad (3.28)$$

Displacement lags the excitation force at an angle θ , defined as:

$$\theta = \arctg \frac{-2\zeta\eta}{1-\eta^2} \quad (3.29)$$

Steady-state solution of the equation of motion can thus be expressed in the form:

$$x(t) = \left[\frac{1}{\sqrt{(1-\eta^2)^2 + (2\zeta\eta)^2}} \right] \cdot \frac{F}{k} e^{i(\omega t - \theta)} \quad (3.30)$$

The expression in square brackets is the absolute value of complex frequency response. It is often called as an *amplification factor* and it expresses a dimensionless ratio between the amplitude of displacement \mathbf{X} and static displacement \mathbf{F}/k .

$$|H(\eta)| = \frac{1}{\sqrt{(1-\eta^2)^2 + (2\zeta\eta)^2}} \quad (3.31)$$

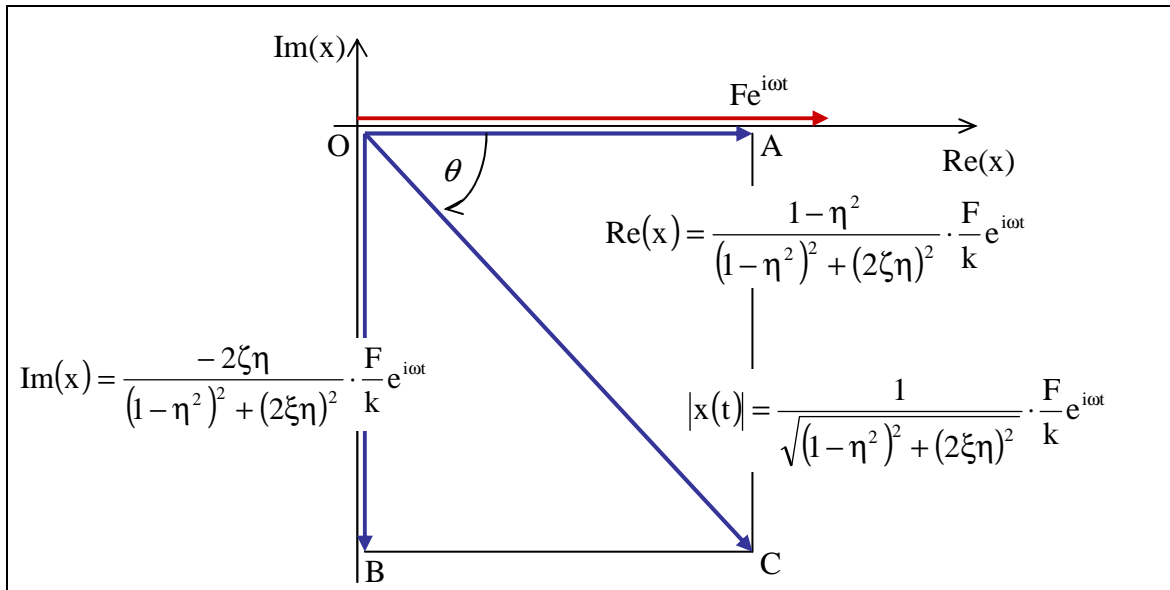


Fig. 3.5 Relationship Between the Complex Displacement and the Excitation Force

Frequency response function (3.24) is complex and it is a function of frequency (or of tuning factor, respectively) at the same time. It means that it can not be displayed in a single two-dimensional plot. Its 3D plot is in Fig. 3.6. The red curve represents a damped system, the green curve represents an undamped system (in that case, the plot lies in the plane η - $\text{Re}(H(\eta))$ and is two-dimensional).

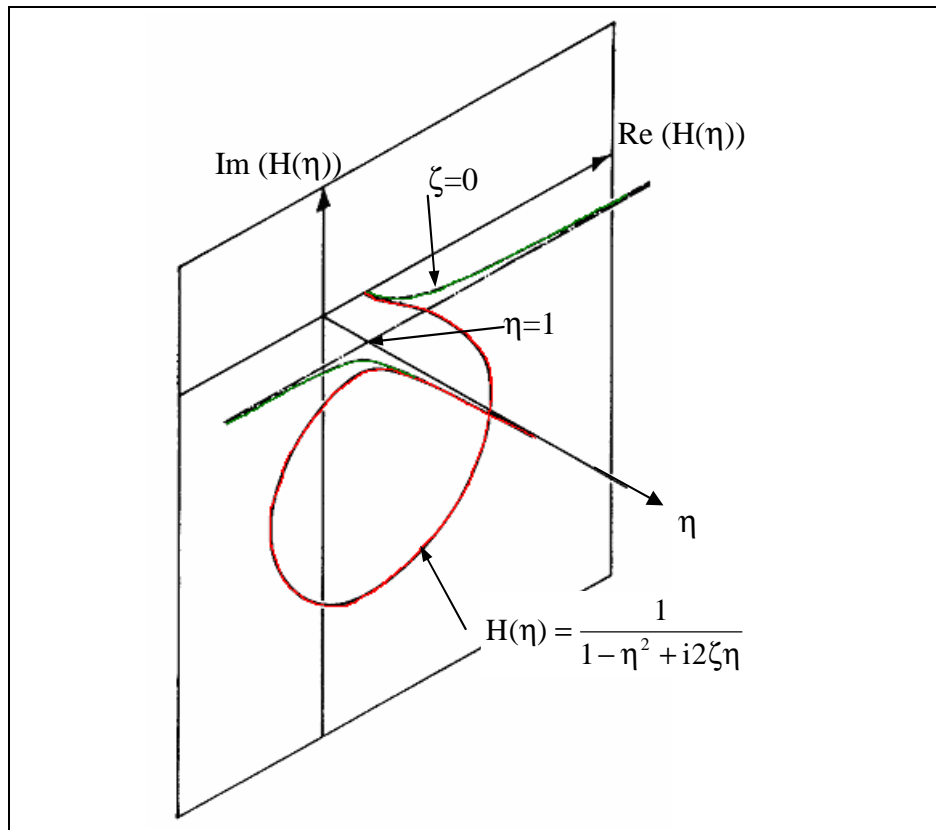


Fig. 3.6 3D plot of the Frequency Response Function - Undamped and Damped

Projection of this 3D plot to the individual planes is in Fig. 3.7. and in Fig. 3.8 (left). In Fig. 3.8, two of the possible ways of displaying FRF are shown - simultaneous displaying of real and imaginary part of FRF as functions of frequency or of tuning factor (top left), or so called Nyquist diagram which is plot in the plane $[\mathbf{Re}(\mathbf{H}(\eta)); \mathbf{Im}(\mathbf{H}(\eta))]$ - bottom left. In Nyquist plot, information about the frequency is hidden - the plot is drawn from the initial frequency to the final frequency clockwise; the major part of the circle represents resonance and its vicinity (more detailed in chapter 4.3.1.2). Different colours of plots are for various levels of damping - from green for an undamped system to magenta for a critically damped system ($\zeta=1$).

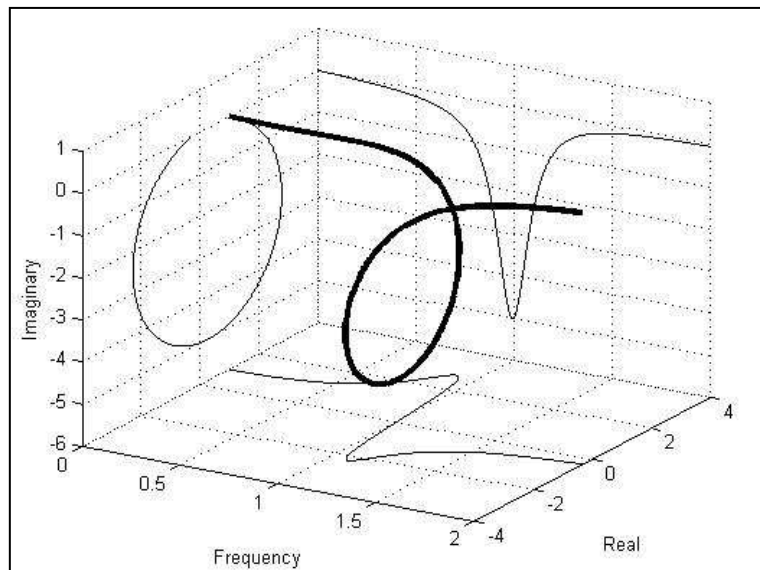


Fig. 3.7 3D Plot of the Frequency Response Function (Receptance)

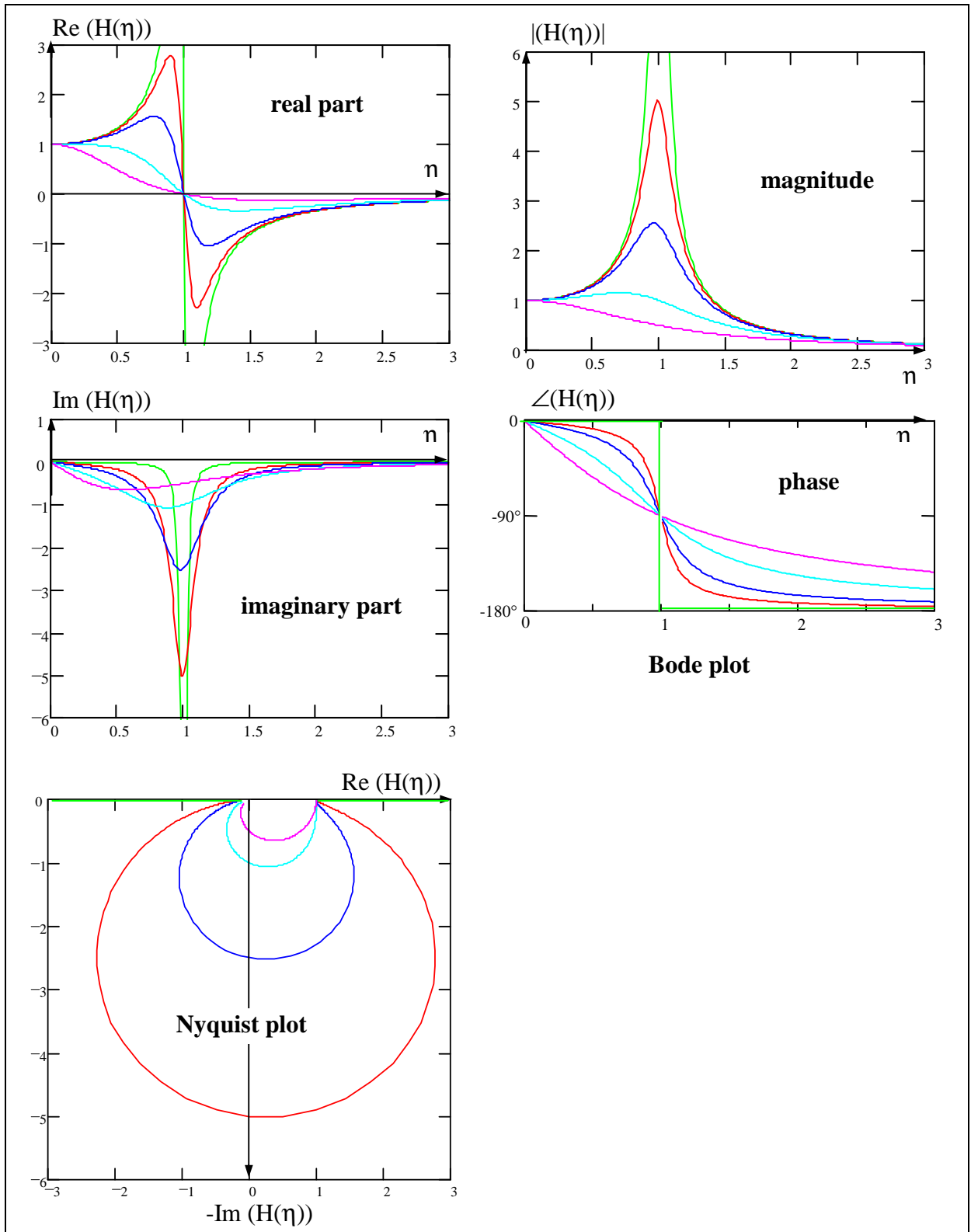


Fig. 3.8 Various Forms of Displaying FRF - Visously Damped System

FRF is frequently displayed as Bode plot, which is simultaneously display of amplitude and phase of FRF, both as a function of frequency (or tuning factor) - see Fig. 3.8 (right).

3.1.2.3 Determination of Resonance Tuning

Resonance can be defined as a state when magnitude of FRF is maximal. The plot of FRF magnitude as a function of tuning factor shows, that resonant peak for undamped system occurs when $\eta=1$ and is shifted to the left when damping increases. To determine the resonant tuning factor, equation (3.31) should be derived with respect to the tuning factor and then put the derivative equal to zero.

$$|H(\eta)| = \frac{1}{\sqrt{(1-\eta^2)^2 + (2\zeta\eta)^2}}$$

$$\frac{dH(\eta)}{d\eta} = 0 \quad \dots\dots\dots\Rightarrow \quad \eta_{\text{res}} = \sqrt{1-2\zeta^2} \quad (3.32)$$

Then, resonant excitation frequency is:

$$\omega_{\text{res}} = \Omega_0 \cdot \sqrt{1-2\zeta^2} \quad (3.33)$$

Magnitude of FRF and displacement in resonance are:

$$H(\omega_{\text{res}}) = \frac{1}{2\zeta\sqrt{1-\zeta^2}} \quad (3.34)$$

$$X_{\text{res}} = X_{\text{st}} \cdot \frac{1}{2\zeta\sqrt{1-\zeta^2}} \quad (3.35)$$

For light damping ($\zeta < 0.05$) the curves are nearly symmetrical along the vertical axis passing through $\eta=1$. Peak value of $|H(\omega)|$ at the immediate vicinity of $\eta=1$ is given by

$$H(\omega_{\text{res}}) \doteq \frac{1}{2\zeta} = Q \quad Q \dots \text{quality factor} \quad (3.36)$$

3.1.2.4 Determination of Damping from FRF Plots

a) *Determination of damping from plot of real part $H(\eta)$ as a function of η*

The following procedure will derive for which tuning factors η_1 and η_2 (and corresponding excitation frequencies ω_1 and ω_2) occur local extremes in the graph of real part of FRF as a function of frequency. These frequency values can be easily read from the graph and using them, damping ratio ζ can be expressed (see Fig. 3.9).

$$H(\eta) = \frac{1}{1-\eta^2 + i2\zeta\eta}$$

$$H(\eta) = \frac{1-\eta^2}{(1-\eta^2)^2 + (2\zeta\eta)^2} + \frac{2\zeta\eta}{(1-\eta^2)^2 + (2\zeta\eta)^2} i$$

$$\text{Re}H(\eta) = \frac{1-\eta^2}{(1-\eta^2)^2 + (2\zeta\eta)^2}$$

$$\frac{d \operatorname{Re} H(\eta)}{d \eta} = \dots = 0 \quad \Rightarrow$$

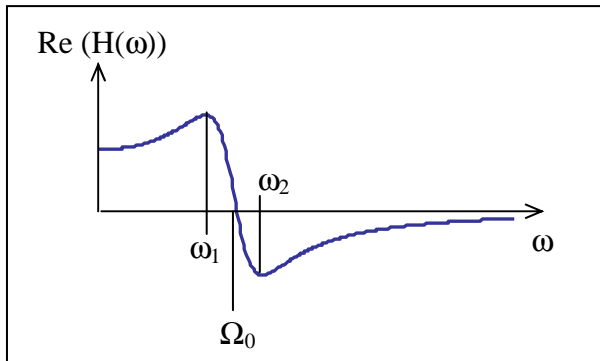


Fig. 3.9 Determination of Damping from $\operatorname{Re}(H(\omega))$

$$\eta_1 = \sqrt{1-2\zeta}$$

$$\eta_2 = \sqrt{1+2\zeta}$$

$$\omega_1 = \Omega_0 \cdot \sqrt{1-2\zeta} \quad (3.37)$$

$$\omega_2 = \Omega_0 \cdot \sqrt{1+2\zeta} \quad (3.38)$$

$$\frac{\omega_2}{\omega_1} = \frac{\sqrt{1+2\zeta}}{\sqrt{1-2\zeta}}$$

$$\left(\frac{\omega_2}{\omega_1}\right)^2 = \frac{1+2\zeta}{1-2\zeta}$$

$$\left(\frac{\omega_2}{\omega_1}\right)^2 \cdot (1-2\zeta) = 1+2\zeta$$

$$\left(\frac{\omega_2}{\omega_1}\right)^2 - \left(\frac{\omega_2}{\omega_1}\right)^2 \cdot 2\zeta - 1 - 2\zeta = 0$$

$$2\zeta = \frac{\left(\frac{\omega_2}{\omega_1}\right)^2 - 1}{\left(\frac{\omega_2}{\omega_1}\right)^2 + 1} \quad (3.39)$$

b) Determination of damping from half-power points

Half-power points are points on the plot of magnitude of $H(\omega)$, in which the magnitude decreases to the value $\frac{1}{\sqrt{2}} \cdot H_{\text{res}}$, which means to the $\frac{1}{\sqrt{2}}$ of the peak value. In the power spectrum, it would be one half of the peak value - hence the name half-power points.

If $H(\omega)$ is plotted in logarithmic scale, in these points the peak magnitude decreases by 3 dB (see Fig. 3.10).

$$\frac{H_{\text{res}}}{H_{\text{halfpower}}} = \sqrt{2}$$

$$20 \cdot \log H_{\text{res}} - 20 \cdot \log H_{\text{halfpower}} = 20 \cdot \log \sqrt{2} = 3$$

$$H_{\text{res}} - H_{\text{halfpower}} = 3\text{dB}$$

If these points are denoted P_1 and P_2 and the corresponding frequencies ω_1 and ω_2 , then the difference between those frequencies $\omega_2 - \omega_1$ is called 3dB band of the system. For light damping:

$$\Delta\omega_{3\text{dB}} = \omega_2 - \omega_1 = 2 \cdot \zeta \cdot \Omega_0$$

where $\Delta\omega_{3dB}$ is 3dB band. Thus:

$$\frac{\omega_2 - \omega_1}{\Omega_0} = 2\zeta \quad (3.40)$$

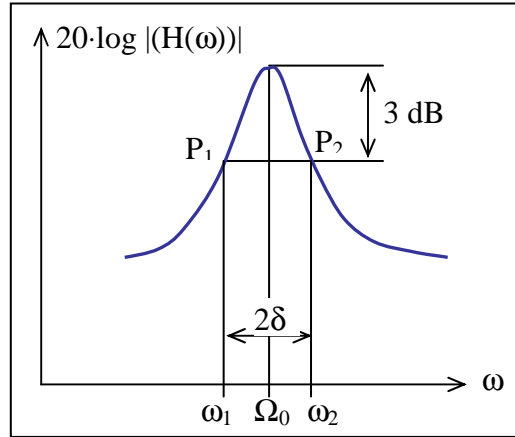


Fig. 3.10 Determination of damping from 3dB band

Now, it will be proved that frequencies ω_1 and ω_2 are the same frequencies (for slight damping) as those that were obtained in the previous paragraph from the extremes of real part FRF. Supposing it is true, put the equations (3.37) and (3.38) into equation (3.40):

$$\frac{\omega_2 - \omega_1}{\Omega_0} = 2\zeta$$

$$\Omega_0 \cdot \sqrt{1+2\zeta} - \Omega_0 \cdot \sqrt{1-2\zeta} = \Omega_0 \cdot 2\zeta$$

$$1+2\zeta - 2 \cdot \sqrt{(1+2\zeta) \cdot (1-2\zeta)} + 1-2\zeta = 4\zeta^2$$

$$2 - 2\sqrt{1-4\zeta^2} = 4\zeta^2$$

$$\sqrt{1-4\zeta^2} = 1-2\zeta^2$$

For light damping ($\zeta < 0,05$) applies :

$$1 \doteq 1$$

To determine damping for lightly damped systems, the simplified equation (3.40) can be used even when reading from real part FRF plot. If this equation is to be valid, the following should apply:

$$\omega_2 - \omega_1 = 2\delta \quad (3.41)$$

As the plot of FRF magnitude is symmetrical in the vicinity of resonance, also applies:

$$\omega_1 = \Omega_0 - \delta \quad (3.42)$$

$$\omega_2 = \Omega_0 + \delta \quad (3.43)$$

3.1.3 Single Degree-of-freedom System with Hysteretic (Structural) Damping

3.1.3.1 Forced Vibration

Close inspection of the behaviour of real structures suggests that the viscous damping model used above is not very representative when applied to MDOF systems. Real structures exhibit a frequency dependence that is not described by the standard viscous dashpot. A large variety of materials, when subjected to cyclic stress (for strains below the elastic limit), exhibits a stress-strain relationship which is characterised by a hysteresis loop. The energy dissipated per cycle due to internal friction in the material is proportional to the area within the hysteresis loop, and hence the name hysteretic damping. Internal friction is independent of the rate of strain (independent of frequency) and over a significant frequency range is proportional to the displacement. Thus the damping force is proportional to the elastic force, since energy is dissipated, it must be in phase with the velocity. Thus for simple harmonic motion, the damping force is given by

$$i\gamma kx = \frac{k\gamma}{\omega} \cdot \dot{x} \quad (3.44)$$

where γ is called *structural damping loss factor*.

Note: In literature, structural damping loss factor is often denoted as η , but here γ will be used in order not to confuse it with tuning coefficient.

Hysteretic model provides a much simpler analysis for MDOF systems but it presents difficulties to a rigorous free vibration analysis. Therefore only forced vibration analysis will be performed.

Equation of motion for a SDOF system with structural damping can be written:

$$m\ddot{x}(t) + \frac{k\gamma}{\omega} \cdot \dot{x}(t) + kx(t) = f(t) \quad (3.45)$$

where $f(t) = Fe^{i\omega t}$... harmonic excitation force

$x(t) = Xe^{i\omega t}$... expected solution and its derivatives:

$\dot{x}(t) = i\omega Xe^{i\omega t}$

$\ddot{x}(t) = -\omega^2 Xe^{i\omega t}$

Equation of motion can be also rewrite as:

$$m\ddot{x}(t) + k(1 + i\gamma)x(t) = f(t)$$

where $k(1 + i\gamma)$ is called the complex stiffness. (3.46)

By setting the expected solution into the equation of motion is obtained:

$$(-m\omega^2 + k(1 + i\gamma)) \cdot X = F$$

After dividing by stiffness k and using equaiton (3.5):

$$\left(1 - \frac{\omega^2}{\Omega_0^2} + i\gamma\right) \cdot \mathbf{X} = \frac{\mathbf{F}}{\mathbf{k}}$$

Then, amplitude of complex displacement is:

$$\mathbf{X} = \frac{1}{1 - \eta^2 + i\gamma} \cdot \frac{\mathbf{F}}{\mathbf{k}} \quad (3.47)$$

$$\mathbf{X} = \frac{1}{1 - \eta^2 + i\gamma} \cdot \mathbf{X}_{st}$$

$$|\mathbf{X}| = \mathbf{X}_{st} \cdot \frac{1}{\sqrt{(1 - \eta^2)^2 + \gamma^2}} \quad \dots \text{amplitude of displacement} \quad (3.48)$$

Following procedure is analogous to the procedure from chapter 3.1.2.2 for a system with viscous damping.

$$\mathbf{x}(t) = \mathbf{X}e^{i\omega t} = \frac{1}{1 - \eta^2 + i\gamma} \cdot \frac{\mathbf{F}}{\mathbf{k}} e^{i\omega t} \quad \dots \text{time history of displacement} \quad (3.49)$$

$$\mathbf{x}(t) = \left[\frac{1 - \eta^2}{(1 - \eta^2)^2 + \gamma^2} - \frac{\gamma}{(1 - \eta^2)^2 + \gamma^2} i \right] \frac{\mathbf{F}}{\mathbf{k}} \cdot e^{i\omega t}$$

$$|\mathbf{x}(t)| = \frac{1}{\sqrt{(1 - \eta^2)^2 + \gamma^2}} \cdot \frac{\mathbf{F}}{\mathbf{k}} e^{i\omega t} \quad (3.50)$$

$$\theta = \arctg \frac{-\gamma}{1 - \eta^2} \quad \dots \text{phase lag between displacement and excitation force} \quad (3.51)$$

$$\mathbf{x}(t) = \left[\frac{1}{\sqrt{(1 - \eta^2)^2 + \gamma^2}} \right] \cdot \frac{\mathbf{F}}{\mathbf{k}} e^{i(\omega t - \theta)} \quad (3.52)$$

The expression in the square brackets is again the absolute value of frequency response, or magnification factor, and again it has the meaning of a dimensionless ratio between displacement amplitude \mathbf{X} and static displacement \mathbf{F}/\mathbf{k} .

$$|\mathbf{H}(\eta)| = \frac{1}{\sqrt{(1 - \eta^2)^2 + \gamma^2}} \quad (3.53)$$

In Fig. 3.11, various types of plots of FRF with the same amount of damping as it was in Fig. 3.8. When a system is structurally damped, resonant peak in the plot of FRF amplitude does not shift to the left with increasing amount of damping, but it still remains on tuning value $\eta=1$. But, as damping increases, the plot does not start with amplitude equal to 1 corresponding to static displacement, but with a value less than 1. Similar differences are evident in all types of plots.

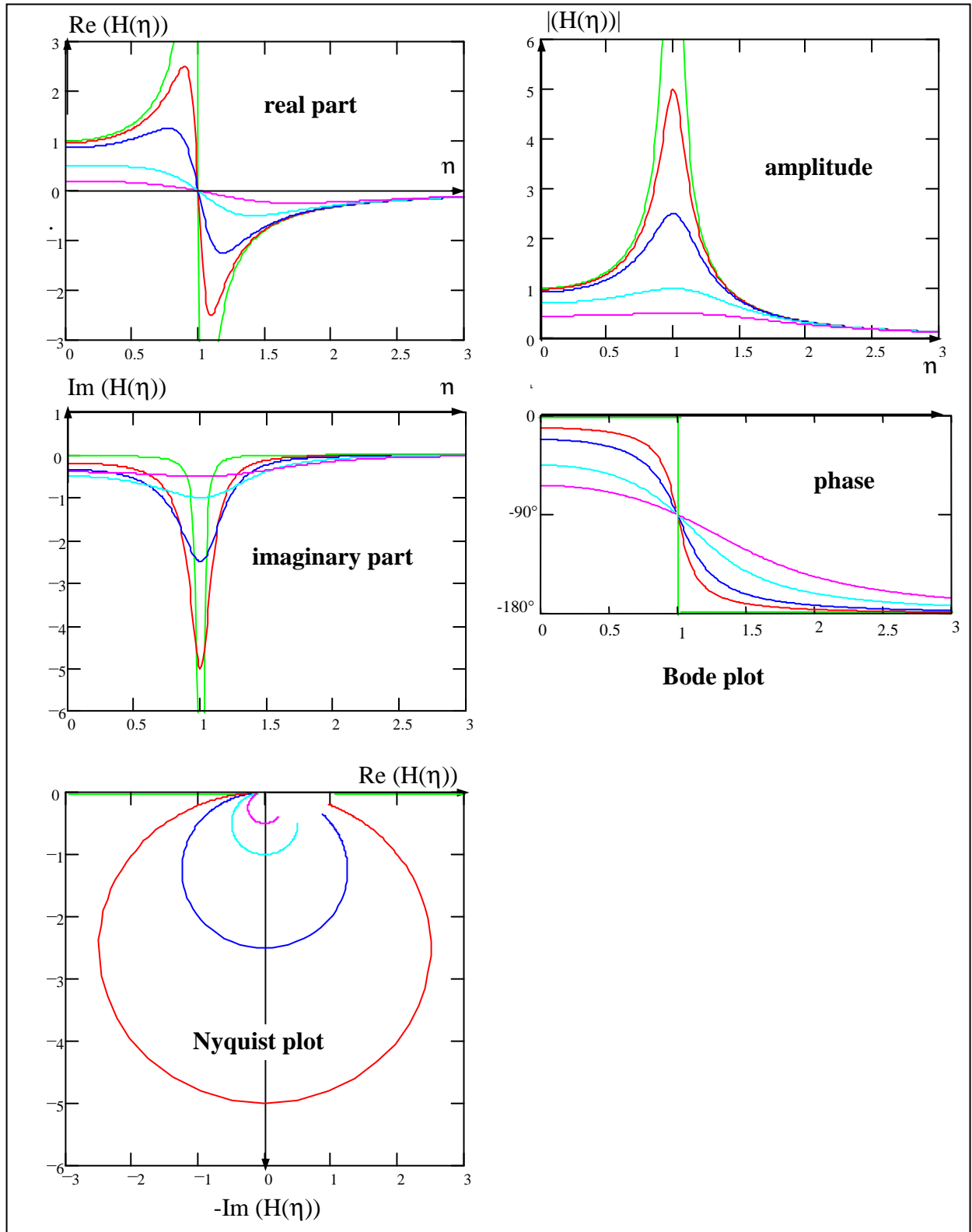
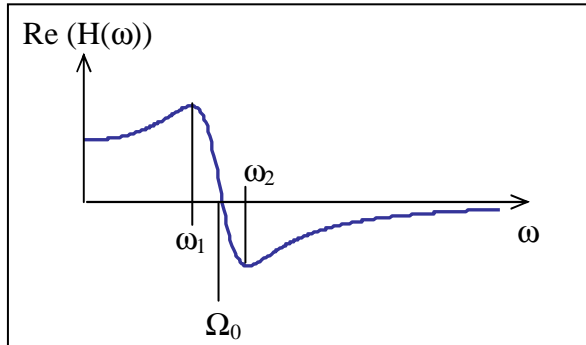


Fig. 3.11 Various Forms of Displaying FRF - Structurally (Hysteretically) Damped System

3.1.3.2 Determination of Damping from FRF Plots

Using the same procedure as in chapter 3.1.2.4, damping from the plot of real part of $H(\eta)$ as a function of tuning coefficient η will be determined.

$$H(\eta) = \frac{1}{1 - \eta^2 + i\gamma}$$



$$H(\eta) = \frac{1 - \eta^2}{(1 - \eta^2)^2 + \gamma^2} - \frac{\gamma}{(1 - \eta^2)^2 + \gamma^2} i$$

$$\text{Re}H(\eta) = \frac{1 - \eta^2}{(1 - \eta^2)^2 + \gamma^2}$$

Fig. 3.12 Determination of Damping from $\text{Re}(H(\omega))$

Determining ω_1 and ω_2 :

$$\frac{d \text{Re}H(\eta)}{d\eta} = \dots\dots\dots = 0$$

$$\Rightarrow \eta_1 = \sqrt{1 - \gamma}$$

$$\eta_2 = \sqrt{1 + \gamma}$$

$$\omega_1 = \Omega_0 \cdot \sqrt{1 - \gamma} \tag{3.54}$$

$$\omega_2 = \Omega_0 \cdot \sqrt{1 + \gamma} \tag{3.55}$$

Using the same procedure as for viscously damped system leads to:

$$\gamma = \frac{\left(\frac{\omega_2}{\omega_1}\right)^2 - 1}{\left(\frac{\omega_2}{\omega_1}\right)^2 + 1} \tag{3.56}$$

For light damping approximately applies:

$$2\zeta = \gamma \tag{3.57}$$

3.1.4 Various Forms of FRF for Single Degree-of-freedom System

For all three types of systems - undamped, viscously and hysteretically damped - frequency response function in the form of receptance, i.e. with displacement as response parameter, has been derived. During modal tests, the response is mostly measured using accelerometers, so FRF in the form of inertance, with acceleration as response parameter, is more common. In chapter 1.3, relations between the individual forms of FRF were discussed together with the fact that in frequency domain, forms of FRF derived from receptance are obtained by simple multiplication by $i\omega$ (see eq. 1.6 and 1.7). From plots of FRF amplitude as a function of

frequency, form of FRF can be detected only in logarithmic scale (see Fig. 3.13). In other plots, shifting by 90° is evident for each derivative. Thus, e.g. Nyquist plot is in the right half-plane for mobility FRF and in the upper half-plane for inertance FRF etc.

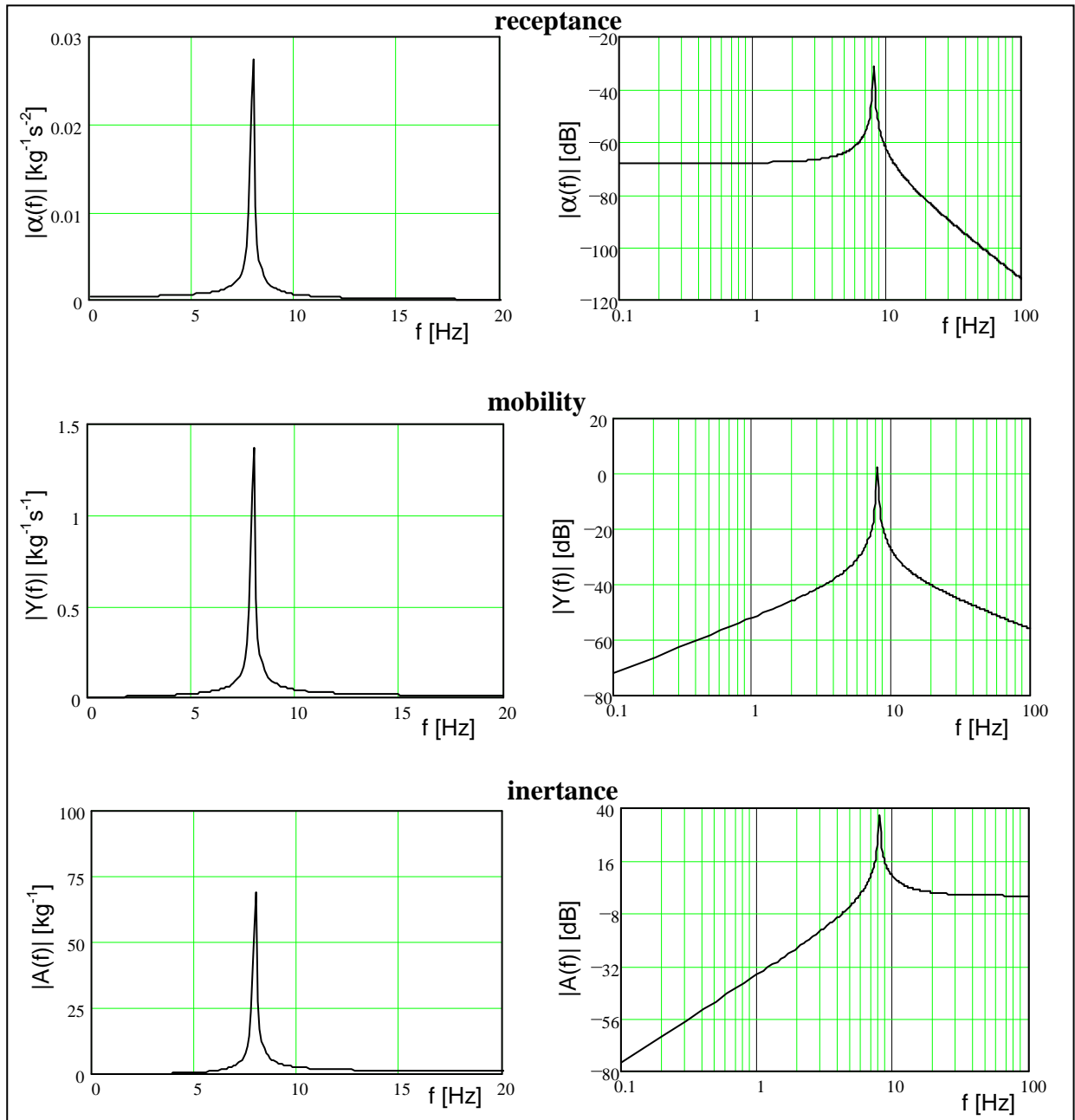


Fig. 3.13 Various Forms of FRF According to Response Parameter

3.2 Multi Degree-of-freedom System (MDOF)

Real structures possess a lot of degrees of freedom and a lot of equations are necessary for their description. Therefore, matrix form is preferably used for MDOF systems as it enables to write a single matrix equation instead a number of equations.

3.2.1 Undamped MDOF System

For undamped MDOF system of N degrees of freedom, the equation of motion in matrix form is:

$$[M]\{\ddot{x}(t)\} + [K]\{x(t)\} = \{f(t)\} \quad (3.58)$$

where $[M]$ and $[K]$ are the mass and stiffness matrices of order $N \times N$ and $\{x(t)\}$ and $\{f(t)\}$ are vectors of time-varying displacements and forces of order N .

3.2.1.1 Free vibration

In order to determine modal properties of the system, free vibration solution will be considered by putting

$$\{f(t)\} = \{0\}$$

In that case, solution can be expected in the form

$$\{x(t)\} = \{X\}e^{i\omega t} \quad \{\ddot{x}\} = -\omega^2 \{X\}e^{i\omega t}$$

where $\{X\}$ is a vector of N time-independent amplitudes. This assumes that the system is able to vibrate on a single frequency ω .

Substituting the homogeneous solution into equation of motion gives:

$$([K] - \omega^2 [M])\{X\} = \{0\} \quad (3.59)$$

The only non-trivial solution is:

$$\det([K] - \omega^2 [M]) = 0 \quad (3.60)$$

When substituting

$$\omega^2 = \lambda \quad (3.61)$$

then:

$$\det([K] - \lambda [M]) = 0 \quad \dots \text{characteristic equation of the system}$$

The characteristic equation can be transcribed to the form:

$$d_N \lambda^N + d_{N-1} \lambda^{N-1} + \dots + d_0 = 0 \quad (3.62)$$

By solving this characteristic equation, N values of λ_i , which are called *eigenvalues*, can be determined. Undamped natural frequencies can be obtained from eigenvalues as:

$$\Omega_{0i}^2 = \lambda_i \quad (3.63)$$

Substituting any of these back into the equation (3.59) yields a corresponding set of relative values for $\{X\}$, i.e. $\{\Psi\}_r$, the so-called *mode shape (or eigenvector)* corresponding to that natural frequency.

The complete solution can be expressed in two $N \times N$ matrices:

$$[\Omega_{0r}^2] \quad \dots \text{spectral matrix (eigenvalue matrix) - diagonal}$$

$[\Psi]$... modal matrix (matrix of modal shapes); its form is

$$[\{\Psi\}_1 \quad \{\Psi\}_2 \quad \dots \quad \{\Psi\}_r \quad \dots \quad \{\Psi\}_N]$$

where Ω_{0r}^2 is the r^{th} eigenvalue, or natural frequency squared, and $\{\Psi\}_r$ is the r^{th} eigenvector that describes the corresponding mode shape.

There are various numerical procedures, that convert the spatial model represented by matrices $[M]$ and $[K]$ to the modal model represented by matrices $[\Omega_{0r}^2]$ and $[\Psi]$.

A spectral matrix is a unique one, but a modal matrix is not. Whereas the natural frequencies are fixed quantities, the mode shapes are subject to an indeterminate scaling factor which does not affect the shape of the vibration mode, only its amplitude. Thus, a mode shape vector of

$$\begin{Bmatrix} 1 \\ 2 \\ 1 \\ 0 \end{Bmatrix} \text{ describes exactly the same vibration mode as } \begin{Bmatrix} 3 \\ 6 \\ 3 \\ 0 \end{Bmatrix} \text{ etc.}$$

What determines how the eigenvectors are scaled, or *normalized*, is largely governed by the numerical procedures followed by the eigensolution.

The actual amplitudes of vibration depend on the initial conditions and positions and magnitudes of exciting forces.

The procedure of obtaining eigenvalues and eigenvectors will be illustrated on the example of two degree-of-freedom undamped system (see Fig.3.14).

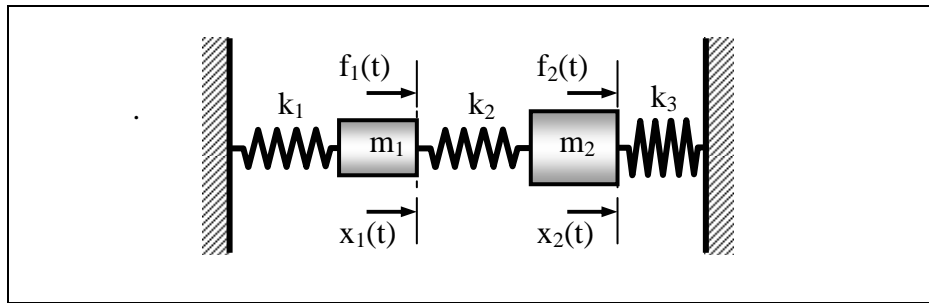


Fig. 3.14 Two Degree-of-freedom System

Equations of motion of this system are:

$$m_1 \ddot{x}_1 + (k_1 + k_2)x_1 - k_2 x_2 = f_1 \quad (3.64)$$

$$m_2 \ddot{x}_2 - k_2 x_1 + (k_2 + k_3)x_2 = f_2 \quad (3.65)$$

or in matrix form:

$$\begin{bmatrix} m_1 & 0 \\ 0 & m_2 \end{bmatrix} \begin{Bmatrix} \ddot{x}_1 \\ \ddot{x}_2 \end{Bmatrix} + \begin{bmatrix} k_1 + k_2 & -k_2 \\ -k_2 & k_2 + k_3 \end{bmatrix} \begin{Bmatrix} x_1 \\ x_2 \end{Bmatrix} = \begin{Bmatrix} f_1 \\ f_2 \end{Bmatrix} \quad (3.66)$$

Consider numerical values:

$$m_1 = 5 \text{ kg}$$

$$m_2 = 10 \text{ kg}$$

$$k_1 = k_2 = 2 \text{ N/m}$$

$$k_3 = 4 \text{ N/m}$$

Substituting in eq. (3.66), for free vibration (i.e. $f_1=0$ and $f_2=0$) yields to:

$$\begin{aligned} \begin{bmatrix} 5 & 0 \\ 0 & 10 \end{bmatrix} \begin{Bmatrix} \ddot{x}_1 \\ \ddot{x}_2 \end{Bmatrix} + \begin{bmatrix} 4 & -2 \\ -2 & 6 \end{bmatrix} \begin{Bmatrix} x_1 \\ x_2 \end{Bmatrix} &= \begin{Bmatrix} 0 \\ 0 \end{Bmatrix} \\ \left(\begin{bmatrix} 4 & -2 \\ -2 & 6 \end{bmatrix} - \lambda \begin{bmatrix} 5 & 0 \\ 0 & 10 \end{bmatrix} \right) \begin{Bmatrix} X_1 \\ X_2 \end{Bmatrix} &= \begin{Bmatrix} 0 \\ 0 \end{Bmatrix} \\ \begin{bmatrix} 4-5\lambda & -2 \\ -2 & 6-10\lambda \end{bmatrix} \begin{Bmatrix} X_1 \\ X_2 \end{Bmatrix} &= 0 \end{aligned} \tag{3.66a}$$

$$\begin{vmatrix} 4-5\lambda & -2 \\ -2 & 6-10\lambda \end{vmatrix} = 0$$

$$(4-5\lambda)(6-10\lambda) - (-2)(-2) = 0$$

$$50\lambda^2 - 70\lambda + 20 = 0$$

$$\lambda_1 = 0,4 \text{ s}^{-2}$$

$$\Omega_{01} = \sqrt{0,4} \text{ s}^{-1}$$

$$\lambda_2 = 1 \text{ s}^{-2}$$

$$\Omega_{02} = 1 \text{ s}^{-1}$$

Substituting back λ_1 and λ_2 into eq. (3.66a) will give the two natural mode shapes:

$$\text{For } \Omega_{01}: \begin{bmatrix} 4-5 \cdot 0,4 & -2 \\ -2 & 6-10 \cdot 0,4 \end{bmatrix} \begin{Bmatrix} X_1 \\ X_2 \end{Bmatrix} = 0$$

$$2X_1 - 2X_2 = 0$$

$$-2X_1 + 2X_2 = 0$$

... One of these equations is enough.

$$\Rightarrow X_1 = X_2$$

$$\text{Thus the mode shape for } \Omega_{01} \text{ is } \{\Psi\}_1 = \begin{Bmatrix} 1 \\ 1 \end{Bmatrix}$$

$$\text{For } \Omega_{02}: \begin{bmatrix} 4-5 \cdot 1 & -2 \\ -2 & 6-10 \cdot 1 \end{bmatrix} \begin{Bmatrix} X_1 \\ X_2 \end{Bmatrix} = 0$$

$$-X_1 - 2X_2 = 0$$

$$\Rightarrow X_2 = -\frac{X_1}{2}$$

$$\text{Thus the mode shape for } \Omega_{02} \text{ is } \{\Psi\}_2 = \begin{Bmatrix} 1 \\ -1/2 \end{Bmatrix}$$

Thus the entire solution is given by matrices:

$$[\Omega_{0r}^2] = \begin{bmatrix} 0,4 & 0 \\ 0 & 1 \end{bmatrix} \quad [\Psi] = \begin{bmatrix} 1 & 1 \\ 1 & -1/2 \end{bmatrix}$$

Mode shapes are shown in Fig. 3.15. It can be seen that the masses move either in phase or 180° out of phase. Since the masses reach their maximum displacements simultaneously, the *nodal points* (points, which do not move) are clearly defined.

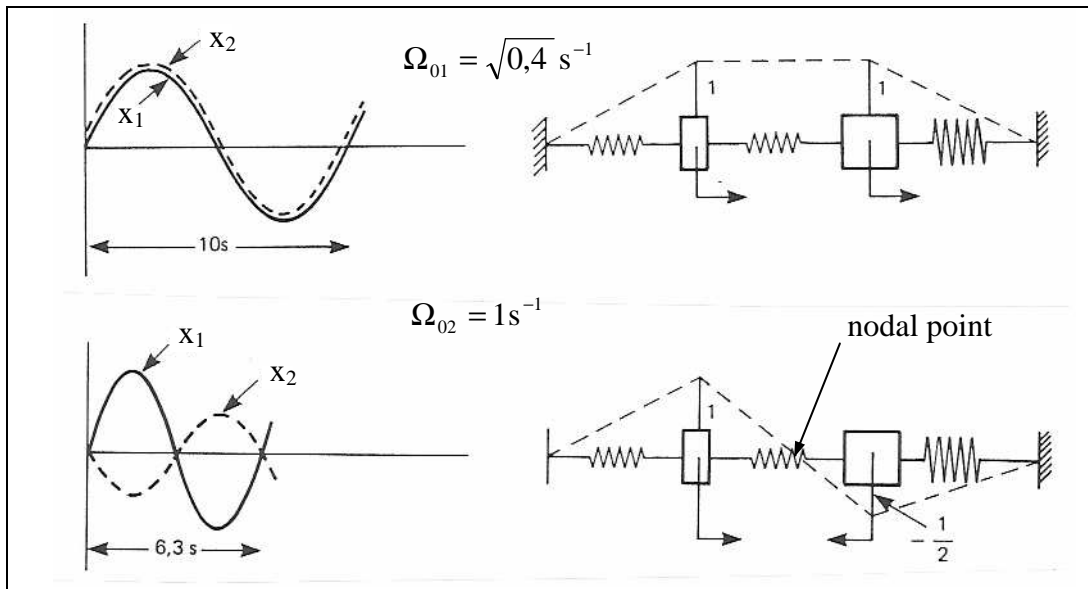


Fig. 3.15 Mode Shapes for the two Degree-of-freedom System

3.2.1.2 Orthogonal Properties of Eigenvectors

Solution of the equation $([K] - \lambda[M])\{X\} = \{0\}$ yields N eigenvalues and N corresponding eigenvectors. A particular r^{th} mode will satisfy:

$$[K]\{\Psi\}_r = \lambda_r [M]\{\Psi\}_r \quad (3.67)$$

Premultiply eq. (3.67) by the transpose of another, s^{th} mode shape:

$$\{\Psi\}_s^T [K]\{\Psi\}_r = \lambda_r \{\Psi\}_s^T [M]\{\Psi\}_r \quad (3.68)$$

Similarly, s^{th} mode will satisfy (after premultiplying by the transpose of r^{th} eigenvector) :

$$\{\Psi\}_r^T [K]\{\Psi\}_s = \lambda_s \{\Psi\}_r^T [M]\{\Psi\}_s \quad (3.69)$$

As $[M]$ and $[K]$ are symmetric matrices, it applies:

$$\{\Psi\}_r^T [K]\{\Psi\}_s = \{\Psi\}_s^T [K]\{\Psi\}_r \quad \text{and}$$

$$\{\Psi\}_r^T [M]\{\Psi\}_s = \{\Psi\}_s^T [M]\{\Psi\}_r$$

Therefore subtracting eq. (3.69) from eq. (3.68) yields to:

$$0 = (\lambda_r - \lambda_s) \{\Psi\}_s^T [M]\{\Psi\}_r \quad (3.70)$$

It is obvious that for $\lambda_r \neq \lambda_s$ (two different natural frequencies) applies:

$$\{\Psi\}_s^T [M]\{\Psi\}_r = 0 \quad \text{and} \quad (3.71)$$

$$\{\Psi\}_s^T [K]\{\Psi\}_r = 0 \quad (3.72)$$

Equations (3.71) and (3.72) define the orthogonal properties of the mode shapes with respect to the system mass and stiffness matrices respectively.

In the case of $\lambda_r = \lambda_s$ it applies:

$$\{\Psi\}_r^T [\mathbf{K}] \{\Psi\}_s = \lambda_r \{\Psi\}_r^T [\mathbf{M}] \{\Psi\}_s$$

Therefore:

$$\{\Psi\}_r^T [\mathbf{K}] \{\Psi\}_s = \mathbf{K}_r \quad \dots \text{generalized (modal) stiffness of the } r^{\text{th}} \text{ mode} \quad (3.73)$$

$$\{\Psi\}_r^T [\mathbf{M}] \{\Psi\}_s = \mathbf{M}_r \quad \dots \text{generalized (modal) mass of the } r^{\text{th}} \text{ mode} \quad (3.74)$$

$$\lambda_r = \Omega_{0r}^2 = \frac{\mathbf{K}_r}{\mathbf{M}_r} \quad (3.75)$$

In matrix notation:

$$\{\Psi\}^T [\mathbf{K}] \{\Psi\} = [\mathbf{K}_r] \quad (3.76)$$

$$\{\Psi\}^T [\mathbf{M}] \{\Psi\} = [\mathbf{M}_r] \quad (3.77)$$

$$[\Omega_{0r}^2] = [\mathbf{M}_r]^{-1} \cdot [\mathbf{K}_r] \quad (3.78)$$

The numerical values of the mode shapes calculated above will be used to determine the generalized mass and generalized stiffness of both modes:

$$\begin{bmatrix} 1 & 1 \\ 1 & -1/2 \end{bmatrix} \cdot \begin{bmatrix} 5 & 0 \\ 0 & 10 \end{bmatrix} \cdot \begin{bmatrix} 1 & 1 \\ 1 & -1/2 \end{bmatrix} = \begin{bmatrix} \mathbf{M}_1 & 0 \\ 0 & \mathbf{M}_2 \end{bmatrix} \quad \Rightarrow \quad \begin{array}{l} \mathbf{M}_1 = 15\text{kg} \\ \mathbf{M}_2 = 7,5\text{kg} \end{array}$$

Then

$$\mathbf{K}_1 = \Omega_{01}^2 \cdot \mathbf{M}_1 = 0,4 \cdot 15 = 6 \text{ N/m}$$

$$\mathbf{K}_2 = \Omega_{02}^2 \cdot \mathbf{M}_2 = 1 \cdot 7,5 = 7,5 \text{ N/m}$$

3.2.1.3 Normalization of Mode Shapes

As the mode shapes are arbitrary scaled, the values \mathbf{M}_r and \mathbf{K}_r are not unique (in contrary to the ratio $\mathbf{K}_r / \mathbf{M}_r$), it is not advisable to refer to a particular generalized mass or stiffness. This problem is eliminated by so-called *normalization* of mode shapes. If one of the elements of the eigenvector is assigned a certain value, the rest of elements are also fixed because the ration between any two elements is constant. This process of adjusting the elements of the natural modes to make their amplitude unique is called normalization. There are several ways how to do it, e.g.:

- mass normalization (to unity modal mass)
- the largest element of the mode shape is set to unity
- the length of the mode vector is set to unity

Mass normalization

This type of normalization is probably the most common and has most relevance to modal testing. The mass-normalized eigenvectors are written as $[\Phi]$ and have the particular property that

$$[\Phi]^T \cdot [M] \cdot [\Phi] = [I] \quad (3.79)$$

$$[\Phi]^T \cdot [K] \cdot [\Phi] = [\Omega_{0r}^2] \quad (3.80)$$

The relation between the mass-normalized mode shape for mode r , $\{\Phi\}_r$, and its more general form, $\{\Psi\}_r$, is simply:

$$\{\Phi\}_r = \frac{1}{\sqrt{M_r}} \cdot \{\Psi\}_r \quad (3.81)$$

or

$$[\Phi] = [\Psi] \cdot [M_r]^{-\frac{1}{2}} \quad (3.82)$$

Mass-normalized shapes can be derived by denoting them u_i and substituting to the equation (3.77):

$$\{\Psi\}_{j_1}^T \cdot [m] \cdot \{\Psi\}_{j_1} = M_1 \quad \{\Psi\}_{j_1} = \begin{Bmatrix} X_1 \\ X_1 \end{Bmatrix} = \begin{Bmatrix} 1 \\ 1 \end{Bmatrix}$$

$$\{\Phi\}_{j_1}^T \cdot [m] \cdot \{\Phi\}_{j_1} = 1$$

$$\{u_1 \quad u_1\} \cdot \begin{bmatrix} 5 & 0 \\ 0 & 10 \end{bmatrix} \cdot \begin{Bmatrix} u_1 \\ u_1 \end{Bmatrix} = 1$$

$$\{5u_1 \quad 10u_1\} \cdot \begin{Bmatrix} u_1 \\ u_1 \end{Bmatrix} = 1$$

$$5u_1^2 + 10u_1^2 = 1$$

$$u_1^2 = \frac{1}{15}$$

$$u_1 = \sqrt{1/15} \quad \{\Phi\}_{j_1} = \begin{Bmatrix} \sqrt{1/15} \\ \sqrt{1/15} \end{Bmatrix}$$

The same can be obtained by substituting the modal mass into equation (3.81):

$$\{\Phi\}_{j_1} = \frac{1}{\sqrt{M_1}} \cdot \{\Psi\}_{j_1} = \frac{1}{\sqrt{15}} \cdot \begin{Bmatrix} 1 \\ 1 \end{Bmatrix} = \begin{Bmatrix} \sqrt{1/15} \\ \sqrt{1/15} \end{Bmatrix}$$

$$\{\Phi\}_{j_2} = \frac{1}{\sqrt{M_2}} \cdot \{\Psi\}_{j_2} = \sqrt{\frac{2}{15}} \cdot \begin{Bmatrix} 1 \\ -1/2 \end{Bmatrix} = \begin{Bmatrix} \sqrt{2/15} \\ -\frac{\sqrt{2/15}}{2} \end{Bmatrix}$$

3.2.1.4 Forced Response Analysis of Multi Degree-of-freedom System

Suppose that the structure is excited harmonically by a set of sinusoidal forces all at the same frequency ω , but with individual amplitudes and phases. Then:

$$\{f(t)\} = \{F\}e^{i\omega t}$$

and solution is assumed to exist of the form:

$$\{x(t)\} = \{X\}e^{i\omega t}$$

where $\{F\}$ and $\{X\}$ are $N \times 1$ vectors of time-independent complex amplitudes.

The equation of motion then becomes:

$$([\mathbf{K}] - \omega^2 [\mathbf{M}]) \cdot \{X\}e^{i\omega t} = \{F\}e^{i\omega t} \quad (3.83)$$

or, rearranging to solve for the unknown responses

$$\{X\} = ([\mathbf{K}] - \omega^2 [\mathbf{M}])^{-1} \cdot \{F\} \quad (3.84)$$

which may be written as

$$\{X\} = [\alpha(\omega)] \cdot \{F\} \quad (3.85)$$

where $[\alpha(\omega)]$ is the $N \times N$ receptance FRF matrix for the system and constitutes its *response model*. The general element in the receptance FRF matrix, $\alpha_{jk}(\omega)$, is defined as follows:

$$\alpha_{jk}(\omega) = \frac{X_j}{F_k} ; \quad F_m = 0; \quad m = 1 \dots N \quad ; \quad m \neq k$$

and as such represents an individual receptance FRF expression very similar to that defined earlier for the SDOF system.

It is possible to determine values for the elements of $[\alpha(\omega)]$ at any frequency of interest simply by substituting the appropriate values into:

$$[\alpha(\omega)] = ([\mathbf{K}] - \omega^2 [\mathbf{M}])^{-1} \quad (3.86)$$

However, this involves inversion of the system matrix at each frequency and this has several disadvantages, namely:

- it becomes costly for large-order systems (lot of DOFs)
- it is inefficient if only a few of the individual FRF expressions are required
- it provides no insight into the form of the various FRF properties

For these reasons, an alternative way of deriving the various FRF parameters is used which makes use of the modal properties of the system.

Come out of inverted eq. (3.86):

$$([\mathbf{K}] - \omega^2 [\mathbf{M}]) = [\alpha(\omega)]^{-1}$$

Premultiply both sides by $[\Phi]^T$ and postmultiply both sides by $[\Phi]$ to obtain

$$[\Phi]^T \cdot ([\mathbf{K}] - \omega^2 [\mathbf{M}]) \cdot [\Phi] = [\Phi]^T \cdot [\alpha(\omega)]^{-1} \cdot [\Phi]$$

$$[(\Omega_{or}^2 - \omega^2)] = [\Phi]^T \cdot [\alpha(\omega)]^{-1} \cdot [\Phi]$$

which leads to

$$[\alpha(\omega)] = [\Phi] \cdot [(\Omega_{0r}^2 - \omega^2)]^{-1} \cdot [\Phi]^T \quad (3.87)$$

It is clear from this equation that the receptance matrix $[\alpha(\omega)]$ is symmetric and this will be recognized as the principle of *reciprocity* which applies to many structural characteristics. Its implications are that:

$$\alpha_{jk} = \frac{X_j}{F_k} = \alpha_{kj} = \frac{X_k}{F_j} \quad (3.88)$$

Equation (3.87) enables to compute any individual FRF parameter, $\alpha_{jk}(\omega)$, using the following formula:

$$\alpha_{jk}(\omega) = \sum_{r=1}^N \frac{(\Phi_j)_r \cdot (\Phi_k)_r}{\Omega_{0r}^2 - \omega^2} = \sum_{r=1}^N \frac{(\Psi_j)_r \cdot (\Psi_k)_r}{m_r(\Omega_{0r}^2 - \omega^2)} \quad (3.89)$$

or

$$\alpha_{jk}(\omega) = \sum_{r=1}^N \frac{rA_{jk}}{\Omega_{0r}^2 - \omega^2} \quad rA_{jk} \quad \dots \text{ modal constant, residuum} \quad (3.90)$$

In the following example it will be proved that the same function α_{11} could be obtained by both ways - by direct inversion (eq. 3.86) and from partial fraction form (eq. 3.89).

Equations of motion of forced undamped vibration of the system from Fig. 3.14 are:

$$(k_1 + k_2 - \omega^2 m_1)X_1 + (-k_2)X_2 = F_1$$

$$(-k_2)X_1 + (k_2 + k_3 - \omega^2 m_2)X_2 = F_2$$

which yields:

$$\left(\frac{X_1}{F_1} \right)_{F_2=0} = \alpha_{11}(\omega) = \frac{k_2 + k_3 - \omega^2 m_2}{\omega^4 m_1 m_2 - \omega^2 (m_1 k_2 + m_1 k_3 + m_2 k_1 + m_2 k_2) + (k_1 k_2 + k_2 k_3 + k_1 k_3)}$$

numerically (for $m_1 = 5$ kg, $m_2 = 10$ kg, $k_1 = k_2 = 2$ N/m, $k_3 = 4$ N/m):

$$\left(\frac{X_1}{F_1} \right)_{F_2=0} = \alpha_{11}(\omega) = \frac{6 - 10\omega^2}{20 - 70\omega^2 + 50\omega^4}$$

Now, the modal summation formula (3.89) will be used together with the results obtained earlier:

$$\alpha_{11}(\omega) = \frac{({}_1\Phi_1)^2}{\Omega_{01}^2 - \omega^2} + \frac{({}_2\Phi_1)^2}{\Omega_{02}^2 - \omega^2}$$

numerically (for $\Omega_{01}^2 = 0.4$ s⁻¹, $\Omega_{02}^2 = 1$ s⁻¹, ${}_1\Phi_1 = \sqrt{1/15}$, ${}_2\Phi_1 = \sqrt{2/15}$):

$$\alpha_{11}(\omega) = \frac{1/15}{0.4 - \omega^2} + \frac{2/15}{1 - \omega^2} = \frac{6 - 10\omega^2}{20 - 70\omega^2 + 50\omega^4}$$

which is the same expression as above.

3.2.2 Characteristics and Presentation of Multi Degree-of-Freedom FRF Data

As for an SDOF system, for MDOF system there are also three alternatives of FRF with using either displacement or velocity or acceleration as a response parameter, thus obtaining receptance, mobility or inertance respectively. These three forms are exactly in the same relation as described earlier, thus:

$$[Y(\omega)] = i\omega[\alpha(\omega)] \quad (3.91)$$

$$[A(\omega)] = i\omega[Y(\omega)] = -\omega^2[\alpha(\omega)] \quad (3.92)$$

According to the place and direction of excitation and response (place + direction = DOF), four types of FRF can be defined:

- *point* - coordinates of excitation and response are equal (e.g. point No 10)
 - *direct* - directions of excitation and response are equal (e.g. DOF 10X)
 - *cross* - directions of excitation and response are different (e.g. excitation at DOF 10Z, response at DOF 10X).
- *transfer* - coordinates of excitation and response are different
 - *direct* (e.g. excitation at DOF 10X, response at DOF 14X)
 - *cross* (e.g. excitation at DOF 10X, response at DOF 14Z)

It is helpful to examine the form which FRF data takes when presented in various graphical formats. This knowledge is necessary in assessing the validity and interpreting measured data.

For the simplest case of an undamped system, for which the receptance expression is given by equation (3.89): $\alpha_{jk}(\omega) = \sum_{r=1}^N \frac{(\Phi_j)_r \cdot (\Phi_k)_r}{\Omega_{0r}^2 - \omega^2}$

Using the type of log-log plot, individual terms in the FRF series can be plotted as separate curves. The total FRF curve is a summation of all the individual curves. However, the exact shape of the curve is not so simple to deduce as first appears because a part of the information (phase) is not shown. In fact, in some sections of each curve, the receptance is actually positive in sign and in others is negative but there is no indication of this on the logarithmic plot which only shows the modulus. However, when addition of the individual components is made to determine the complete receptance expression, the signs of various terms are of considerable importance.

Examine some of the important features using a simple example with just two modes:

$[\Phi] = \begin{bmatrix} 1 & 1 \\ 1 & -1/2 \end{bmatrix}$. Two FRF plots, point receptance α_{11} and transfer receptance α_{21} will be created.

Expressions for the receptances are:

$$\alpha_{11}(\omega) = \frac{1}{\Omega_{01}^2 - \omega^2} + \frac{1}{\Omega_{02}^2 - \omega^2} \qquad \alpha_{21}(\omega) = \frac{1}{\Omega_{01}^2 - \omega^2} - \frac{0.5}{\Omega_{02}^2 - \omega^2}$$

from which it can be seen that the main difference between the point and transfer receptances is in the sign of the modal constant (the numerator) of the second mode. As the plots only show the modulus, they are apparently insensitive to this difference. However, when the two terms are added to produce the actual FRF for the MDOF system, the following characteristics will arise, which is illustrated in Fig. 3.16. In this figure, receptance is plotted, but the following remarks apply for all types of FRF (receptance, mobility and inertance).

When considering a point receptance, the numerator in the eq. (3.89) for all modes will always be positive, as it is a square of modal vector element. In transfer receptance, the numerator can be either positive or negative according to the signs of elements of eigenvectors.

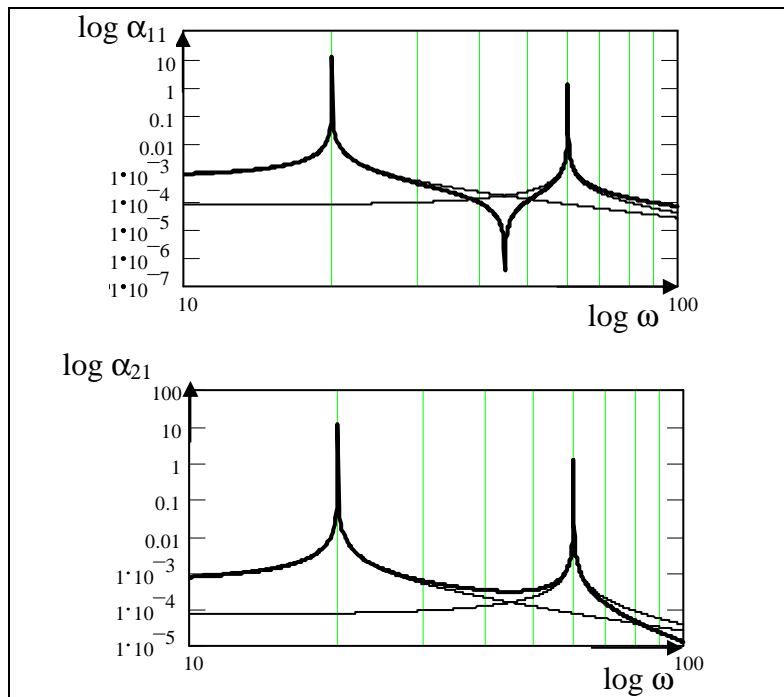


Fig.3.16 Point (upper) and Transfer Receptance (below) FRF Plot for Undamped 2DOF System

Point Receptance

At frequencies below the first natural frequency, both terms in the sum have the same sign and thus are additive, making the total FRF curve higher than each component, but as the plot uses a logarithmic scale, the contribution of the second mode at these low frequencies is relatively insignificant. Hence, the total FRF curve is only slightly above that for the first term. A similar argument and result apply at the high frequency end, above the second natural frequency, where the total plot is just above that for the second term alone. However, in the region between the two resonances, the two components have opposite signs to each other so that they are subtractive, and at the point where they cross, their sum is zero since they are of equal magnitude but of opposite sign there. On a logarithmic plot of this type, this produces the antiresonance characteristic which reflects that of resonance. In the immediate vicinity of

any resonance, the contribution of the term whose natural frequency is nearby is so much greater than the other one that the total is, in effect, the same as that one term. Physically, the response of the MDOF system just at one of its natural frequencies is dominated by that mode and other modes have very little influence (it applies for undamped or very slightly damped systems).

Transfer Receptance

Similar reasoning as for point receptance can be applied when progressing along the frequency range with the only difference that the signs of the two terms in the sum are opposite in this case. Thus, at very low and very high frequencies, the total FRF curve lies just below that of the nearest individual component while in the region between the resonances, the two components now have the same sign and so the cancelling-out feature is not encountered and only a minimum, rather than antiresonance, occurs.

The principles illustrated here may be extended to any number of degrees of freedom. There is a fundamental rule that if two consecutive modes have the same sign for the modal constants, then there will be an antiresonance at some frequency between the natural frequencies of those two modes. If they have opposite signs, there will not be an antiresonance but just a minimum. The most important feature of antiresonance is perhaps the fact that there is a phase change associated with it, as well as a very low magnitude.

It is also interesting to determine what controls whether a particular FRF will have positive or negative modal constants, and thus whether it will exhibit antiresonances or not. A considerable insight may be gained by considering the origin of the modal constant: it is the product of two eigenvector elements, one at the response point and the other at the excitation point. For point mobility, the total modal constant for every mode must be positive, it being the square of a number. This means that for point FRF, there must be an antiresonance following every resonance, without exception.

The situation for transfer FRFs is less categorical because the modal constant will sometimes be positive and sometimes negative, depending upon whether the excitation and response move in phase or not. Thus, we expect transfer FRF measurements to show a mixture of antiresonances and minima (valleys). However, the mixture can be anticipated to some extent because it can be shown that the further apart are the two points in question, the more likely are the two eigenvector elements to alternate in sign as progressed through the modes. Thus, it might be expected that the transfer FRF between two positions widely separated on the structure will exhibit fewer antiresonances than the one for two points relatively close together.

A clear example of this is given in Fig. 3.17 for a 4DOF system, showing a complete set of FRFs for excitation at one extreme point in the form of mobility.

Finally, it should be remarked that if either the excitation or the response coordinates happen to coincide with a node for one of the modes (i.e. ${}_r\Phi_{j_r} \cdot \Phi_k = 0$), then this mode will not appear as a resonance on the FRF plot. In that case, ${}_rA_{jk} = 0$ and so the only response which will be encountered at or near $\omega = \Omega_{or}$ will be due to the off-resonant contribution of all the other modes.

The form of the FRF plot of a damped system is quite similar to those for an undamped system described above. The resonances and antiresonances are blunted by inclusion of damping, and the phase angles (not shown) are no longer exactly 0° or 180° , but the general appearance of the plot is an extension of that for the system without damping. This applies as long as the modes are relatively well separated. This condition is satisfied unless the separation between adjacent natural frequencies (expressed as a percentage of their mean) is of the same order as, or less than, the modal damping factors, in which case it becomes difficult to distinguish the individual modes.

Fig. 3.18 shows a receptance plot of a 2DOF system - the same system as in Fig. 3.16, with damping added.

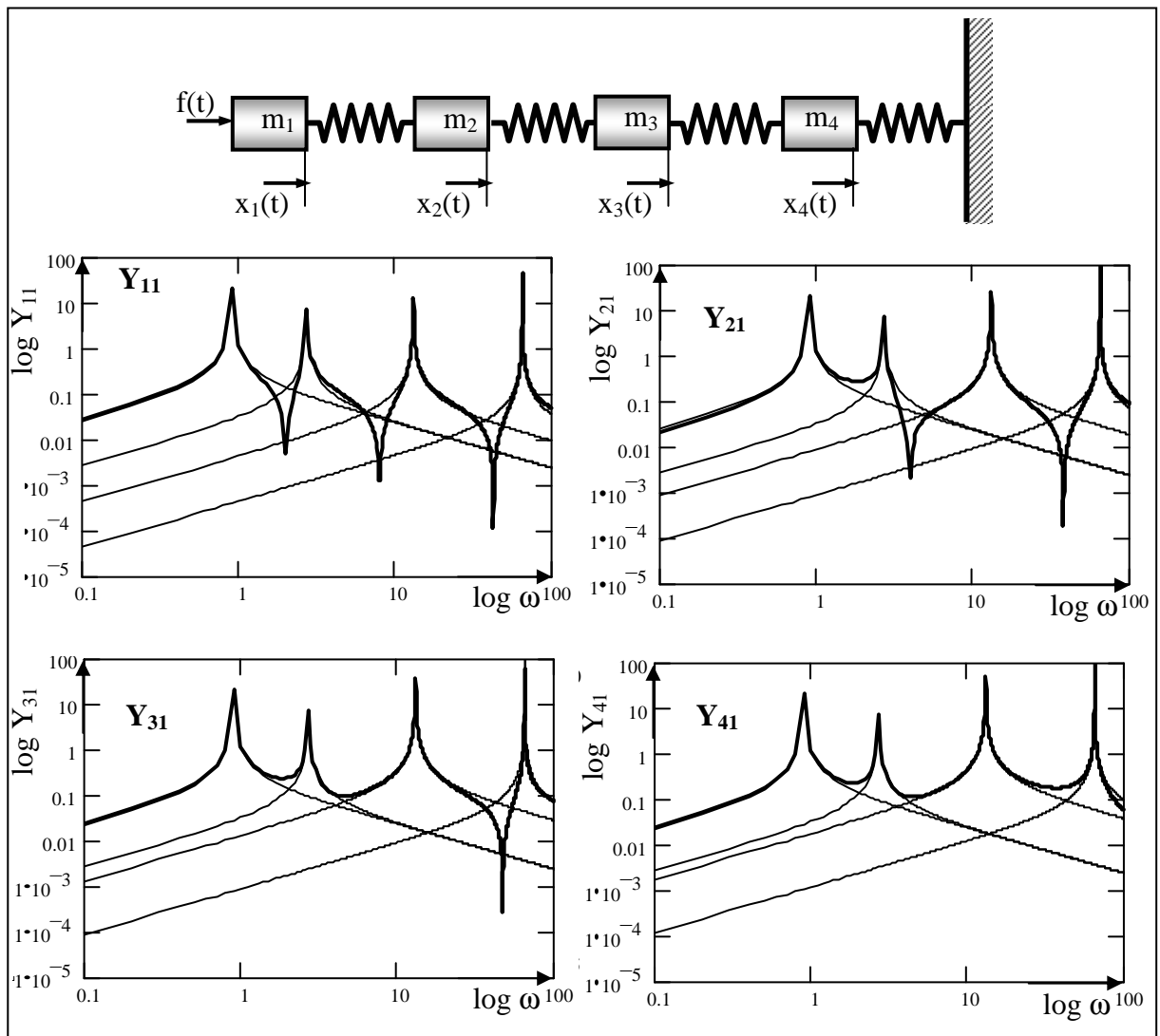


Fig.3.17 Mobility Plots of a 4DOF System

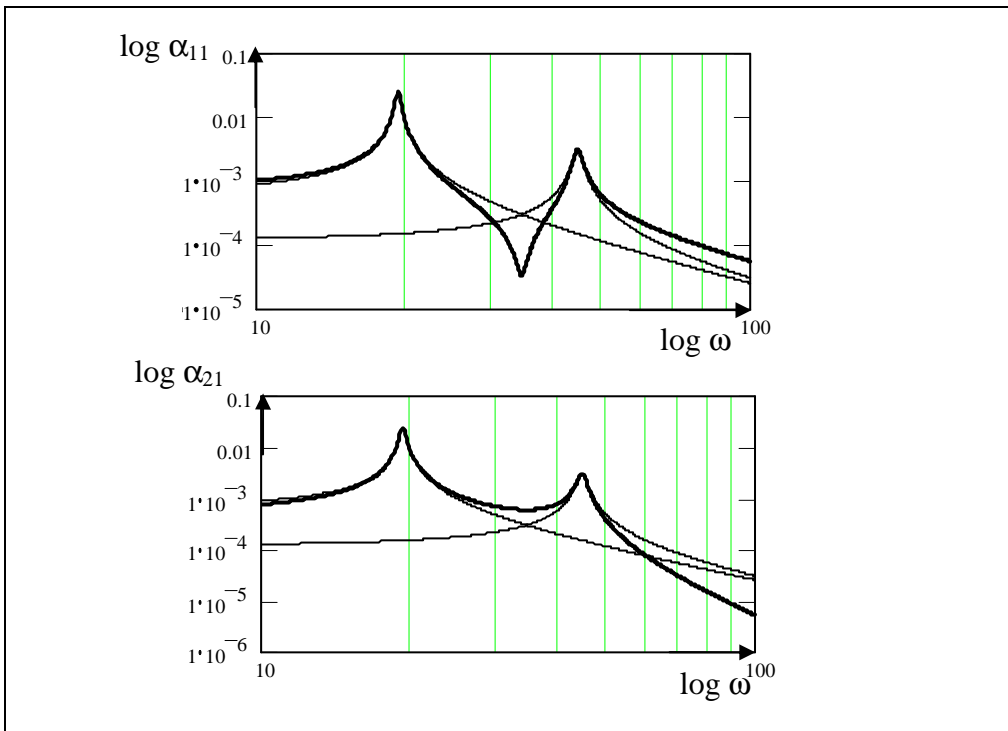


Fig. 3.18 Point (upper) and Transfer Receptance (below) FRF Plot for Damped 2DOF system

As for the SDOF case, it is interesting to examine the form of Nyquist circle for an MDOF system as well. Nyquist plot of 2DOF system is shown in Fig. 3.19 - point receptance on the left and transfer receptance on the right. Receptance of a proportionally damped system is plotted in a solid line, receptance of non-proportionally damped system in a dashed line (in that case, modal circles are rotated). Non-proportional damping will be discussed in detail in chapter 3.2.3.4.

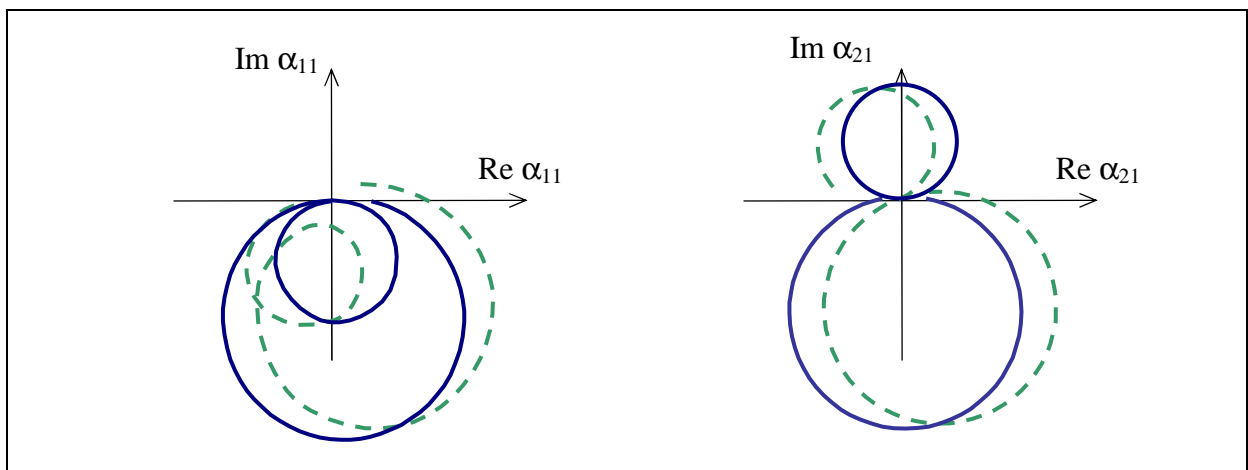


Fig.3.19 Nyquist Plots of Point and Transfer Receptances

3D plot of the point receptance of a 3DOF proportionally damped system and its projections to the individual planes is shown in Fig. 3.20.

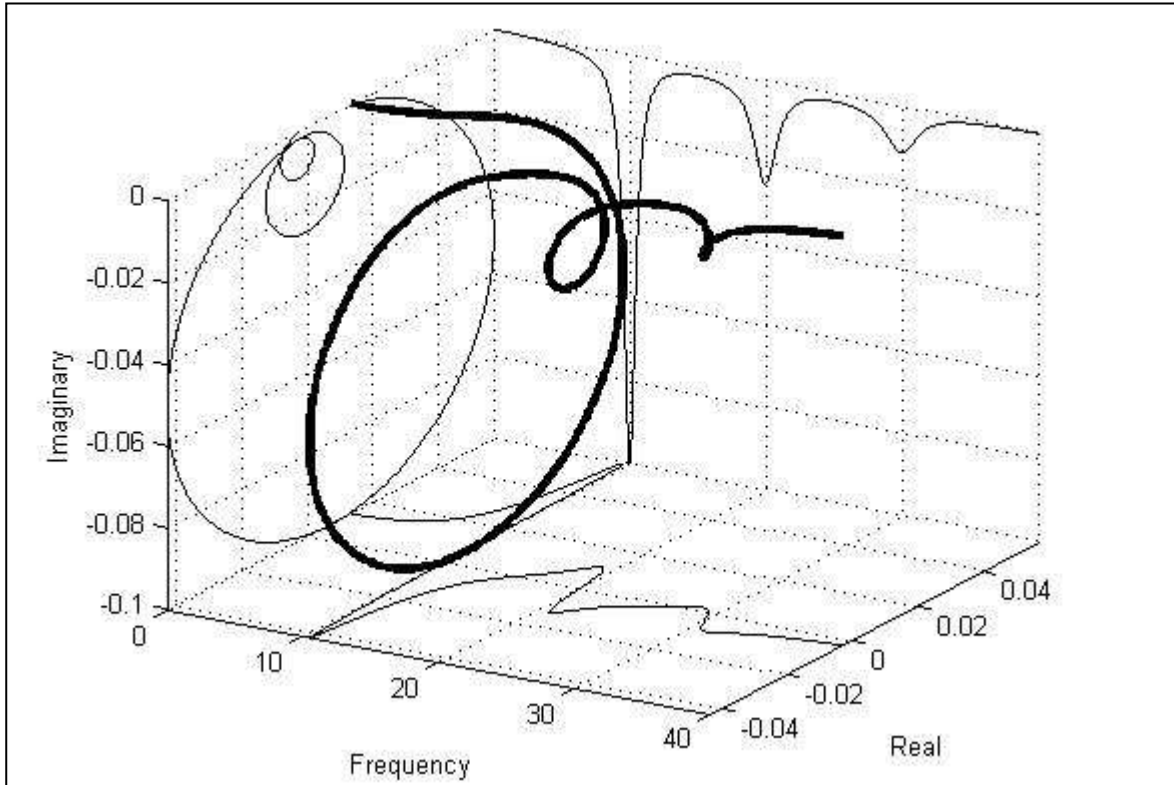


Fig.3.20 3D Receptance Plot of a 3DOF System

3.2.3 Damped Multi Degree-of-Freedom System

3.2.3.1 Proportional Viscous Damping

A special type of damping that is quite easy to include in analysis is so-called *proportional damping*. The advantage of using a proportional damping model in the analysis of structures is that the modes of such a structure are almost identical to those of the undamped version of the model. Specifically, the mode shapes are identical and the natural frequencies are very similar to those of the simpler undamped system. It is possible to derive modal properties of a proportionally damped system by fully analysing the undamped version and then making a correction for the presence of damping. While this procedure is often used in the theoretical analysis of structures, it should be mentioned that it is only valid in the case of this special type or distribution of damping, which may not apply to real structures studied in modal tests.

Adding a viscous damping matrix [B] to the general equation of motion for an MDOF system, following equation applies :

$$[M]\{\ddot{x}\} + [B]\{\dot{x}\} + [K]\{x\} = \{f\} \quad (3.93)$$

First, the case where the damping matrix is directly proportional to the stiffness matrix, will be discussed:

$$[B] = \beta[K] \quad (3.94)$$

If the damping matrix is pre- and post-multiplied by the eigenvector matrix $[\Psi]$ in just the same way as it was done previously for the mass and stiffness matrices, it becomes:

$$[\Psi]^T [B][\Psi] = \beta[k_r] = [b_r] \quad (3.95)$$

where the diagonal elements \mathbf{b}_r represent the modal damping of the various modes of the system. The fact that this matrix is also diagonal means that the undamped system mode shapes are also those of the damped system, and this is a particular feature of this type of damping. This can easily be demonstrated. Substituting modal coordinates $\{p\}$ for $\{x\}$

$$\{x\} = [\Psi] \cdot \{p\} \quad (3.96)$$

into the equation of motion and pre-multiplying it by $[\Psi]^T$ leads to :

$$[m_r] \cdot \{\ddot{p}\} + [b_r] \cdot \{\dot{p}\} + [k_r] \cdot \{p\} = \{0\} \quad (3.97)$$

from where the r^{th} equation is :

$$m_r \ddot{p}_r + b_r \dot{p}_r + k_r p_r = 0 \quad (3.98)$$

which is a equation of a single degree-of-freedom system, or of a single mode of the system. This mode has a complex eigenvalue $p_r = -\delta_r \pm i\Omega_r$ with an oscillatory part:

$$\Omega_r = \Omega_{0r} \sqrt{1 - \zeta_r^2} \quad \Omega_{0r}^2 = \frac{k_r}{m_r} \quad \zeta_r = \frac{b_r}{2\sqrt{k_r m_r}} = \frac{1}{2} \beta \Omega_{0r} \quad (3.99)$$

and a decay part:

$$\delta_r = \zeta_r \Omega_{0r} = \frac{\beta}{2} \cdot \Omega_{0r}^2 \quad (3.100)$$

A simple extension of the steps performed in forced response analysis of undamped systems (equations 3.83 to 3.89) lead to the definition for the general receptance FRF as:

$$[\alpha(\omega)] = [K + i\omega B - \omega^2 M]^{-1} \quad (3.101)$$

or

$$\alpha_{jk}(\omega) = \sum_{r=1}^N \frac{\Psi_j \cdot \Psi_k}{(k_r - \omega^2 m_r) + i(\omega b_r)} = \sum_{r=1}^N \frac{\Phi_j \cdot \Phi_k}{\Omega_{0r}^2 - \omega^2 + 2i\omega \Omega_{0r} \zeta_r} \quad (3.102)$$

which has a very similar form to that for the undamped system except that now it becomes complex in the denominator as a result of the inclusion of damping.

General Forms of Proportional Damping

Other distributions of damping bring about the same result and they are included in the classification *proportional damping*. The usual definition of proportional damping is that the damping matrix $[B]$ should be of the form:

$$[B] = \beta[K] + \gamma[M] \quad (3.103)$$

In this case, the damped system will have eigenvalues and eigenvectors as follows:

$$\Omega_r = \Omega_{0r} \sqrt{1 - \zeta_r^2} \quad ; \quad \zeta_r = \frac{\beta \Omega_{0r}}{2} + \frac{\gamma}{2\Omega_{0r}} \quad (3.104)$$

and $[\Psi^{\text{damped}}] = [\Psi^{\text{undamped}}]$

Distribution of damping of this type is often plausible from the practical standpoint - the actual damping mechanisms are usually analogous to stiffness elements (for internal material or hysteretic damping) or to mass elements (for friction damping). There is a more general definition of the condition required for the damped system to possess the same mode shapes as its undamped counterpart, and that is:

$$([M]^{-1}[K]) \cdot ([M]^{-1}[B]) = ([M]^{-1}[B]) \cdot ([M]^{-1}[K]) \quad (3.105)$$

although it is more difficult to make a direct physical interpretation of its form.

3.2.3.2 Proportional Hysteretic Damping

An identical procedure can be used for an MDOF system with proportional hysteretic damping, producing the same essential results. If the general system equations of motion are expressed as

$$[M]\{\ddot{x}\} + [K + iH]\{x\} = \{f\} \quad (3.106)$$

and the hysteretic damping matrix [H] is proportional, typically:

$$[H] = \beta'[K] + \gamma'[M] \quad (3.107)$$

then the mode shapes for the damped system are again identical to those of the undamped system and the eigenvalues take the complex form:

$$\lambda_r^2 = \Omega_{0r}^2 (1 + i\eta_r) \quad \Omega_{0r}^2 = \frac{k_r}{m_r} \quad \eta_r = \beta' + \frac{\gamma'}{\Omega_{0r}^2} \quad (3.108)$$

Note: η_r is the hysteretic damping loss factor. In the chapter 3.1.3.1, this loss factor was denoted as γ (and in the entire chapter 3.1, η was used for tuning coefficient). In the following text, the loss factor will be denoted as η in accordance with common notation in literature.

The general FRF expression is:

$$\alpha_{jk}(\omega) = \sum_{r=1}^N \frac{\Psi_{j,r} \Psi_{k,r}}{(k_r - \omega^2 m_r) + i\eta_r k_r} = \sum_{r=1}^N \frac{\Phi_{j,r} \Phi_{k,r}}{\Omega_{0r}^2 - \omega^2 + i\eta_r \Omega_{0r}^2} \quad (3.109)$$

3.2.3.3 Hysteretic Damping - General Case

As stated above, the case of proportional damping is a particular one which does not always apply. It is justified in a theoretical analysis because it is realistic and also because of a lack of any more accurate model. However, it is important to consider the most general case in order to be able to interpret and analyse correctly the data observed on real structures.

The general equation of motion for an MDOF system with hysteretic damping and harmonic excitation is:

$$[M]\{\ddot{x}\} + [K]\{x\} + i[H]\{x\} = \{F\}e^{i\omega t} \quad (3.110)$$

Now, first consider the case where there is no excitation and assume a solution of the form:

$$\{x\} = \{X\}e^{i\lambda t} \quad (3.111)$$

Substituted to the equation of motion, this trial solution leads to a complex eigenproblem whose solution is in the form of two matrices (as for the earlier undamped case), containing the eigenvalues and eigenvectors. In this case, both matrices are complex, meaning that each natural frequency and each mode shape is described in terms of complex quantities. The r^{th} eigenvalue is written as

$$\lambda_r^2 = \Omega_r^2(1 + i\eta_r) \quad (3.112)$$

where Ω_r is the natural frequency and η_r is the damping loss factor for that mode. The natural frequency Ω_r is not necessarily equal to the natural frequency of the undamped system, Ω_{0r} , as was the case for proportional hysteretic damping, although the two values will generally be very close in practice.

The complex mode shapes means that the amplitude of each DOF has both magnitude and phase angle. This is only very slightly different from the undamped case where there is also both magnitude and phase, but the phase angle is either 0° or 180° , which can be completely described using real numbers (0° - positive magnitude, 180° - negative magnitude).

Eigensolution of the damped system possess the same type of orthogonality properties as those demonstrated in chapter 3.2.1.2 for the undamped system and may be defined by equations:

$$[\Psi]^T [M][\Psi] = [m_r] \quad (3.113)$$

$$[\Psi]^T [K + iH][\Psi] = [k_r] \quad (3.114)$$

Again, the modal mass and stiffness parameters (now complex) depend upon normalisation of the mode shape vectors for their magnitudes but always obey the relationship:

$$\lambda_r^2 = \frac{k_r}{m_r} \quad (3.115)$$

and a set of mass-normalized eigenvectors can be defined as:

$$\{\Phi\}_r = m_r^{-\frac{1}{2}} \cdot \{\Psi\}_r \quad (3.116)$$

3.2.3.4 MDOF System with General Hysteretic Damping - Forced Response Solution

The equation of motion for a forced response analysis of an MDOF system with harmonic excitation and response is:

$$[K + iH - \omega^2 M]\{X\}e^{i\omega t} = \{F\}e^{i\omega t} \quad (3.117)$$

Again, a direct solution to this problem may be obtained by using the equations of motion to give:

$$\{X\} = [K + iH - \omega^2 M]^{-1} \{F\} = [\alpha(\omega)]\{F\} \quad (3.118)$$

but this is again very inefficient for numerical application and the procedure by multiplying both sides of the equation by the eigenvectors will be used. Following the same procedures as between equations (3.86) and (3.87), it can be written:

$$[\alpha(\omega)] = [\Phi][(\lambda_r^2 - \omega^2)]^{-1}[\Phi]^T \quad (3.119)$$

From this matrix equation, any FRF element $\alpha_{jk}(\omega)$ can be extracted and expressed explicitly in a series form:

$$\alpha_{jk}(\omega) = \sum_{r=1}^N \frac{\Phi_{j,r} \Phi_{k,r}}{\Omega_r^2 - \omega^2 + i\eta_r \Omega_r^2} \quad (3.120)$$

which can also be rewritten in various alternative ways, such as:

$$\alpha_{jk}(\omega) = \sum_{r=1}^N \frac{\Psi_{j,r} \Psi_{k,r}}{m_r (\Omega_r^2 - \omega^2 + i\eta_r \Omega_r^2)} \quad \text{or} \quad \alpha_{jk}(\omega) = \sum_{r=1}^N \frac{A_{jk,r}}{\Omega_r^2 - \omega^2 + i\eta_r \Omega_r^2} \quad (3.121)$$

In these expressions, both the numerator and denominator are complex as a result of the complexity of the eigenvectors. It is in this respect that the general damping case differs from that for proportional damping.

3.2.3.5 MDOF Systems - Summary for Various Types of Damping

An analysis of an MDOF system with a general form of viscous damping is omitted in this text, because it constitutes a much more difficult problem than that of an analysis of an MDOF system with a general form of hysteretic damping. Only results are stated here - in table 3.1., definitions of FRFs and "natural frequencies" are summarized for all types of damping.

The basic definition of "natural frequency" derives from the undamped system's eigenvalues which yield the frequencies at which free vibration of the system can take place. These undamped system natural frequencies are given by the square roots of the eigenvalues and identified by the symbol Ω_{0r} and they occur in expressions for both free vibration response:

$$x(t) = \sum_{r=1}^N X_r e^{i\Omega_{0r}t} \quad (3.122)$$

and for forced vibration, the FRF:

$$\alpha(\omega) = \sum_{r=1}^N \frac{A_r}{\Omega_{0r}^2 - \omega^2} \quad (3.123)$$

For damped systems, the situation is more complicated and leads to two alternative characteristic frequency parameters being defined - both called "natural frequencies" - one for free vibration (Ω_r) and the second for forced vibration (Ω_r').

SYSTEM	EQUATION FOR FRF	C	D	NATURAL FREQ.	
				free Ω_r	forced Ω'_r
undamped	$\alpha_{jk}(\omega) = \sum_{r=1}^N \frac{\Phi_{j,r} \cdot \Phi_{k,r}}{\Omega_{0r}^2 - \omega^2}$	real constant	0	Ω_{0r}	Ω_{0r}
proportional hysteretic	$\alpha_{jk}(\omega) = \sum_{r=1}^N \frac{\Phi_{j,r} \cdot \Phi_{k,r}}{\Omega_{0r}^2 - \omega^2 + i\eta_r \Omega_{0r}^2}$	real constant	real constant	Ω_{0r}	Ω_{0r}
proportional viscous	$\alpha_{jk}(\omega) = \sum_{r=1}^N \frac{\Phi_{j,r} \cdot \Phi_{k,r}}{\Omega_{0r}^2 - \omega^2 + 2i\omega \Omega_{0r} \zeta_r}$	real constant	real (ω)	$\Omega_{0r} \sqrt{1 - \zeta_r^2}$	Ω_{0r}
general hysteretic	$\alpha_{jk}(\omega) = \sum_{r=1}^N \frac{\Phi_{j,r} \cdot \Phi_{k,r}}{\Omega_r^2 - \omega^2 + i\eta_r \Omega_r^2}$	complex constant	real constant	Ω_r	Ω_r
general viscous	$\alpha_{jk}(\omega) = \sum_{r=1}^N \frac{R_{jk} + i \frac{\omega}{\Omega'_r} S_{jk}}{\Omega_r'^2 - \omega^2 + 2i\omega \Omega_r' \zeta_r}$	complex (ω)	real (ω)	$\Omega_r' \sqrt{1 - \zeta_r^2}$	Ω_r'

Tab 3.1 FRF Formulae and Natural Frequencies for All Types of Damping

The natural frequency Ω_r constitutes the oscillatory part of the free vibration characteristic which, being complex, contains an exponential decay term as well. Thus:

$$x(t) = \sum_{r=1}^N X_r e^{-\delta_r t} e^{i\Omega_r t} \quad (3.124)$$

where Ω_r may or may not be equal to Ω_{0r} , depending on the type and distribution of the damping.

The "natural frequency" Ω_r' comes from the general form of the FRF expression which, combining all the previous cases, may be written in the form:

$$\alpha(\omega) = \sum_{r=1}^N \frac{C_r}{\Omega_r'^2 - \omega^2 + iD_r} \quad (3.125)$$

Here, C_r may be real or complex and D_r will be real; both may be constant or frequency dependent and Ω_r' will, in general, be different to both Ω_{0r} and Ω_r .

Table 3.1 summarizes systems with all the above mentioned types of damping.

3.2.3.6 Excitation by a General Force Vector

Now, a hysteretically damped MDOF system will be considered again. Its equation of motion in the case of harmonic excitation has the form (3.117):

$$[K + iH - \omega^2 M] \{X\} e^{i\omega t} = \{F\} e^{i\omega t}$$

If the system is excited simultaneously at several points (rather than at just one, as in the case of the individual FRF expression), the solution is given by eq. (3.118):

$$\{X\} = [K + iH - \omega^2 M]^{-1} \{F\} = [\alpha(\omega)]\{F\}$$

A more explicit solution can be derived in the form:

$$\{X\} = \sum_{r=1}^N \frac{\{\Phi\}_r^T \{F\} \{\Phi\}_r}{\Omega_r^2 - \omega^2 + i\eta_r \Omega_r^2} \quad (3.126)$$

This equation permits the calculation of one or more individual responses to excitation of several simultaneous harmonic forces, all of which must have the same frequency but may vary in amplitude and phase.

The resulting vector of responses is sometimes referred to as *forced vibration mode* or, more commonly, as *operating deflection shape* (ODS). When the excitation frequency is close to one of the system's natural frequencies, the ODS will reflect the shape of the nearby mode because one term in the series of (3.126) will dominate, but it will not be identical to it because of the contributions of all the other modes.

3.2.3.7 Excitation by a Vector of Mono-Phased Forces

Consider a special case where the structure will be excited by a vector of mono-phased forces. All the forces will have the same frequency and phase, only their amplitudes may differ. In this case, it would be of interest to know whether there exist some conditions under which it is possible to obtain a similarly mono-phased response (the whole system responding with a single phase angle).

So, let the force and response vectors be represented by:

$$\{f\} = \{F\} e^{i\omega t} \quad (3.127)$$

$$\{x\} = \{X\} e^{i(\omega t - \phi)} \quad (3.128)$$

where $\{F\}$ and $\{X\}$ are vectors of real quantities. Substituting them into equation of motion, (3.117) yields to :

$$[K + iH - \omega^2 M] \{X\} e^{i\omega t} \cdot e^{-i\phi} = \{F\} e^{i\omega t} \quad (3.129)$$

$$[K + iH - \omega^2 M] \{X\} \cdot e^{-i\phi} = \{F\}$$

$$[K + iH - \omega^2 M] \{X\} \cdot (\cos \phi - i \cdot \sin \phi) = \{F\} \quad (3.130)$$

After splitting (3.130) into real and imaginary part:

$$([K - \omega^2 M] \cos \phi + [H] \sin \phi) \{X\} = \{F\} \quad (3.131)$$

$$(-[K - \omega^2 M] \sin \phi + [H] \cos \phi) \{X\} = \{0\} \quad (3.132)$$

Equation (3.132) can be considered as an eigenvalue problem which has "roots" ϕ_s and corresponding "vectors" $\{k\}_s$. These may be inserted back into (3.131) in order to establish the form of the mono-phased force vector necessary to bring out the mono-phased response vector described by $\{k\}_s$. Thus, a set of N mono-phased force vectors is obtained, each of

which results in a mono-phased response characteristics, when applied as excitation to the system.

The equations used to obtain the above mentioned solution are functions of frequency and thus each solution applies only at one specific frequency, ω_s .

A situation of particular interest occurs when a phase lag ϕ between all the forces and all the responses is exactly 90° . In this case, the eq. (3.132) reduces to:

$$[K - \omega^2 M]\{X\} = \{0\} \quad (3.133)$$

Solving this equation, natural frequencies and mode shapes of an undamped system are determined. This is a very important result revealing that it is always possible to find a set of mono-phased forces which will cause a mono-phased set of responses and, moreover, if these two sets of mono-phased parameters are separated by exactly 90° , then the frequency at which the system is vibrating is identical to one of its undamped natural frequencies and the displacement shape is the corresponding undamped mode shape.

This very important result is the basis for many of the multi-shaker test procedures used to isolate the undamped modes of structures for comparison with the theoretical prediction. It is commonly used in the aircraft industry.

It should be emphasized that, by this method, undamped modes are directly obtained, whereas almost all other methods extract the actual damped modes of the system under test. The physical principle of this method is that the force vector is chosen so that it exactly balances all the damping forces whatever these may be and so the principle applies equally to all types of damping.

4. Modal Test

In this chapter, the procedure how to perform modal test will be discussed. This procedure involves three or four main stages:

- 1) preparation of the measured structure and creating a geometrical model for measurement
- 2) measurement itself
- 3) identification of modal parameters from the measured data
- 4) (verification of the obtained modal model, its comparison with a computational model etc.)

All these stages will be discussed step by step. It is clear that using various procedures in the individual stages will highly depend on the purpose of modal test (see chapter 1.1).

4.1 Preparation

4.1.1 Preparation of the Measured Structure

Various types of how to support the structure during measurement were briefly mentioned in chapter 1.4. Here, the individual possibilities will be discussed in more detail.

4.1.1.1 Free Support

Free support (free-free conditions) is theoretically such a type of support where the tested object is not attached to ground at any of its coordinates and is freely suspended in space. In theoretical analysis, a freely supported body exhibits 6 rigid body modes, i.e. 3 displacements in the direction of 3 coordinates and 3 rotations around the coordinate axes. All those six modes have the natural frequency equal to zero.

In practice, free support is realized either by putting the body on a very soft pad (e.g. foam) or suspending it on soft springs. It is obvious that frequencies of rigid body modes will not be equal to zero in that case, but the values will be very low. Such support is considered to be free if the highest natural frequency of rigid body modes is less than 10% of the value of the lowest deformation natural frequency. So, if the first bending mode of a beam is e.g. 150 Hz, all of the rigid body modes should be less than 15 Hz. When this condition is satisfied, the influence of support to deformation natural frequencies is negligible.

Damping of the individual modes, rather than natural frequencies, could be influenced by the support. Thus, if the measurement is performed with the aim to determine precise values of damping, the influence of the support could be minimized by placing soft suspension springs into nodal points. But, nodal points are different for each of the modes, so for obtaining as precise values of damping as possible it would be necessary to measure each mode with different placing of suspension springs.

Free support is both the simplest and the most suitable if the modal model obtained from measurements is to be compared with the computational modal model. Thus, it is worth to use it whenever it is possible.

4.1.1.2 Grounded (Fixed) Support

Grounded (fixed, clamped) support is theoretically such a type of support where some points on the body (some DOFs) are completely fixed by connecting to the ground. This could not be reached in practice, so the support is considered to be fixed if the response of the fixed DOFs is less than 10% of the response of the other DOFs. This type of support causes difficulties when comparing experimental modal model with the computational modal model, because the differences in both models could be caused namely by different boundary conditions. But, sometimes it is necessary to use this type of support, if modal properties have no importance when the structure is freely supported (e.g. for turbine blades).

Another difficulty with such a type of support is with repeatability of the measurements. Despite any effort (tighten the screws connecting the structure with the measurement base using a torque wrench, etc.), 100% repeatability is failing if disassembly and reassembly of the measurement base is performed. According to experience, natural frequencies of the individual modes could differ after such mount - demount in the range up to $\pm 5\%$.

4.1.1.3 Support in-situ

This type of support is the simplest as for preparation - there is no preparation, measurement is performed in the actual operational conditions. This type of support is used when there is no other possibility (when measuring a very heavy structure, large machine, etc.) or, when modal properties in operational conditions are of interest. It is clear that it is even more difficult to compare an experimental model with its computational model with this type of support than it is with fixed support.

4.1.2 Preparation of Experimental Model

In this chapter, a *model* will denote a geometrical model of the measured structure with defined points and degrees of freedom in which measurements are to be performed. This means no kind of mathematical model (spatial, modal or response).

A mesh of points representing the measured structure is to be selected. In each of these points, it should be decided in which directions the measurements are to be performed, i.e. degrees of freedom are to be defined. Most often, only the transversal degrees of freedom are measured (i.e. directions X, Y and Z). In special cases, rotational degrees of freedom could be measured as well, but these require special transducer and procedures that are not common and are not supported by most of modal software packages.

The density of the mesh of the measurement points highly depends on the frequency range of the measurements or, more precisely defined, on the number of modes that would be identified - it is important to consider that the higher the mode, the more nodal lines possess its mode shape and the more points are necessary to display it realistically. So, the rule for defining the density of the mesh (i.e. number of points) is: define just enough points to be able to reliably identify all of the modes in the measured frequency range, but not too many points (or DOFs), because redundant points mean a more time-consuming modal test.

It should be mentioned, that the density of mesh does not affect the precision of the obtained modal parameters! It only affects the quality of displaying mode shapes and thus the

possibility to identify them correctly. It is a completely different situation from finite element calculations where the density of the mesh highly influences the precision of the solution.

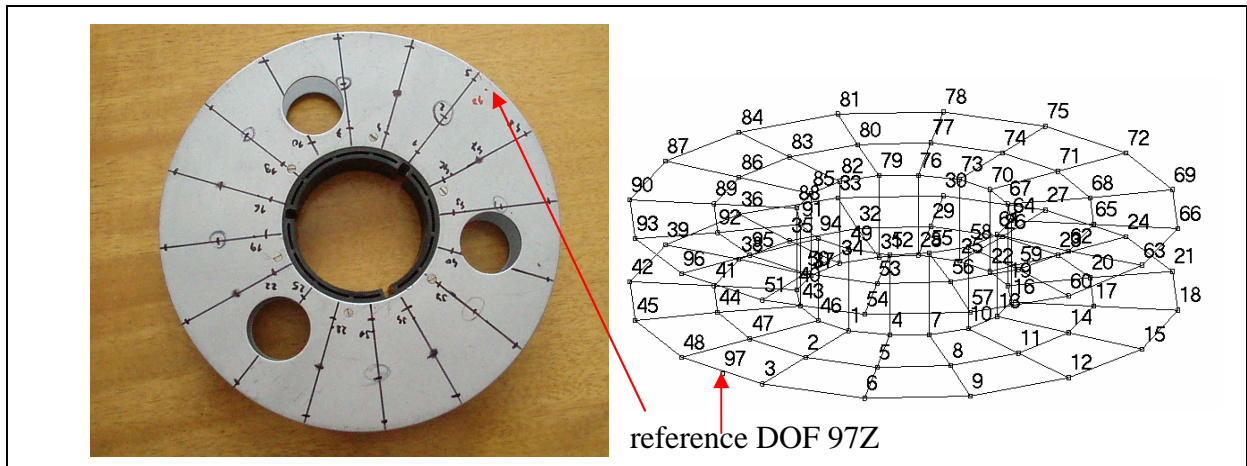


Fig. 4.1 Example of the Geometrical Model for Modal Test

A mesh of points should be drawn on the measured structure (see Fig. 4.1) and the same model should be created in the modal test software. Also, so-called *reference DOF* is to be defined - this is the DOF, in which point direct FRF is measured, which means that the DOF of excitation and of response is the same. When a modal test is performed using impact excitation, an accelerometer is usually fixed in the reference point. When a dynamic exciter is used for excitation, it is connected to the structure in the reference point. Requirements for the location of the reference point are somewhat contradictory:

1. It should be placed in a way that there is an adequate response by all of the modes so that the signal to noise ratio is as good as possible.
2. It should be placed in a way that the influence of attaching accelerometer or dynamic exciter is as low as possible.

It is obvious that these two requirements are in contradiction, because the highest influence on the structure caused by attaching accelerometer or exciter would be at position, where the structure exhibits the highest response. Thus, in practice it is necessary to choose a reasonable compromise between those two requirements. Moreover, when the mass of accelerometer in comparison to the mass of the measured structure is negligible, its influence is also negligible.

The first requirement is related to the fact that one must be careful that the reference point would not also be a nodal point of one mode from those which are of interest. In this case, the response of this mode is zero and it would not be possible to identify it. One of the ways to avoid this situation is to approximately know the mode shapes in advance, e.g. from a computational model. Another option, if mode shapes are not known and can not be estimated, is to try different locations of the reference point before the entire modal test and watch if the number of resonances in the measured FRF is stable. If some of the resonances disappears at any point, it means that at this point is a nodal point of the particular mode shape and that this point can not serve as a reference.

4.2 Measurement Techniques

This chapter deals with measurement techniques which are used for modal testing. There are two types of vibration measurement:

- Those in which just one type of parameter is measured (usually the response levels)
- Those in which both input and response output parameters are measured.

According to the basic relationship:

$$\text{RESPONSE} = \text{PROPERTIES} \times \text{INPUT}$$

it is clear that only when two of the three terms in this equation have been measured, it can be defined completely what is going on in the vibration of the test object. If we measure only the response, we are unable to say whether a particularly high response level is due to a strong excitation or to a resonance of the structure. Nevertheless, both types of measurements have their applications and much of the equipment and instruments used is the same in both cases.

This text is focused on the second type of measurement, where both excitation and response are measured simultaneously so that the basic equation can be used to deduce the system properties directly from the measured data. Within this category there are a number of different approaches which can be used, but it should be started with a method referred as the *single-point excitation* (although this point may change its location during the modal test). Using this method, either one row or one column of the frequency response function matrix is measured. There are two principally identical modifications of the single-point excitation method:

- SISO (Single Input Single Output)
- SIMO (Single Input Multiple Output) - the number of outputs (responses) depends on the number of channels that are at disposal on the analyzer, i.e. how many responses can be captured simultaneously. The principle of signal post-processing is the same as for SISO - the classical FRF is used according to eq. (1.1).

Another type of measurement is so called MIMO (Multiple Input Multiple Output), during which excitation at multiple points is applied simultaneously. This type of measurements is essential for modal testing in these cases:

- Large structures that are impossible to be excited using only one exciter.
- Complex structures that exhibit local modes. Local modes are modes when only a part of structure vibrates and it is impossible to excite all these modes simultaneously with a single exciter.
- Symmetrical structures that exhibit multiple modes (two or more modes at the same frequency). In order to isolate these modes, it is necessary to have as many reference points as is the number of modes at the same frequency.

MIMO method is a common standard in aircraft and automotive industries, but it has a slightly different theoretical background than single-point excitation and thus it will not be discussed in detail in this text.

4.2.1 Basic Measurement Setup

The experimental setup used for FRF measurements basically consists of three or four major items:

- an excitation mechanism
- a transduction system, to measure the various parameters of interest
- an analyzer, to extract the desired information form the measured signals
- (computing system, to post-process the measured data, extract modal parameters, animate mode shapes etc.)

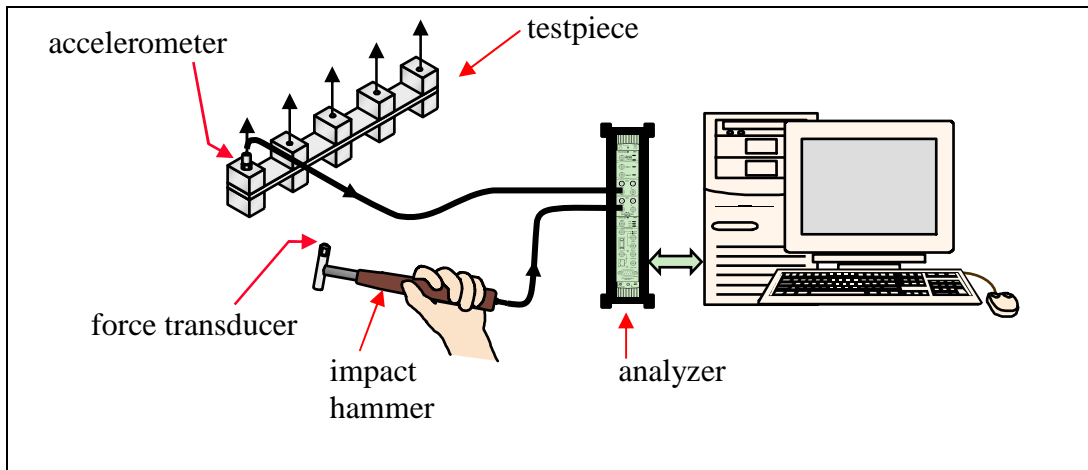


Fig. 4.2 Experimental Setup Where Impact Hammer is Used for Excitation

A typical experimental setup for excitation using impact an hammer is shown in Fig. 4.2. In this case, the accelerometer is fixed in the reference point and the structure is subsequently excited at all the points. It provides one row of the FRF matrix. A typical experimental setup for excitation using dynamic exciter is shown in Fig. 4.3. In this case, the exciter is fixed in the reference point and the response is subsequently measured at all the points (or at all the points simultaneously, depending on how many analyzer's channels are at disposal). It provides one column of the FRF matrix.

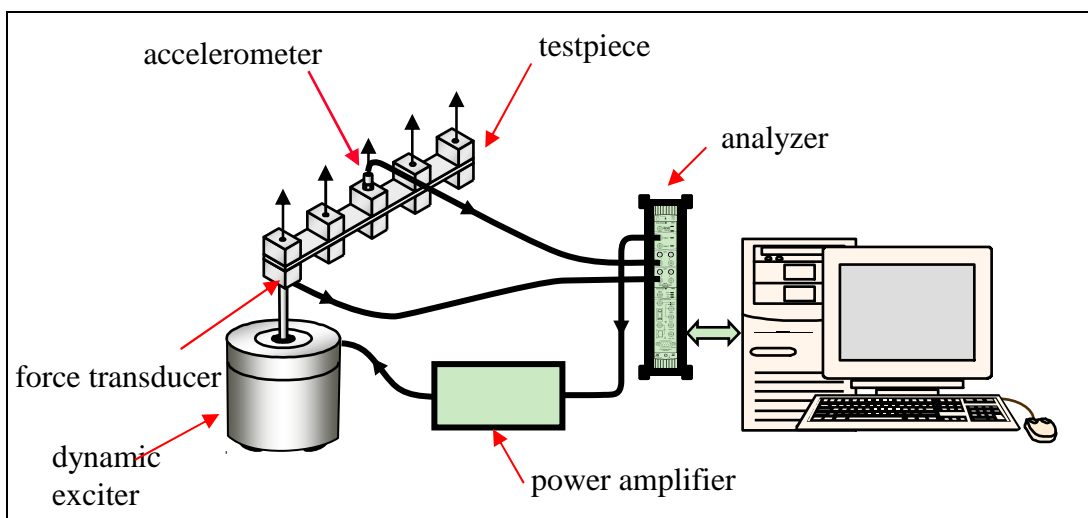


Fig. 4.3 Experimental Setup Where Dynamic Exciter is Used for Excitation

4.2.1.1 Excitation Techniques

There are several ways how to excite vibration of a structure. They can be divided into two major groups:

1. impact excitation

- using impact (modal) hammer - the most common method
- releasing from the deformed position - e.g. by cutting across the suspension cable
- hitting by a falling mass
- using a pendulum impactor

2. excitation using an attached exciter

- electromagnetic exciter - the most common method
- electro-hydraulic exciter
- mechanical exciter - eccentric rotating masses

There are other, non-standard excitation methods that are used for large structures (bridges, off-shore platforms etc.):

- using jet engines
- natural excitation (by wind, sea waves, traffic)

They are used in so called *operational modal analysis* (see chapter 6) and lead to an unscaled modal model.

4.2.1.1.1 *Impact Excitation Using Impact Hammer*

Using an impact hammer is the simplest and fastest way of exciting a structure into vibration. It requires no preparation work and thus is very suitable to use in operational conditions. Moreover, it does not influence the structure by attaching the exciter, which is an advantage itself.

The hammer consists of a head, force transducer, tip and handle. An impactor can also be used - it is basically a hammer without a handle (see Fig. 4.4). The equipment of a hammer is usually completed with a set of tips of different stiffness and with a set of heads of different masses. A force transducer detects the magnitude of the force felt by the impactor which is assumed to be equal and opposite to that experienced by the structure.

The magnitude of the impact is basically determined by the mass of the hammer head and the velocity with which it is moving when it hits the structure. The operator controls the velocity rather than the force level itself, and so an appropriate way of adjusting the order of the force level is by varying the mass of the hammer head.

The frequency range which is effectively excited by this type of device is controlled by the stiffness of the contacted surfaces and the mass of the hammer head: there is a system

resonance at a frequency given by $\sqrt{\frac{\text{contact stiffness}}{\text{impactor mass}}}$ above which it is difficult to deliver

energy into the test structure. When the hammer tip impacts the test structure, this will experience a force pulse which is substantially that of a half-sine shape, as shown in Fig. 4.5 (left). A pulse of this type has a frequency content of the form illustrated in Fig. 4.5 (right)

which is essentially flat up to a certain frequency (f_c) and then it is of uncertain strength above this frequency. This means that it is relatively ineffective at exciting vibrations in the frequency range above f_c and so it is necessary to have some control over this parameter. It can be shown that there is a direct relationship between the first cut-off frequency, f_c , and the duration of the pulse, T_c , and that in order to raise the frequency range it is necessary to induce a shorter pulse length. This, in turn, is related to the stiffness (not the hardness) of the contacting surfaces and the mass of the impactor head. The stiffer the materials, the shorter will be the duration of the pulse and the higher will be the frequency range covered by the impact. Similarly, the lighter the impactor mass, the higher the effective frequency range. It is for this purpose that a set of different hammer tips and heads are used to enable the regulation of the frequency range. Generally, it can be said that a tip as soft as possible has to be used in order to supply input energy only to the frequency range of interest. Using a stiffer tip than necessary leads to the fact that the supplied energy causes vibrations outside the frequency band of interest at the expense of those within this zone.

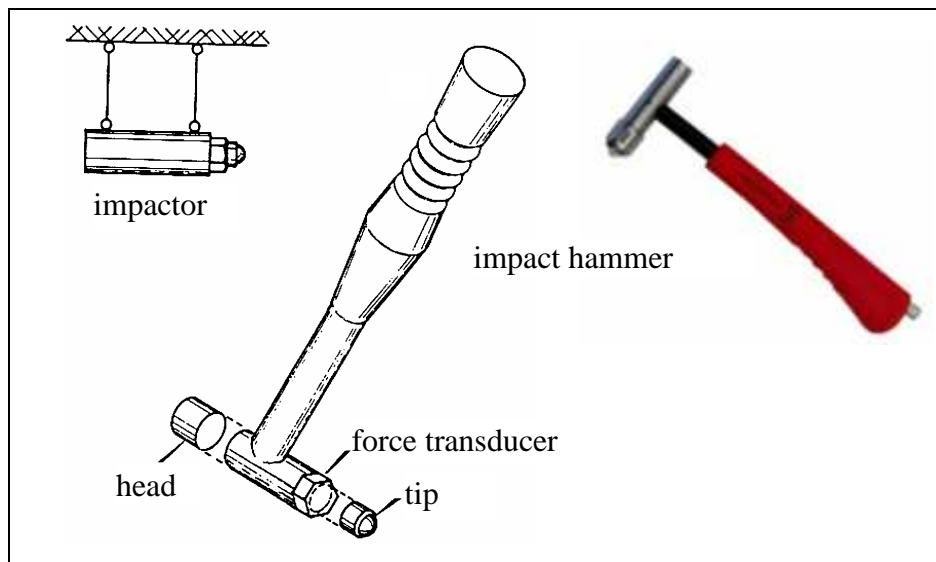


Fig. 4.4 Impactor and Impact Hammer Details

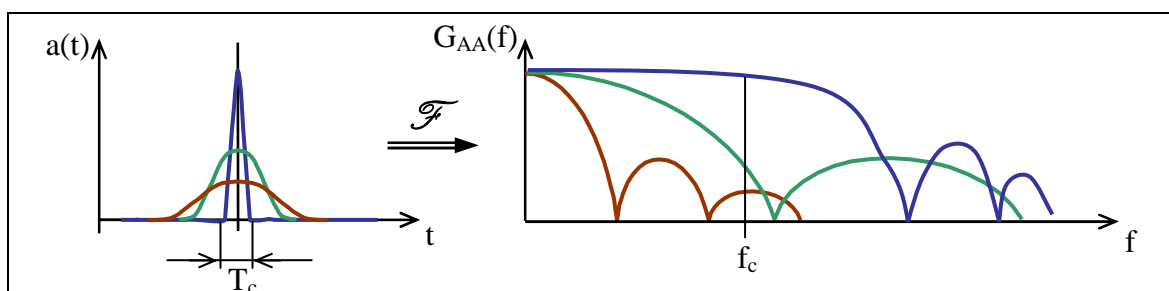


Fig. 4.5 Impact Force Pulse and its Spectrum

There are some disadvantages associated with using an impact hammer:

- Control of the frequency range of excitation is limited and, moreover, it is rarely possible to use frequency zoom.
- Crest factor is very high and due to a high peak level of the acting force there is a danger of causing a local damage to the structure and exciting its nonlinear behaviour.

- Window (weighting) functions have to be used both for input and output signal.

When using impact excitation, different weighting functions are used for input and output signals. The input signal is weighted with *transient window* that serves for suppressing noise to zero in the time period when the impact force is not acting but the measurement of response is in progress. In order to be sure that the shift and length of the transient window are set correctly, it is worth to expand the vertical axis so that level of noise is visible. For the output signal (response), exponential window is often used to improve the analysis by minimizing leakage error that is caused by truncating the time signal. The length of the exponential window (its time constant τ) should be set with regard to the requirement that the signal at its end should be attenuated to the level of noise or at least by 40 dB. The windows for both signals should started at the same time if there is no system delay. Weighting windows are shown in Fig. 4.6.

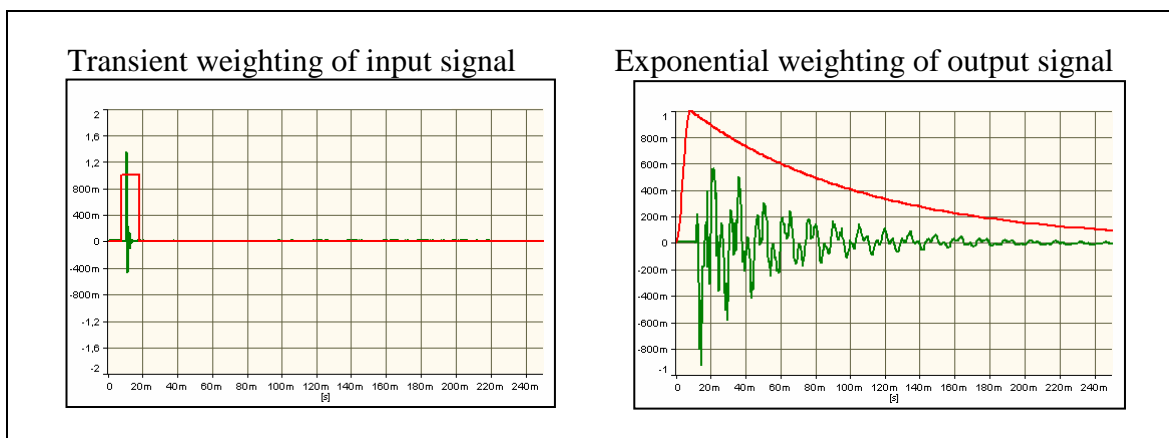


Fig. 4.6 Weighting Windows for Impact Excitation

By applying exponential weighting, an electronic damping is added to the system. Under this condition, the damping value determined by measurement will be over-estimated and for obtaining the true value, compensation for the exponential window should be performed (see Fig. 4.7).

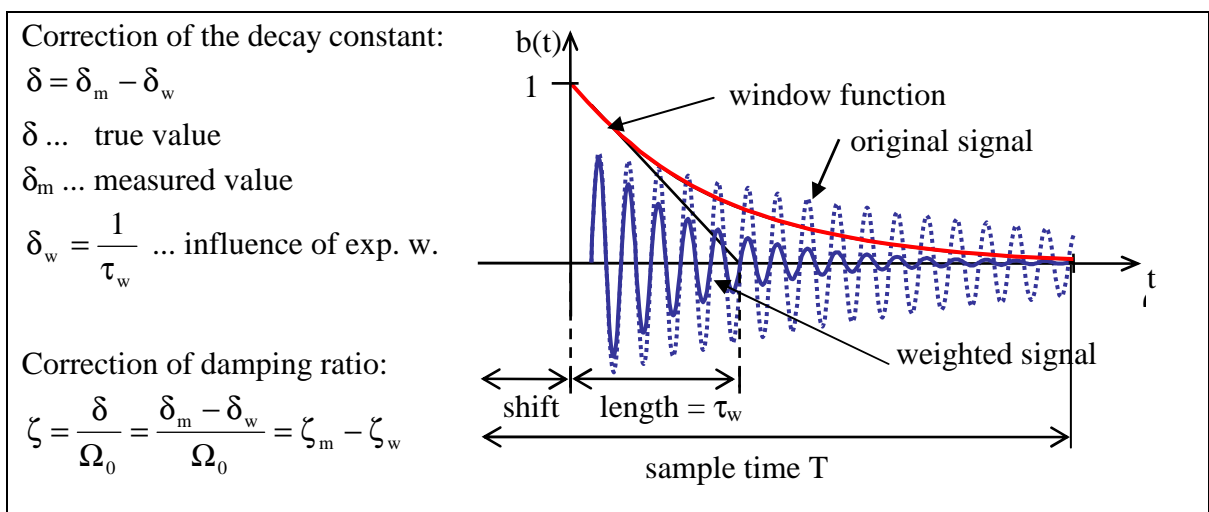


Fig. 4.7 Compensation for Exponential Weighting

Some of the disadvantages of application of impact hammer excitation can be avoided by applying so-called *random impact excitation*. This means several consecutive hits during the record (see Fig. 4.8). In this case, Hanning window is used both for input and output signals in order to push the signals to zero in their edges and minimize the error caused by leakage. As the windows applied to the input and output signals are the same, their influence on FRF will be cancelled out and no compensation for weighting window is necessary when damping is estimated.

Random impact excitation introduces more energy than a single impact during one record and the crest factor is lower. All advantages of impact excitation remain unchanged, namely its easy use in operational conditions. Moreover, this type of excitation may be used for measurements in a narrow frequency band or with frequency zoom. In these cases, record time is quite long and if only a single impact was used, the structure would vibrate for much shorter time period than the measurement period was. By applying more hits, this problem is avoided, but still there is a risk that most of the energy supplied to the structure will be out of the measurement range, because control over the frequency range of excitation is always limited when an impact hammer is used.

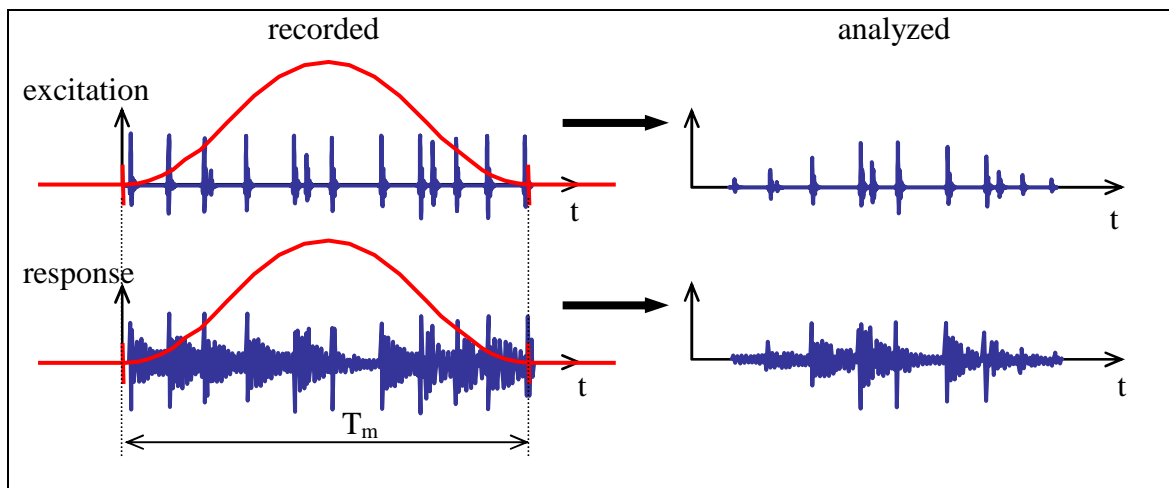


Fig. 4.8 Signals Involved in Random Impact Excitation

4.2.1.1.2 Excitation with the Help of Dynamic Exciter

Perhaps the most common type of exciter is the *electromagnetic* (or electrodynamic) *shaker* in which the supplied input signal is converted to an alternating magnetic field where a coil is placed which is attached to the drive part of the device and to the structure. In this case, the frequency and amplitude of excitation are controlled independently of each other, giving more operational flexibility. It is useful because it is often better to vary the level of the excitation as resonances are passed through. However, it must be mentioned that electrical impedance of these devices varies with the amplitude of motion of the moving coil and so it is not possible to deduce the excitation force either from a measurement of the voltage applied to the shaker or by measuring the current passing through the shaker because this measures the force applied not to the structure itself, but to the assembly of structure and shaker drive. The difference between this force and that applied to the structure is quite small, but near the resonance a very little force is required to produce a large response and without altering the

settings on the power amplifier or signal generator, there is a marked reduction in the force level at frequencies adjacent to the structure's natural frequencies. As a result, measurement of force at frequencies adjacent to natural frequencies inclines to be contaminated by noise. So, the force acting on the structure should be measured as close as possible to the structure's surface, the same as with impact excitation.

Generally, the larger the shaker, the greater the force which may be generated for exciting the structure, but the working frequency range is limited at the same time. An effective excitation is possible only as long as the moving parts of the exciter remain a rigid mass. Once the frequency of vibration approaches and passes the first natural frequency of the coil and drive platform, there is a severe attenuation of the force which is available for driving the test object and although some excitation is possible above this critical frequency, it does impose a natural limit on the useful working range of the device. This frequency is of course lower for larger shakers.

In special cases, it is appropriate to use an *electrohydraulic exciter*. These are cases of testing structures or materials, the normal vibration ambience of which is associated with higher static load that may quite often alter their dynamic characteristics or even their geometry. An advantage of electrohydraulic exciters is their ability to apply simultaneously a static load as well as dynamic vibratory load that is necessary in such cases. Another advantage that may hydraulic exciters offer is the possibility of providing a relatively long stroke, thereby permitting the excitation of structures at large amplitudes. On the other hand, hydraulic exciters tend to be limited in operational frequency range above 1 kHz, whereas electromagnetic exciters can operate well into the 30-50 kHz region, depending on their size. Hydraulic exciters are more complex and expensive, although generally compact and lightweight compared with electromagnetic exciters.

Another type of exciter that is worth to be mentioned is a *mechanical exciter*. It is realized by means of eccentric rotating masses (unbalances) and it is able to generate the prescribed force at various frequencies, although its control is not much flexible. The amplitude of the exciting force is given by the unbalanced mass and it can be changed only by changing either the mass or its radius which both is impossible to perform during operation. This type of exciter is also relatively ineffective at lower frequencies, because the exciting force depends on the square of rotational speed. However, if vibration amplitudes caused by this type of exciter is not too large in reference to the orbit of rotating mass, amplitude and phase of the excitation force are exactly known and require no additional measurements unlike other type of exciters. A mechanical exciter is used to measure large structures such as bridges or bedplates of turbogenerators.

Attachment of an Exciter to a Structure

When using an electromagnetic or electrohydraulic exciter, it is necessary to connect the driving platform of the shaker to the structure, usually incorporating a force transducer. Some precautions must be taken in order to avoid the introduction of unwanted excitations or inadvertent modification of the structure. From the definition of a single FRF as a ratio between the harmonic response at DOF \mathbf{j} caused by a single harmonic force applied in DOF \mathbf{k}

it is evident that this single force must be the only excitation of the structure and this requirement should be met in the modal test. Although it may seem that the exciter is capable of applying the force in one direction only, as it is essentially a unidirectional device, there exists a problem on most practical structures whose motion is generally complex and multidirectional. The problem is that when pushed in one direction, the structure responds not only in the same direction but also in others. Such motion is expected but it is possible that it can give rise to a secondary form of excitation if the shaker is incorrectly attached to the structure.

The moving part of the shaker is usually very mobile along the axis of its drive but very stiff in the other directions. Thus, if the structure wishes to respond both in line of action of the exciter and in lateral direction, then the stiffness of the exciter will cause resisting forces or moments to be generated which are, in effect, exerted on the structure in the form of secondary excitation. The response transducers know nothing of this and they pick up the total response, which is caused not only by the driving force which is known, but also by the secondary and unknown forces.

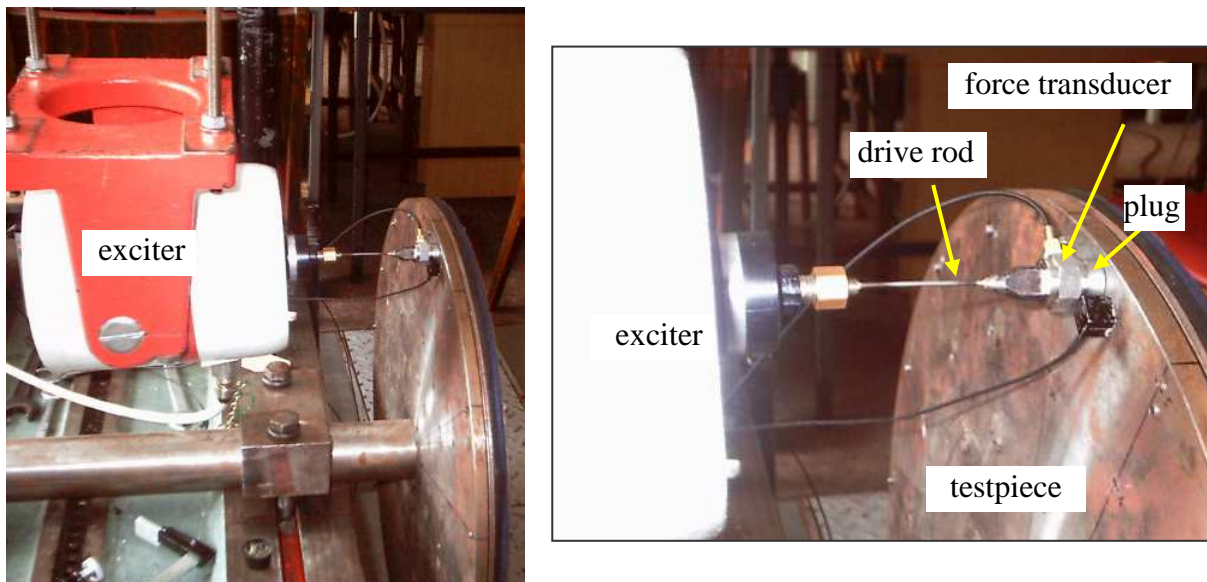


Fig. 4.9 Exciter Attachment and Drive Rod Assembly

The solution is to attach the shaker to the structure through a *drive rod* or similar connector which has the characteristic of being stiff in one direction (that of the intended excitation) while at the same time being relatively flexible in the other five directions. A suitable drive rod, or *stinger*, is shown in Fig. 4.9. It is made of 1 mm diameter wire of the length of about 10 to 50 mm. Care must be taken not to over-compensate: if the drive rod is too long or too flexible, it begins to introduce the effects of its own resonances into the measurements and contaminates the genuine data.

Another requirement that has to be met in order to have the precise measurements of the excitation force is to place the force transducer as close to the measured structure as possible. Correct arrangement of the connection that is necessary for reliable FRF measurements is shown in Fig. 4.10 and also in a practical example in Fig. 4.9.

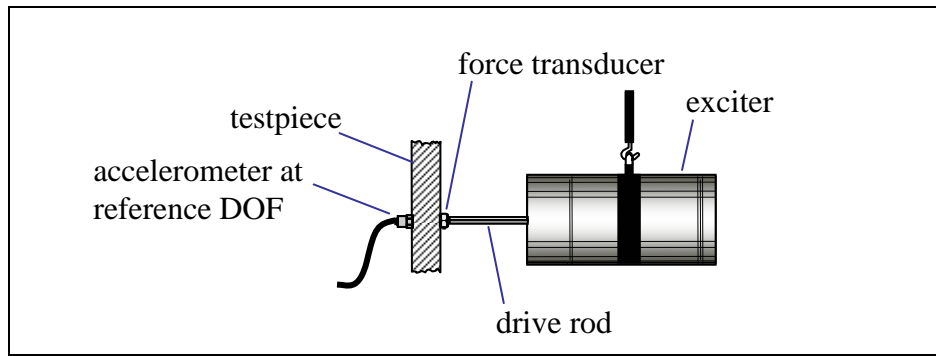


Fig. 4.10 Placing of Force Transducer and Attachment of the Exciter to the Testpiece

Another consideration which concerns the shaker is the question of how it should be supported, or mounted, in relation to the test structure. Several possibilities are shown in Fig. 4.11 - three of them are acceptable and one is unsatisfactory. Generally, it can be said that either the shaker or the structure should be freely supported.

In Fig. 4.11 (left), and also in Fig. 4.12, the shaker is fixed to the ground while the test structure is supported by a soft suspension. It is the most satisfactory arrangement and it is often used for light structures that can be supported freely. In the middle of Fig. 4.11, two arrangements in which the shaker is resiliently supported are shown. In this case, the measured structure can be either grounded or freely supported. The problem with this arrangement is that the reaction force causes a movement of the shaker body which, at low frequencies, can be of large displacement. This in turn causes a reduction in the force acting on the structure and thereby adding an additional inertia mass to the shaker may be necessary.

The arrangement in Fig. 4.11 (right) is unsatisfactory for the modal test, because reaction forces in shaker's support introduce an additional excitation to the structure that is not measured by the force transducer.

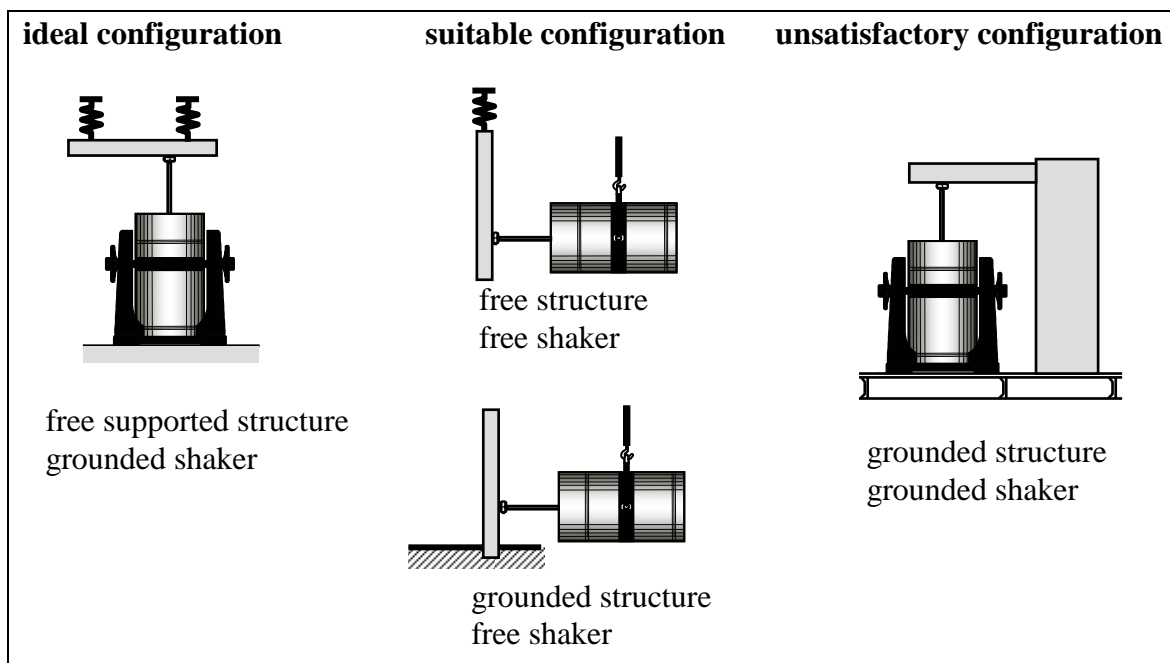


Fig. 4.11 Various Mounting Arrangements for Exciter with Respect to Reaction Forces



Fig. 4.12 Practical Realization - Free Structure, Fixed Exciter

4.2.1.1.3 Types of Excitation Signals

When an attached shaker is used for excitation, there are various possibilities regarding types of the excitation signals. The types of signals can be divided into (see Fig.4.13):

- harmonic (sinusoidal) - spectrum contains only a single frequency of the sinewave
- broadband - spectrum contains a band of frequencies. It further splits into:
 - impulse (transient)
 - single pulse (or impact)
 - periodic pulse
 - random impact
 - random
 - pseudorandom
 - swept sine (chirp)

Impulse excitation is mostly applied in the form of an impact or random impact using an impact hammer (see chapter 4.2.1.1.1), but it can also be applied with the help of an attached shaker. In this case, it would be most likely a single or periodic pulse. All of the above mentioned signals are usually provided by a signal generator which is usually part of the analyzer. The signal from the generator goes through the power amplifier, then to the dynamic exciter and then to the structure.

Note.: Swept sine signal can also be produced by a mechanical vibration exciter, while nature excitation by sea waves or road traffic produces a random signal.

Sine signal

The single sine signal of constant frequency can hardly be applied in modal tests. This type of signal can be used in the form of *stepped sine* in FRA analyzers (FRA = Frequency Response Analyzer) that, in contrast to FFT analyzers, do not perform the Fourier transform of signals, but directly measure the steady-state response of the system to the steady-state harmonic excitation. The frequency of excitation is changed step by step and the ratio of the response to the excitation is recorded. In this way, subsequently, the entire FRF in the

frequency range of interest is obtained. This procedure is very time consuming, but it is basically the only option if the nonlinearities in structures are to be examined in detail. The frequency range of the measurement can be set almost arbitrarily, thus this procedure is applied with the use of the frequency zoom to examine frequency regions near resonances.

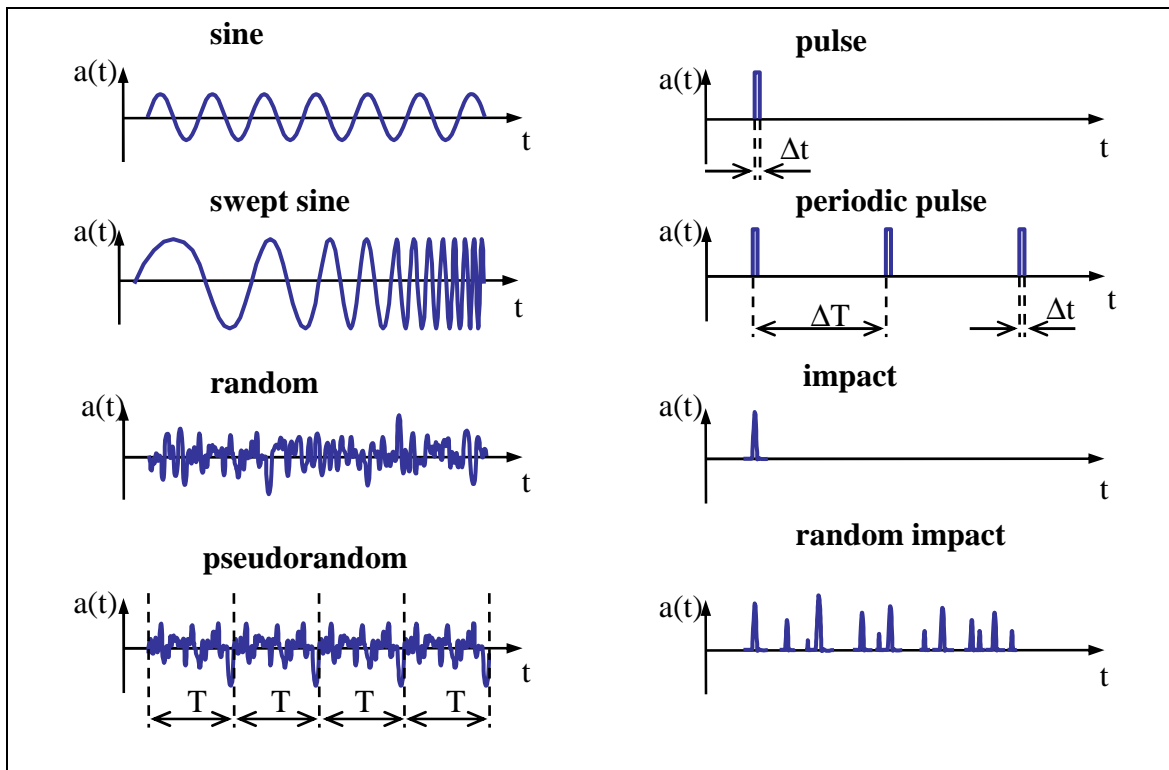


Fig. 4.13 Basic Types of Excitation Signals

Random Signal

Random signal is characterized by its power spectral density $G_{AA}(f)$ and the amplitude probability density $p(a)$ with Gaussian normal distribution (see Fig. 4.14). Crest factor and signal to noise ratio are quite good with this type of signal.

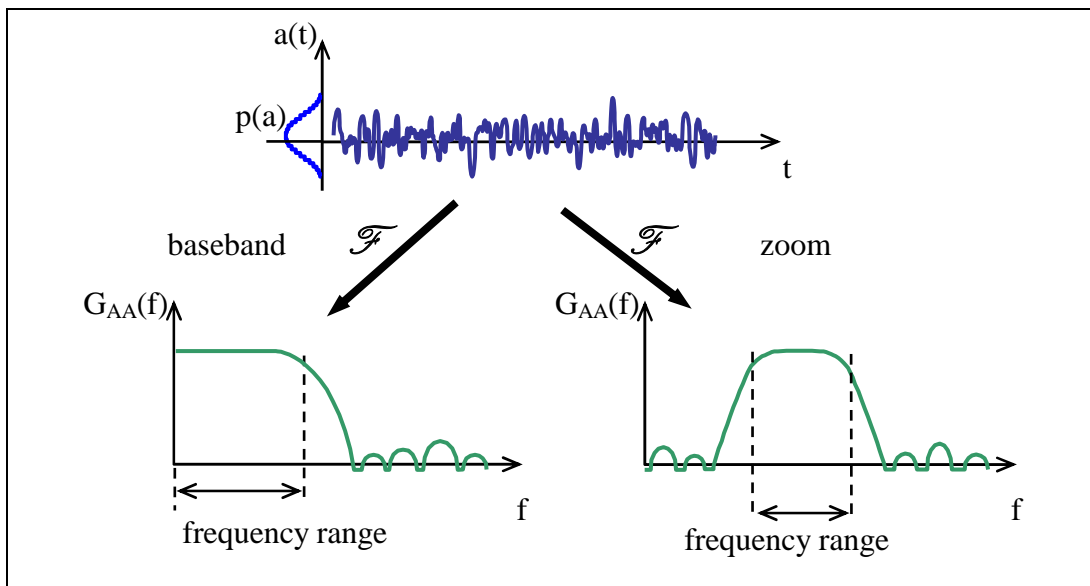


Fig. 4.14 Random Signal - Time History and Spectrum

Random signal can be generated in a limited frequency band according to the frequency range of interest. It can be used for baseband measurements as well as for zoom measurements. The signal is not periodic within the record time, so it is necessary to apply Hanning window to both input and output signals to minimize the leakage error. Changes in amplitudes and phases of the excitation signal are random, thus averaging is necessary. The influence of the eventual nonlinearities is averaged out and the ideal linearized FRF estimate is obtained.

Pseudorandom signal

Pseudorandom signal is essentially a piece of random signal that is repeating with the period **T**. This period is equal to the record length in the analyzer. Consequently, no leakage error occurs because the signal is periodic in the record time so that no weighting windows are necessary (rectangular window = no window). This implies that the signal only contains frequencies coinciding with the lines computed in the analyzer. Normally it is designed to have the same level in each line. At a given frequency, a system will always be excited at the same level since each recording contains the same information. Therefore no averaging of non-linearities can be obtained and this type of signal is only suitable for a perfectly linear system. As with the random signal, the pseudorandom signal can be used both for baseband and zoom measurements.

A special type of pseudorandom signal is a chirp signal. It is a swept sine signal with a high sweep rate when sweep from the minimal to the maximal frequency is repeated each period **T** and this period is equal to the record length.

4.2.1.2 Transducers Used for Excitation Force and Response Measurements

A detailed description of the individual types of transducers is not the subject of this text. It should only be emphasized here that each sensor measures exactly what is happening with it itself. It should be ensured by proper attachment of the sensor to the structure so that this would be the same as what is happening to the structure and what should be measured. Further, it is important to realize that each transducer has its own resonant frequency which mostly depends on the mass of the transducer and which is further more or less influenced by the attachment of the transducer to the structure. The effective frequency range in which a transducer may be used is to approximately 1/3 of the value of this frequency. Various ways of transducer attachment that are sorted according to how much they reduce the transducer's natural frequency (from the best to the worst) are:

- screw (stud)
- special cement
- thin double adhesive stud
- beeswax (up to 40° C only)
- magnet

Beeswax is very often used in modal tests for attachment of accelerometers because it is quite undemanding and quick and does not significantly reduce the effective frequency range of the transducer. On the contrary, attachment with the use of magnet is not appropriate and it

is mostly used for operational measurement but only up to about 1500 Hz. If a structure with a curved surface is to be measured, mounting with swivel base can be used.

When an impact hammer is used for excitation, a force transducer is an integral part of the hammer and it is not attached to the structure. When a dynamic exciter is used for excitation, a force transducer should be attached to the structure, as described in chapter 4.2.1.1.2. (Fig. 4.10). It is mostly attached with a screw. If it is not possible to drill a thread for a screw into the measured structure, it is possible to use so-called "plug". It is a small cylinder, one base of which is smooth and cemented to the surface of the measured structure and a screw thread is drilled into its second base. The force transducer is screwed into this thread as shown in Fig. 4.9.

Another aspect that should be considered in the context of selecting transducers for modal tests is the mass of the transducer in relation to the mass of the measured structure to avoid dynamic properties of the measured structure to be altered significantly by the transducer. It was already mentioned in chapter 4.1.2. regarding the selection of reference point, where the influence of transducer placement to the dynamic properties of the structure was discussed. Mass of the transducer plays a role especially in light structures. Generally, it should be less than 10% of the mass of the structure. From the principle of design of accelerometers, it is obvious that the smaller the transducer, the lower its sensitivity but higher the frequency range of the measurement. For special applications, it could happen that a transducer that would be light enough not to alter the structure would have at the same time inadequate sensitivity. In these cases, a non-contact transducer can be used, e.g. laser doppler vibrometer.

4.2.1.3 Analyzer

Two types of analyzers - FRA or FFT - can be used to perform modal tests.

Frequency Response Analyzer (FRA)

This type of analyzer has been already mentioned in chapter 4.2.1.1.3 in relation to the stepped-sine excitation. It does not perform Fourier transform of time signals. The principle of its operation is as follows: The source or *command* signal is a sine-wave at the desired frequency. Measured signals from the force and response transducers undergo a digital filtering process during which all components with frequency different to that of the command signal are eliminated. Non-synchronous component rejection is improved by filtering over a longer period of time. This is quantified by the number of cycles of the command signal during which the computations are performed. By this process, a very accurate measurement of the signal component at the desired frequency is obtained. FRF at the desired frequency is directly given by the ratio of amplitudes of the response and force signals. Then, the frequency of the command signal is changed by a step corresponding to frequency resolution and the process is repeated. Step by step, the entire frequency band of interest is measured. This is a very accurate and very time consuming measurement. That is why this type of analyzer is not commonly used for modal tests, but only for special applications, namely for studying non-linearities.

Fast Fourier Transform (FFT) Analyzer (frequency, spectral analyzer)

The principle of operation of this type of analyzer was described in detail in the chapter 2 - Dual-channel Analysis. Basic principles can be summarized as:

- All the frequency components present in the complex time varying signal are measured simultaneously.
- The output is a spectrum containing a finite number of components, describing the relative amplitudes of the entire range of frequencies present in the signal.
- Calculates additional functions and all calculations are based on the discrete Fourier transform.
- Signal should always be subjected to the anti-aliasing filter prior to entering the A/D converter.

4.2.2 Preparation of Measurement

After the tested structure is prepared (supported) and the geometrical model is created, the measurement can start. Remember that when a structure is excited with an attached shaker, the shaker and the force transducer are placed in the reference point (DOF) and the response transducer (usually accelerometer) is placed successively to all the points (see Fig. 4.15). If the number of measured DOFs is not greater than analyzer's channels that are at disposal, responses at all the DOFs can be captured simultaneously. In any case, one column of the FRF matrix is obtained.

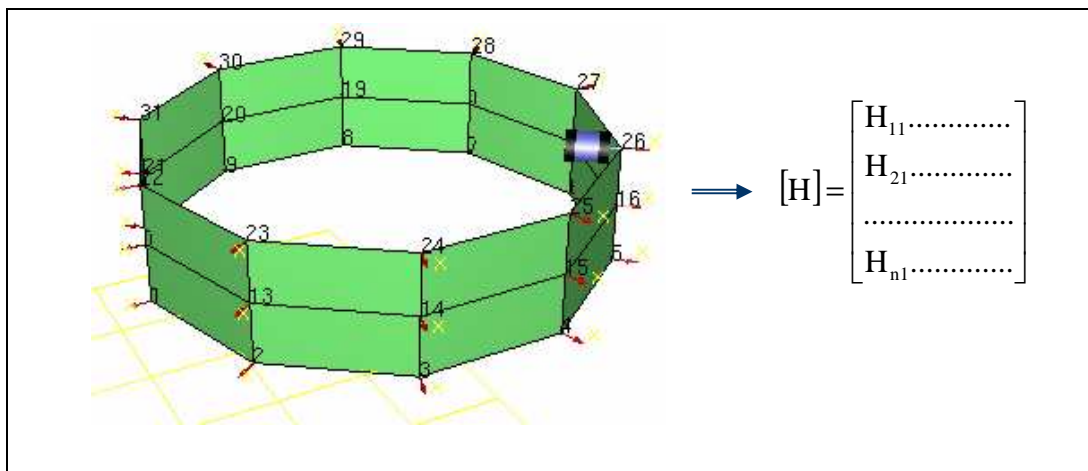


Fig. 4.15 Preparation of Measurements - Shaker Excitation

When hammer excitation is used, the accelerometer is usually placed in the reference point and the structure is excited successively in all the points, thus producing one row of the FRF matrix (see Fig. 4.16). However, this is not a strict rule. If the tested structure is quite complex and some of the DOFs that have to be measured are hardly accessible, it might be easier to place an accelerometer to them rather than to induce an impact in them. In that case, the structure might be excited with an impact hammer in a fixed (reference) point and the response accelerometer might be roving. Likewise, if a triaxial accelerometer is used to capture responses, it can not be used as reference, because only one degree-of-freedom is the reference one (supposing SISO or SIMO technique). Thus, when a triaxial accelerometer is

used, it is always a roving one and the DOF of excitation is fixed, regardless whether hammer or shaker excitation is applied.

Prior to starting with the entire modal test, it is appropriate to perform some checks in order to be sure that the measured data will be correct. With hammer excitation, it is simple to perform the reciprocity check. Theoretically, if a structure is excited in DOF i and the response is captured in DOF j , it should be the same as the reciprocal situation (excitation in DOF j and response in DOF i). In both case, an identical FRF should be obtained - $H_{ij}(f)=H_{ji}(f)$.

The most important check that should never be omitted is that of checking the accuracy of reference point measurement.

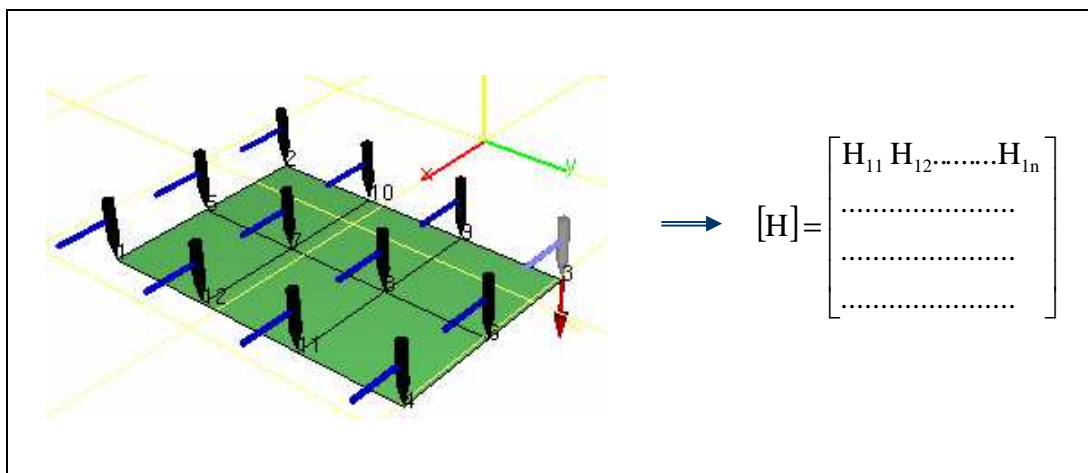


Fig. 4.16 Preparation of Measurements - Hammer Excitation

4.2.2.1 Reference Point Measurement

In chapter 4.1.2, the requirements regarding the reference point were discussed. It is a good idea to start a modal test with reference point measurement and to perform all the possible checks to ensure that this measurement is correct prior to continuing with measurements in all other points. One should always keep in mind that from low-quality data, it is not possible to obtain a reliable modal model whatever sophisticated post-processing is used. From this perspective, the care given to the initial checks of the accuracy of data appears to be excellent investment. The correct reference point should exhibit the following features (see Fig. 4.17):

- There is an antiresonance behind each resonance in an FRF plot when displayed in dB.
- In a phase FRF plot, the phase only varies in the range of 180° .
- In the plot of imaginary part of inertance or receptance and in the plot of real part of mobility, all the peaks are of the same signs.

There are some other requirements that apply to all measurements, not only to the reference point measurement. However, if they are satisfied for the reference point measurement, they are usually satisfied for all the other measurement as well. These are the following:

- Coherence function (eq. 2.10) should have the value as close to 1 as possible. Generally, this cannot be achieved in the whole frequency range. Usually, even for

good quality measurements, coherence in antiresonances is far below 1 (see Fig. 4.17) as a result of the fact that the level of the signal is at these frequencies comparable to the noise level. On the contrary, near resonances the coherence function use to be close to 1 even for measurements of lower quality.

- Nyquist plot should draw a distinct circle section for each resonance. In Fig. 4.17 (below) it can be seen that one of the modes (it is the first mode actually) didn't draw a very distinct circle. This is the sign of the leakage error and related insufficient frequency resolution of measurement. (Of course, it has its effect to coherence function as well.) This case will be discussed in more detail in chapter 4.3.1.2 after learning about modal circle properties.

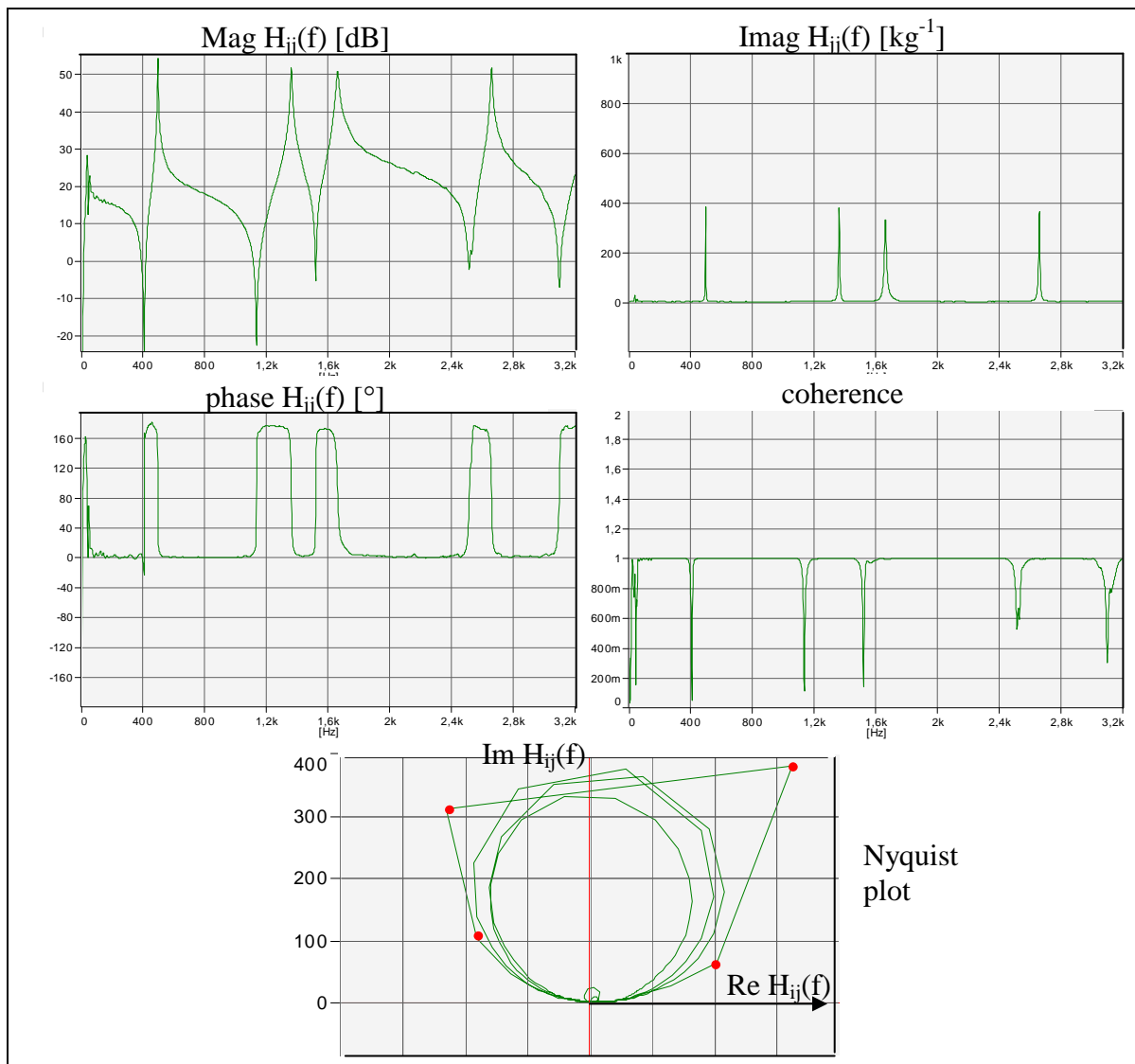


Fig. 4.17 Checking of Accuracy of Reference Point Measurement

4.3 Experimental Modal Analysis - Modal Parameters Identification

After acquiring all the data by performing measurements at all the DOFs, thus obtaining either one row or one column of the FRF matrix, modal analysis software is to be used to

post-process this data. This part of modal test is called *experimental modal analysis* as this is the stage of the experimental approach corresponding to the stages called *modal analysis* also in theoretical approach. In both cases, modal analysis leads to identification of modal properties of the system. However, it should be noticed that these two processes are somehow different: experimental approach deals with curve-fitting theoretical expressions to the actual measured data, while theoretical analysis deals with the eigenvalue problem.

Nowadays, a lot of software packages for the experimental modal analysis exist and the analyst is not supposed to carry out this stage without software support. In each software package, several methods for post-processing of the measured data are at disposal, and it is the responsibility of the analyst to choose the most appropriate method for each application. In increasing complexity, the methods involve the analysis of a part of a single FRF curve encompassing single resonance, then of a complete curve encompassing several resonances and, finally, of a set of many FRF plots all on the same structure. In every case, however, the task undertaken is basically the same: to find the coefficients in a theoretical expression for the FRF which most closely matches the measured data. This task is most readily tackled by using the partial fraction series-form for the FRF, as developed in chapter 3 for different types of system. The particular advantage of the series-form FRF approach is that the coefficients thus determined are directly related to the modal properties of the system under test, and these are generally the very parameters that are sought.

In this text, only three of all the existing methods will be described.

4.3.1 Single Degree-of-Freedom Approach

There are several modal analysis methods that exploit the same basic assumption: that in the vicinity of resonance, the entire response of the system is dominated by the nearest mode. These methods can be further divided into:

- those based on an assumption that all the response is given by this single mode (e.g. the simplest method call peak-amplitude or peak-picking)
- those based on an assumption that contribution of other modes are represented by a single approximation (e.g. the circle-fit method).

4.3.1.1 Peak-picking method

This is a method that works adequately for structures whose FRFs exhibit well separated modes which are not so lightly damped that accurate measurements at resonances are difficult to obtain but which, on the other hand, are not so heavily damped that the response at a resonance is strongly influenced by more than one mode. The applicability of this method is limited, but it can be useful in more difficult cases for obtaining initial estimates to the parameters required, thereby speeding up more general curve-fitting procedures which require starting estimates. This method is also used in identification of operational deflection shapes. Its application is as follows:

- 1) On the FRF plot, the individual resonant peaks are identified and frequencies with maximum response are considered to be natural frequencies Ω_r .
- 2) Local maximum value $|H|$ of FRF at the natural frequency is noted.
- 3) 3dB bandwidth $\Delta\omega$ is detected and damping value is determined from half-power points - ω_a and ω_b (eq. 3.40):

$$\eta_r = \frac{(\omega_a^2 - \omega_b^2)}{\Omega_r^2} \cong \frac{\Delta\omega}{\Omega_r} \qquad \eta_r = 2\zeta_r$$

- 4) An estimate for the modal constant can be obtained by assuming that the total response in the resonant region is attributed to a single term in the general FRF series (eq.

$$3.121): \alpha_{jk}(\omega) = \sum_{r=1}^N \frac{r A_{jk}}{\Omega_r^2 - \omega^2 + i\eta_r \Omega_r^2} \qquad \text{for } \omega = \Omega_r$$

Modal constant can be found from $|H| = \frac{A_r}{\Omega_r^2 \eta_r}$, thus $A_r = |H| \cdot \Omega_r^2 \eta_r$

4.3.1.2 Circle-fit Method

For the general SDOF system, a Nyquist plot of frequency response properties produces circle-like curves and in two special cases it produces an exact circle (mobility of the viscously damped system and receptance of the hysteretically damped system). The MDOF systems also produce Nyquist plots of FRF data which include sections of near-circular arcs corresponding to the regions near the natural frequencies. This characteristic provides the basis of one of the most important types of modal analysis - SDOF circle-fit method.

In this text, the described procedure will be based on a system with structural damping and thus the receptance form of FRF shall be used. However, if it is required to use a model incorporating viscous damping, then mobility form of FRF should be used. Although this gives a different general appearance to the plots - as they are rotated by 90° on the complex plane - most of the following analysis and comments apply equally to both cases. Some of the more discriminating modal analysis packages offer the choice between the two types of damping and simply take receptance or mobility data for the circle-fitting according to the selection.

The circle-fit method exploits the fact that in the vicinity of a resonance, the behaviour of most systems is dominated by a single mode. Algebraically, this means that the magnitude of the FRF is effectively controlled by one of the terms in the series, that being the one relating to the mode whose resonance is being observed. The assumption can be expressed as follows. From eq. (3.121):

$$\alpha_{jk}(\omega) = \sum_{s=1}^N \frac{s A_{jk}}{\Omega_s^2 - \omega^2 + i\eta_s \Omega_s^2} \qquad (4.1a)$$

This can be rewritten, without simplification, as

$$\alpha_{jk}(\omega) = \frac{r A_{jk}}{\Omega_r^2 - \omega^2 + i\eta_r \Omega_r^2} + \sum_{s=1, s \neq r}^N \frac{s A_{jk}}{\Omega_s^2 - \omega^2 + i\eta_s \Omega_s^2} \qquad (4.1b)$$

The SDOF assumption is that for a small range of frequency in the vicinity of the natural frequency of the r^{th} mode, the second of the two terms in (4.1b) is nearly independent of frequency ω , and the expression for the receptance may be written as:

$$\alpha_{jk}(\omega)_{\omega \approx \Omega_r} \cong \frac{{}_r A_{jk}}{\Omega_r^2 - \omega^2 + i\eta_r \Omega_r^2} + {}_r B_{jk} \quad (4.2)$$

The total receptance plot may be treated as a circle with the same properties as the modal circle for the specific mode in question but which is displaced from the origin of the complex plane by an amount determined by the contribution of all the other modes. It cannot be said that other modes are unimportant or negligible - quite the reverse, their influence can be considerable - but rather that their combined effect can be represented as a constant term around this resonance.

Properties of modal circle:

Assuming a system with structural damping, the basic function under consideration is:

$$\alpha(\omega) = \sum_{r=1}^N \frac{1}{\Omega_r^2 \cdot \left(1 - \left(\frac{\omega}{\Omega_r} \right)^2 + i\eta_r \right)} \quad (4.3)$$

since the only effect of including the modal constant ${}_r A_{jk}$ is to scale the size of the circle (by $|{}_r A_{jk}|$) and to rotate it (by $\angle {}_r A_{jk}$). A plot of the quantity $\alpha(\omega)$ is given in Fig. 4.18. It can be seen that for any frequency ω , following relationships may be written:

$$\text{tg}(\gamma) = \frac{\text{Im}(\alpha)}{\text{Re}(\alpha)} = \frac{\eta_r}{1 - \left(\frac{\omega}{\Omega_r} \right)^2} \quad (4.4a)$$

$$\text{tg}(90^\circ - \gamma) = \frac{\text{Re}(\alpha)}{\text{Im}(\alpha)} = \text{tg}(\theta/2) = \frac{1 - \left(\frac{\omega}{\Omega_r} \right)^2}{\eta_r} \quad (4.4b)$$

from which is obtained:

$$\omega^2 = \Omega_r^2 \cdot (1 - \eta_r \cdot \text{tg}(\theta/2)) \quad (4.4c)$$

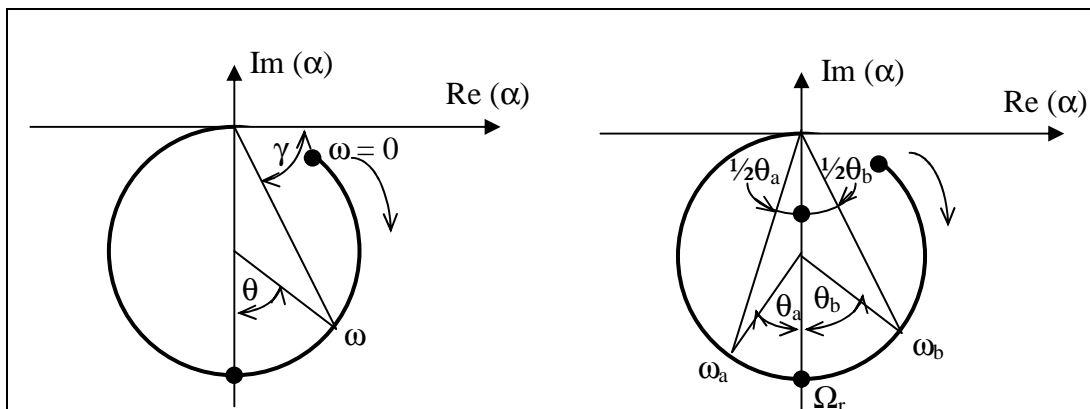


Fig. 4.18 Properties of Modal Circle

Differentiating the equation 4.4c with respect to θ yields to:

$$\frac{d\omega^2}{d\theta} = -\frac{\Omega_r^2 \cdot \eta_r}{2} \cdot \left(1 + \frac{\left(1 - \left(\frac{\omega}{\Omega_r} \right)^2 \right)^2}{\eta_r^2} \right) \quad (4.5)$$

The reciprocal of this quantity is the measure of the rate at which the locus sweeps around the circular arc. It can be seen to reach a maximum value (maximum sweep rate) when $\omega = \Omega_r$, the natural frequency of the mode. This is shown by further differentiation, this time with respect to the frequency:

$$\frac{d}{d\omega} \left(\frac{d\omega^2}{d\theta} \right) = 0 \quad \text{pro} \quad \Omega_r^2 - \omega^2 = 0 \quad (4.6)$$

The above property proves useful in analysing MDOF systems data since, in general, it is not known exactly where is the natural frequency, but if relative spacing of the measured data points around the circular arc near each resonance can be examined, it should be possible to determine its value.

Damping can be determined with the help of two points on the circle - ω_a above resonance and ω_b below resonance. Substituting to (4.4b) leads to:

$$\text{tg}(\theta_b / 2) = \frac{1 - \left(\frac{\omega_b}{\Omega_r} \right)^2}{\eta_r} \quad \text{tg}(\theta_a / 2) = \frac{\left(\frac{\omega_a}{\Omega_r} \right)^2 - 1}{\eta_r}$$

and from these two equations, an expression for the damping of the mode can be obtained:

$$\eta_r = \frac{\omega_a^2 - \omega_b^2}{\Omega_r^2 \cdot (\text{tg}(\theta_a / 2) + \text{tg}(\theta_b / 2))} \quad (4.7)$$

This is an exact expression, and applies for all levels of damping. If light damping is considered (loss factor about 2-3%), the expression (4.7) simplifies to:

$$\eta_r \cong 2 \cdot \frac{\omega_a - \omega_b}{\Omega_r \cdot (\text{tg}(\theta_a / 2) + \text{tg}(\theta_b / 2))} \quad (4.8)$$

When the two point are considered for which $\theta_a = \theta_b = 90^\circ$ (the half-power points), the familiar formula is obtained:

$$\eta_r = \frac{\omega_2 - \omega_1}{\Omega_r} \quad (4.9a)$$

or, if the damping is not light:

$$\eta_r = \frac{\omega_a^2 - \omega_b^2}{2\Omega_r^2} \quad (4.9b)$$

The final property relates to the diameter of modal circle that is for the quantity specified by the eq. (4.3) given as $\frac{1}{\Omega_r^2 \eta_r}$. When scaled by a modal constant added in the numerator, the diameter will be:

$${}_r D_{jk} = \frac{|{}_r A_{jk}|}{\Omega_r^2 \cdot \eta_r} \quad (4.10)$$

and, as mentioned before, the whole circle will be rotated so that the principal diameter - the one that passes through the point pertinent to the natural frequency - is oriented at an angle $\angle {}_r A_{jk}$ to the negative imaginary axis. This means that if A is negative, the circle will lie in the upper half-plane and this is a situation that cannot arise for a point FRF, only for a transfer FRF. The constant ${}_r B_{jk}$ from the eq. (4.2) is determined as a distance of the "top" of the main diameter of the modal circle from the origin (see Fig. 4.19).

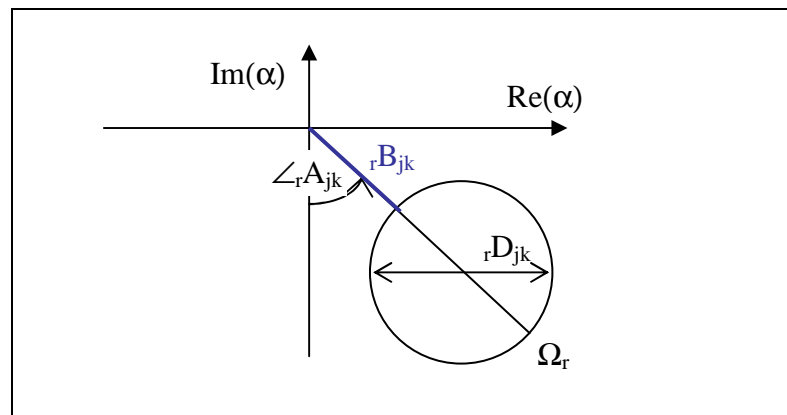


Fig. 4.19 Shift and Rotation of the Modal Circle

When modal parameters are extracted from the measured data, typically not the whole modal circle is available. For a system with well separated modes it can be expected that each resonance will form a larger part of circle, but with increasing modal interference when close modes or high level of damping occurs, it should be expected that only small circular sections will be detectable (maybe 45° or 60°). If the Nyquist plot will not form a distinct circular section in the vicinity of the resonance, the identification of modal parameters is problematic.

In Fig 4.17 (at the bottom) is the Nyquist plot from measurement of a system with well separated modes. It is the reference point measurement and all the other plots in this figure indicate measurement of sufficient quality. However, the Nyquist plot of the first mode did not form a distinct circular part. In this case, it is due to leakage error and associated insufficient frequency resolution. In the figure, four points closest to the resonance are marked with the red colour and it can be seen that the sweep rate around the resonance is so high that it did not manage to form a circle. From this measurement, the accurate value of natural frequency could be identified without any problem, but the damping estimate would not be reliable. To fix this situation, the frequency range of the measurement should be decreased. This will cause prolonging of the measurement time, consequently suppressing leakage error and obtaining finer frequency resolution of the measurement.

4.3.2 MDOF System Approximation Methods

There is a lot of situations in which the SDOF approach to the modal analysis is either inadequate or inappropriate. Several alternative methods that can commonly be classified as multi degree-of-freedom approximation can be used in these cases.

One of the particular cases is that for very lightly damped systems, for which measurements in resonances are inaccurate and difficult to obtain. These are not of concern of this text.

The opposite case represents systems with very closely coupled modes, for which approximation by a single mode is inappropriate. By closely coupled modes are meant those modes whose natural frequencies are very close to each other or which are relatively heavily damped or both. With these systems, the response is not determined by a single mode (or by one member of FRF series) even in resonance. Here, either a simple extension of a SDOF method or a general approximation approach can be used. Its principle will be briefly described below.

General approximation approach

The individual measured FRF data will be denoted as:

$$\alpha_{jk}^m(\omega_\ell) = \alpha_\ell^m \quad (4.11a)$$

while the corresponding "theoretical" values will be denoted as

$$\alpha_{jk}(\omega_\ell) = \alpha_\ell = \sum_{s=m_1}^{m_2} \frac{{}_s A_{jk}}{\Omega_s^2 - \omega_\ell^2 + i\eta_s \Omega_s^2} + \frac{1}{K_{jk}^R} - \frac{1}{\omega_\ell^2 M_{jk}^R} \quad (4.11b)$$

where the coefficients ${}_1 A_{jk}, {}_2 A_{jk}, \dots, \Omega_1, \Omega_2, \dots, \eta_1, \eta_2, \dots, K_{jk}^R$ a M_{jk}^R are all to be determined.

The member $\frac{1}{\omega_\ell^2 M_{jk}^R}$ represents the effect of low-frequency modes (those that lie below the lower limit of the measured frequency band) and the member $\frac{1}{K_{jk}^R}$ represents the effect of high-frequency modes (those that lie above the upper limit of the measured frequency band).

An individual error, ε_ℓ , can be defined as

$$\varepsilon_\ell = (\alpha_\ell^m - \alpha_\ell) \quad (4.12)$$

and this will be expressed as a scalar value:

$$E_\ell = |\varepsilon_\ell|^2 \quad (4.13)$$

If a weighting factor w_ℓ is added to each frequency point under investigation, the process of approximation has to determine the values of the unknown coefficients in (4.11) so that the overall error

$$E = \sum_{\ell=1}^p w_{\ell} E_{\ell} \quad (4.14)$$

is minimized. This is achieved by derivative of the expression (4.14) with respect to each of the unknowns separately, thus creating a set of as many equations as is the number of unknowns, each in the form:

$$\frac{dE}{dq} = 0 \quad ; \quad q = {}_1A_{jk}, {}_2A_{jk}, \dots, \text{etc.} \quad (4.15)$$

A set of equations created like this is not, unfortunately, linear for many of the coefficients (all parameters Ω_s a η_s) and thus it can not be solved directly. Therefore, various algorithms use their own procedures and apply various simplifications. Most of them use some form of iterative solution, some of them use linearization and nearly all of them rely on good initial estimates.

4.4 Modal Model

Whichever of the approximation method has been used, the approximation process should result in a consistent modal model. When global methods are used, the consistent model is their direct output. But when simpler SDOF methods have been used, some additional steps should be done such as averaging of natural frequencies and modal damping values obtained from the individual FRF characteristics. However, all these steps are built-in in software packages for experimental modal analysis and the analyst need not to care for them.

- spectral matrix: eigenvalues - natural frequencies and damping - are on the diagonal
- modal matrix: its columns are eigenvectors pertinent to individual natural frequencies

4.4.1 Presentation of the Obtained Modal Model

The actual output from modal analysis software can be represented in the form of tables. Such tables (results from StarStruct software) are shown in Figs. 4.20 and 4.22. In Fig. 4.20 is a table with the estimated natural frequencies and damping values. Damping is stated in two forms there: damp [Hz] determines one half of 3dB band while damp [%] is the damping ratio multiplied by 100. Other software packages may give damping values in different forms, e.g. as loss factors η . In Fig. 4.22 is a table of mode shapes where the individual mode shapes are given numerically - in the form of relative displacements and phase angles in the individual degrees of freedom. In the displayed table, values for the first mode for the few first points can be seen. Data originates from the measurement when a triaxial accelerometer was used so that each point has 3 DOF - directions X, Y and Z.

Software packages usually enable to export and import data files in the standard Universal file format (UFF) and many of them enable data exchange with other software packages as well, not only for experimental modal analysis, but also for a finite element analysis (quite common is communication with ANSYS software etc.).

Presenting results in a table form may be useful, but in the case of mode shapes it is not very transparent and it is only used for numerical comparison of mode shapes obtained from experiment and from computations (for more details see chapter 4.4.3). For mode shape inspection and assessment, its drawing, either static or animated, is used. All software packages for modal analysis enable to display mode shapes in animation and some of them enable their export in AVI format as well. If the mode shape has to be presented in the printed form, it is only possible to use static pictures, e.g. such as in Fig. 4.21. - here, the two utmost positions of the 3rd mode shape from the table in Fig. 4.20 are shown; the undeformed structure is in red, the mode shape in black colour.

70.47601			
Mode	Freq.(Hz)	Damp.(Hz)	Damp.(%)
1	70.48	453.68e-3	643.72e-3
2	214.44	935.13e-3	436.08e-3
3	290.18	657.11e-3	226.45e-3
4	323.65	723.52e-3	223.55e-3
5	364.30	1.32	362.46e-3
6	438.70	1.77	403.64e-3
7	453.08	3.85	849.61e-3
8	521.10	1.34	256.90e-3
9	533.50	991.38e-3	185.82e-3
10	580.03	2.44	419.96e-3
11	589.30	1.37	233.02e-3
12	759.17	4.51	594.52e-3
13	780.55	4.13	529.62e-3

Fig. 4.20 STAR Software Results - Table of Natural Frequencies and Damping Values

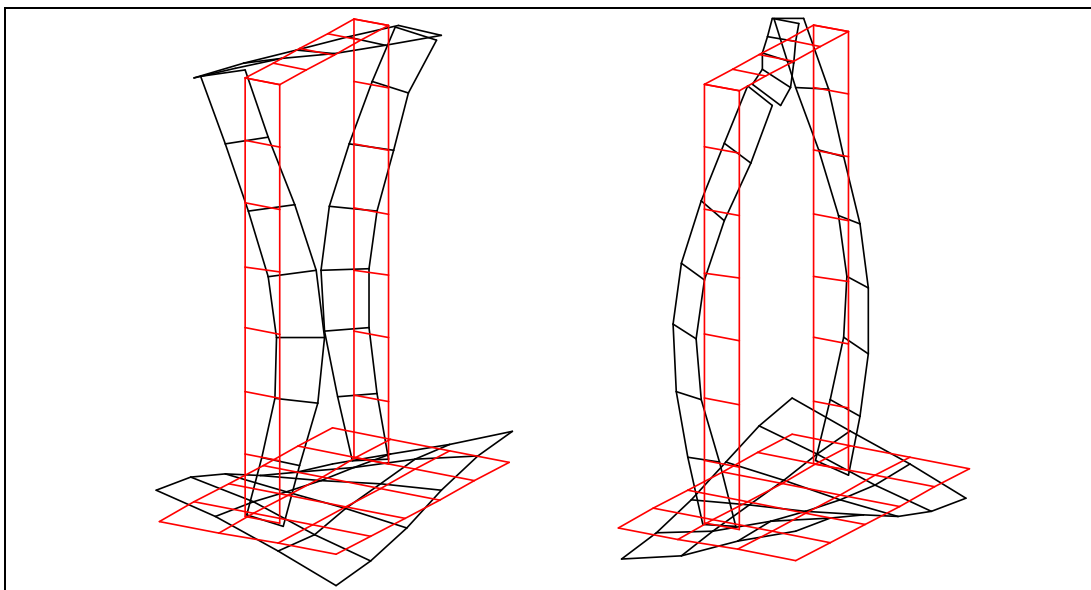


Fig. 4.21 Static Display of the Mode Shape

Point	Dir.1 Mag.	Dir.1 Phase	Dir.2 Mag.	Dir.2 Phase	Dir.3 Mag.	Dir.3 Phase
1	2.12	187.63	3.45	187.64	1.88	7.27
2	2.09	187.32	3.37	7.52	1.51	187.01
3	2.15	7.04	3.42	6.93	1.31	6.80
4	2.11	6.98	3.26	186.44	1.58	187.92
5	2.15	187.36	2.43	8.04	1.38	188.00
6	2.22	187.51	903.14e-3	8.28	475.36e-3	187.97
7	2.18	187.13	624.01e-3	187.86	616.94e-3	7.97
8	2.15	187.10	2.01	187.39	1.39	7.23
9	2.18	7.29	2.16	6.25	1.39	8.58
10	2.22	6.84	1.01	6.64	526.27e-3	6.88
11	2.23	7.39	230.25e-3	179.35	642.15e-3	190.33
12	2.10	6.80	1.78	186.56	1.23	186.87
13	950.13e-3	187.35	2.35	8.09	861.78e-3	188.79
14	938.74e-3	7.28	2.08	7.02	619.62e-3	8.12
15	823.21e-3	187.63	779.29e-3	7.80	180.60e-3	187.14
16	882.33e-3	7.51	913.71e-3	8.17	163.18e-3	3.27
17	858.27e-3	188.09	525.07e-3	188.12	215.31e-3	8.43
18	933.97e-3	7.10	603.51e-3	188.34	266.58e-3	184.25
19	913.82e-3	187.22	2.20	187.53	914.45e-3	7.23
20	717.38e-3	7.42	1.68	186.05	930.07e-3	189.75

Fig. 4.22 STAR Software Results - Table of Mode Shapes

4.4.2 Verification of the Obtained Modal Model

Just the same as the accuracy of the reference point measurement was checked before the modal test proceeded to all the other measurements, it is now appropriate to review, at least briefly, the accuracy of the obtained modal model, prior to comparing it with another model, mostly with a computational model obtained by finite element calculations.

If a structure whose modes are well separated is measured (and moreover, if it is measured freely supported), probably no problems with modal parameters identification occur and the obtained modal model will be most likely correct. When a more complex structure with coupled modes and with a large amount of (nonproportional) damping is measured, the process of modal parameters extraction will be more complicated. It is often necessary or at least useful to try various approximation methods and choose the one that gives the best results. But which will be the best to choose? If the extracted mode shapes are inspected visually in animation, they should exhibit systematic motion. Some of the "mode shapes" could exhibit chaotic motion, could be something like "bumpy", etc. If this happens, there are two possibilities:

- It is so-called *computational mode* or *false mode*. If the software is asked to extract the mode (or two or more modes) in the given frequency range, it always meets this

requirement. But it might happen that if, let's say, three modes are required and there are only two true modes in the frequency band, the third extracted mode is a false mode.

To decide which of the two above possibilities apply for the particular case, the analyst should mainly rely on his experience, but there are some possibilities that could help, e.g.:

- If computationally derived modal parameters are at disposal for the given structure, the knowledge of how the mode shapes should look like is available and all the redundant modes may be excluded from the measured set. It sounds logical, but it is not so clear: When the structure is measured supported otherwise than in free conditions, the actual boundary conditions could be different from that used in computation and, consequently, the computed mode shapes could differ as well. This situation could be discovered by obtaining nice smooth mode shapes from the measurement that are missing in the computational model. In this case, error will be most likely on the computational side. In any case, the knowledge of theoretical mode shapes is helpful in rejecting the false mode shapes from the experimental model (or in realizing that some of the modes should be identified more carefully).
- *Complexity* of the mode shapes could be examined. It means to examine to which extent the displacements in the mode shapes are complex numbers. Generally, it can be said that the less complex the mode shape is, the more probably it is correct. This assumption applies especially for lightly damped structures measured in free conditions. For such structures, complex mode shape may not occur. On the contrary, when a structure is heavily damped and the damping is non-proportionally distributed (e.g. a structure comprising rubber parts), high complexity of mode shapes is expected and it might not signify an approximation error.

A complex mode shape is easily identified in animation by its waving movement. This visual effect originates from the fact that the displacements in the individual points do not reach their utmost positions simultaneously. Consequently, nodal lines change their positions. Thus, complex mode shapes cannot be displayed using static pictures, it is only possible to display them in animation. A poor attempt to display them statically can be done by so called *normalization* - displacements are transformed to the real numbers by assigning zero to phase angles of those displacements that have phase angles more close to zero (thus obtaining positive amplitude) and by assigning 180° to phase angles of those displacements that have phase angles more close to 180° (thus obtaining negative amplitude). Doing this, a real approximation of the complex shapes is obtained. It can be seen in Fig 4.20 that the mode shape stated there is very slightly complex, as the phase angles are mostly very close to 0° or 180° .

If two or more mode shapes look similar, it again might be an approximation error. It might happen when the software identifies false modes from the reason described above (more modes are required in the frequency bands than really exist). In this case, it is worth to examine the MAC matrix. It will be discussed in detail in the next chapter, because its main purpose is in comparing of two models obtained by different methods, but it can be used also for a single model only. In this case, all values on the main diagonal will be equal to 1 and all the other values should be numbers close to zero. If a number close to 1 appears out of the

main diagonal, it most likely indicates a false mode. This applies for modes whose frequency are quite close.

Different situation occurs when two mode shapes look very similar, but their frequencies are quite apart from each other. In this case, the mode shapes differ very likely in something that was not measured (e.g. movement in direction Y if only measurements in directions X and Z were performed). The geometrical model used for modal test is usually quite simple and it could easily happen that it would not capture all the details of the movement. Thus, two modes could appear as being the same even if they are not. In this case, it is not a measurement or approximation error, but the consequence of insufficiently fine model.

4.4.3 Comparison of the Experimentally and Computationally Derived Models

In chapter 1.1 it was stated that a modal test is very often performed with the aim to compare dynamic behaviour of the structure derived from computations and those that is really observed in practise. Sometimes, this process is called *verification (updating)* of the theoretical model and it takes several steps:

- comparison of the dynamic properties - experimental vs. theoretical model
- quantification of the differences between those two data sets
- making changes in one of the sets of results in order to achieve better correspondence

If this is achieved, the theoretical model can be considered as verified and thus it is ready for use in a subsequent analysis.

Comparison of dynamic properties of the experimental and theoretical models can be performed for all the three types of dynamic models (spatial, modal and response). From the opposite procedures used in experimental and theoretical analysis it is clear that what is the most convenient type of model for a theoretical analysis would be worst accessible for an experimental analysis and vice versa. A theoretical analysis starts with the spatial model, but it is quite difficult to achieve it through the measured data - it requires application of additional data processing procedures that are usually not the part of software packages. On the contrary, frequency response functions that are directly obtained by measurements are relatively tedious to acquire in the theoretical model. Therefore, the most common form for comparing the two sets of data is the modal model. Several possibilities of comparing modal models are stated below.

4.4.3.1 Comparison of Natural Frequencies

Quite obvious is to compare measured vs. calculated natural frequencies. This is often done by a simple tabelation of both result sets, but a more useful form is to draw the experimental value vs. the theoretical value for all the modes included into comparison, as is shown in Fig. 4.23. In this way, not only the degree of consistency between the two sets of results can be seen, but also the nature and possible causes of the discrepancies. The drawn points should lie on the line with the slope 1 or near this line. If they lie near a line with the slope other than 1, the cause of this discrepancy is quite sure in incorrect material properties used for computation. If the points are widely spread along the line, there is a serious error in the model that represents the structure and a basic reassessment should be done. Particular

attention has to be paid to the case where the points deviate slightly from the ideal line, but in a systematic rather than random manner, since this situation implies that there is a specific feature which is responsible for the deviation and can not simply be attributed to experimental errors.

If the scatter is small and randomly distributed along the line of the 45° slope, the values are supposed to originate from the normal process of modelling and measurement. Generally, the higher (in order) is the frequency, the larger is the difference between theoretical (computed) and measured values. The differences should have the tendency that the theoretical values of frequencies are higher than the measured ones, because usually damping is not included in the theoretical values whereas measured frequencies are always damped and thus of lower values.

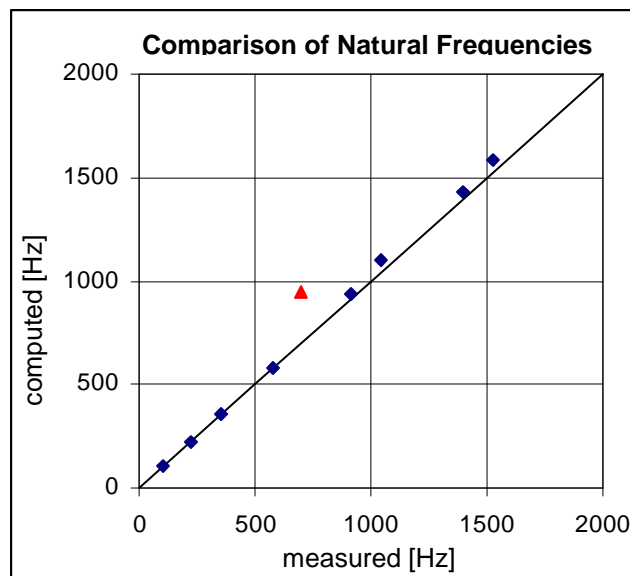


Fig. 4.23 Graphical Comparison of Natural Frequencies

When most of the points are near the ideal line (blue points in Fig. 4.23) and some points are far from this line (red point in Fig. 4.23), it could be the case that different modes are compared. This is quite a frequent mistake that students allow to happen. It should be emphasized that if 10 modes are identified from measurements and 10 modes in the same frequency band are identified from theoretical analysis, it cannot be guaranteed that the 1st mode may be assigned to the 1st one from the different analysis, the 10th to the 10th etc. It could happen that:

- The order of two modes close in frequency is changed in the two compared models.
- One mode is missing in the experimental model (maybe because the reference point was at the nodal line of that mode), and at the same time one mode is missing in the theoretical model (because its frequency in theoretical analysis is above the frequency range in which comparison is performed). Thus, the number of modes is the same in both models, but not all of them create pertinent pairs to be compared.

It is clear from the above that the identified modes cannot be compared automatically, because in all the methods discussed here it would lead to erroneous conclusions. It is

essential to check the mode shapes visually and match the pertinent modes together prior to starting with any comparison of the two models. Doing this, the risk of comparing two modes that do not match is eliminated. This risk is quite high, as it is quite a common situation that some modes are missing in the experimental model. Nevertheless, if the modes are correctly matched, the fact of a missing mode in the experimental model cannot be considered as a mistake that would prevent good comparison of the two models or verifying the theoretical model. It is quite sufficient to verify and update the theoretical model in accordance with those modes that are at disposal (it is supposed that some higher modes might be missing rather than lower ones).

4.4.3.2 Graphical Comparison of Modal Shapes

One of the possibilities how to compare the mode shapes is to draw the deformed shapes for both models - theoretical and experimental - and overlay the two pictures. A disadvantage of this approach is that even though the differences can be seen, it is difficult to interpret them and often the obtained pictures are very confusing as there is a lot of information in them.

A more convenient method is similar to that for graphical comparison of natural frequencies. Mode shape elements are drawn to the x-y plot, again measured vs. computed, and in an ideal case, they should again be scattered near the line with the slope 1. For this comparison, it is necessary to choose those points from the theoretical model (which usually has much more degrees-of-freedom than experimental model) that coincide with the experimental model.

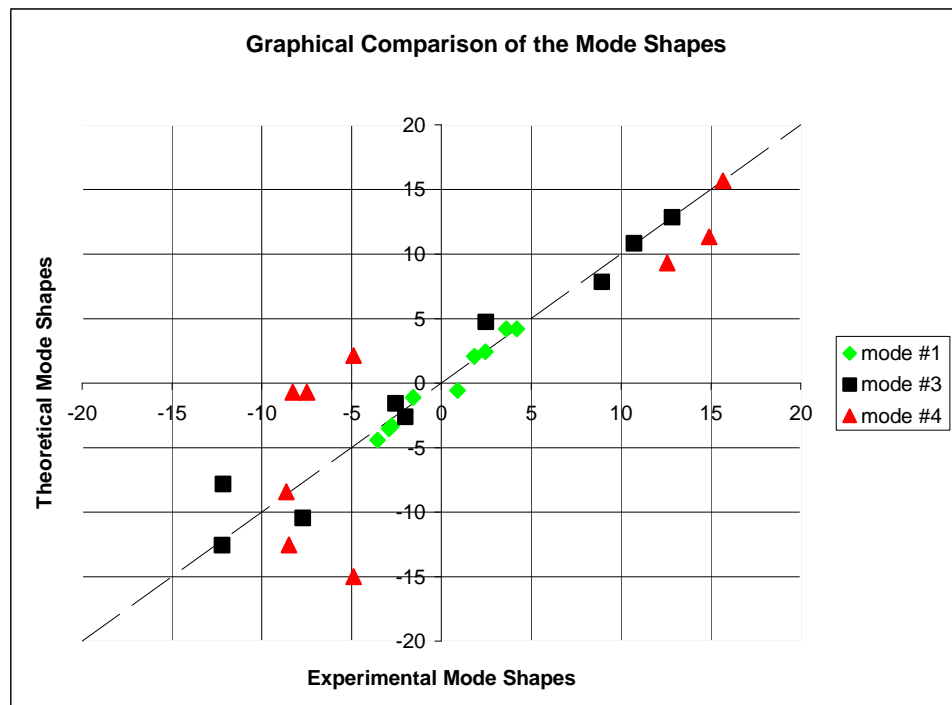


Fig. 4.24 Graphical Comparison of the Mode Shapes

The nature of deviations from the ideal state can again quite clearly indicate the cause of the discrepancy: if the points lie near a line with the slope other than 1, then one of the compared mode shapes is not normalized to the unity modal mass or there is some other scale

error. If the scatter is large, then there is a severe inaccuracy in one of the data sets and if the scatter is excessive, two different modal vectors that do not belong to the same mode might be compared.

In Fig. 4.24, comparison of three mode shapes, each of different colour, is shown. It can be seen that the 1st and the 3rd shape exhibit a good accordance, while this is worse for the 4th shape. This is quite a typical result, as with increasing order of modal shapes it is more difficult to achieve accordance.

4.4.3.3 Numerical Comparison of Mode Shapes

As an alternative to the above introduced graphical approach, numerical comparison of the mode shapes can be used. The expressions (4.16) and (4.17) below suppose that mode shapes data may be complex. The experimental (measured) mode shape is denoted as $\{\phi_X\}$ and the theoretical (computed, analytical) mode shape is denoted as $\{\phi_A\}$. These concepts are in fact useful for all types of comparisons, not only experiment vs. theory, but they can be used to compare any pair of mode shape estimates.

The first criterion deals with the quantity called *Modal Scale Factor* (MSF) and it represents the slope of the best line fitted to the points in Fig. 4.24. This quantity is defined as (two forms are possible according to which of the mode shapes is taken as reference):

$$\text{MSF}(X, A) = \frac{\sum_{j=1}^n (\phi_X)_j (\phi_A)_j^*}{\sum_{j=1}^n (\phi_A)_j (\phi_A)_j^*} \quad \text{MSF}(A, X) = \frac{\sum_{j=1}^n (\phi_A)_j (\phi_X)_j^*}{\sum_{j=1}^n (\phi_X)_j (\phi_X)_j^*} \quad (4.16)$$

It should be noted that this criterion provides no indication concerning the quality of fitting the line to the points, but only its slope.

The second criterion is called *Mode Shape Correlation Coefficient* (MSCC) or *Modal Assurance Criterion* (MAC) and provides the measure of distances of point from the ideal line in the least square sense. It is defined as:

$$\text{MAC}(A, X) = \frac{\left| \sum_{j=1}^n (\phi_X)_j (\phi_A)_j^* \right|^2}{\left(\sum_{j=1}^n (\phi_X)_j (\phi_X)_j^* \right) \cdot \left(\sum_{j=1}^n (\phi_A)_j (\phi_A)_j^* \right)} \quad (4.17)$$

and it is a scalar value, although the data of mode shapes are complex. As the modal scale factor does not indicate the degree of correspondence, the modal assurance criterion does not distinguish between a random scatter responsible for the discrepancies and systematic discrepancies either. So even though these parameters are useful means to quantify the comparison between the two data sets of mode shapes, they do not give a complete insight and should be considered primarily in connection with plots such as the one shown in Fig 4.22.

It is worth to consider two special cases: (1) that when two mode shapes are identical and (2) that when two mode shapes differ by a simple scalar multiple. In the case (1) applies:

$$\{\Phi_X\} \equiv \{\Phi_A\}$$

from which it can be seen that

$$\text{MSF}(X, A) = \text{MSF}(A, X) = 1$$

and also that

$$\text{MAC}(X, A) = 1$$

In the case (2), $\{\Phi_X\} = \gamma\{\Phi_A\}$ and it is found out that

$$\text{MSF}(X, A) = \gamma \quad , \quad \text{whilst} \quad \text{MSF}(A, X) = \frac{1}{\gamma}$$

but since the two modes are still quite perfectly correlated, it still applies:

$$\text{MAC}(X, A) = 1$$

In practice, a typical data would be less ideal than these and what is expected is that if the involved experimental and theoretical mode shapes would really belong to the same mode, then the MAC value would be close to 1, whilst if they would belong to different modes, the MAC value would be close to zero. If a set of m_X experimental modes and a set of m_A theoretical modes are taken into account, a MAC matrix $m_X \times m_A$ can be computed and displayed in a matrix that would clearly indicate which experimental mode matches to which theoretical mode. It is difficult to give exact values that should the MAC values be to ensure good results. Generally, the values greater than 0.9 should be obtained for the same modes and values less than 0.05 for the different modes.

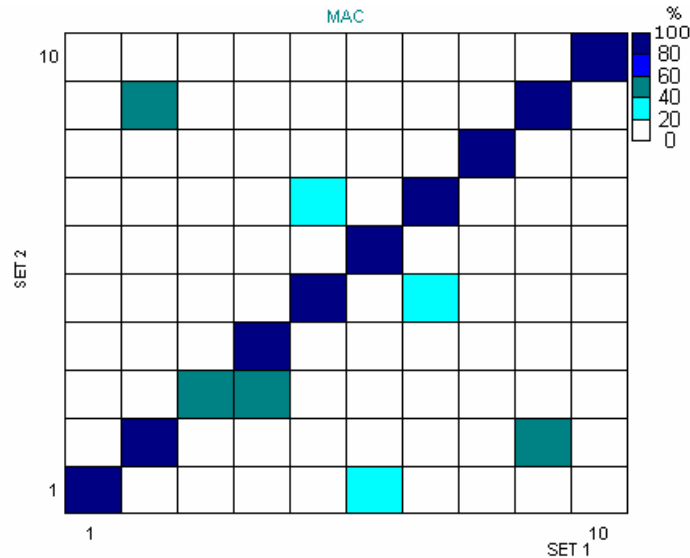


Fig. 4.25 MAC Matrix - Graphical Form

It is worth to mention some possible causes of imperfect results of these calculations. Apart from the obvious reason that the model is defective, MAC values less than 1 can be caused by:

- non-linearities in the tested structures
- noise in measured data that was not averaged out
- weak modal analysis of the measured data
- incorrect selection of DOFs included into correlation

In Fig. 4.25 is an example of MAC matrix that comes from comparison of two sets of experimental data, both from the same structure, one from a modal test when hammer excitation was used, the second when shaker excitation was used. The structure had very similar mode shapes of the 3rd and the 4th mode, and these modes were spaced only 0.4 Hz in frequency. Their identification was very difficult and it can be seen from the MAC matrix where the element (3,3) is less than 0.8 and the element (3,4) is greater than 0.4.

Note.: MAC criterion has already been mentioned in the chapter 4.4.2. If MAC criterion is applied on one set of results, the values on the main diagonal are all exactly equal to 1 and significant are the out-of-diagonal values only - they should be close to zero. If they are not, there is a risk of false mode existence.

5. Operational Deflection Shapes (ODS)

The issue of visualization the operational deflection shapes belongs to the area of vibration diagnostics, where it is used to solve specific problems related to operation of machines. If this issue is sometimes assigned to a modal analysis, it is probably because it uses the same tools, both technical and software. Basic equipment for operational deflection shapes identification comprises a dual or multi-channel analyzer, set of two or more accelerometers and for one of the ODS types, so called spectral ODS, software for experimental modal analysis can also be used.

Operational deflection shapes are used as a diagnostic tool for visualization of the actual dynamic behaviour of machines. This visualization serves for better understanding of what is happening with the given equipment and thus provides a basis for decisions on problem solving. If the vibration levels are unsatisfactory, the ODS is to find the "weak point" of the structure at given operating conditions. Application of ODS is indicated especially when the structure vibrates on a single predominant frequency - in this case it is possible that the system returned itself close to the resonance. This can happen by reducing the stiffness of the support due to mechanical looseness - it may be a loose baseplate, anchor bolt cracked, etc. If defects of this type are suspected, they can be easily detected using ODS visualization, if well-defined model is used. Conversely, this method is not suitable if vibrations are excessive in a wide range of operating conditions.

Another possible application of ODS is verification of forced response simulation which was performed on a modal model, obtained experimentally or by calculation.

Operational deflection shapes
visualize vibration behaviour of structures
under the actual operational conditions.

Thus, operational deflection shapes are about identification of the forced vibrations. The system and the input excitation forces are not observed, no assumptions about the linear behaviour of the system are made, only the vibration response of the system is measured (see Fig. 5.1). The advantage of the ODS is that the dynamic behaviour of the structure under the actual operational conditions and under actual boundary conditions is identified. The disadvantage is (in comparison with a modal test) that no model of the system is obtained and thus no estimates about its response under different conditions could be made.

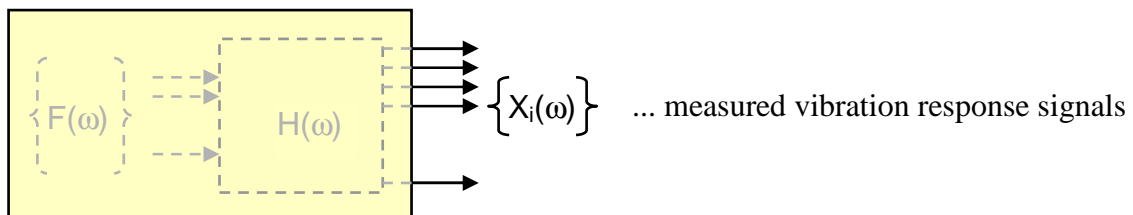


Fig. 5.1 Signals Measured for ODS

Operational conditions refers to rotational speed, load, pressure, temperature, flow, etc. These conditions could be stationary, quasi-stationary (slightly varying rotational speed, run-up, run-down) or transient (e.g. a piece of a rock falls on the measured structure). According to the operational conditions, the type of ODS should be chosen. Basically, there are two types of ODS:

1. *Spectral ODS* - deflection shapes on the individual frequencies or orders are obtained. When the operational conditions are stationary, frequency spectra are used; when they are quasi-stationary, order spectra are used. As a result of measurements, relative amplitudes and phase angles of the individual degrees-of-freedom on the individual frequencies (or order components) are obtained. The individual DOFs could be measured simultaneously (if enough of accelerometers and analyzer channels are at disposal) or successively. In principle, two accelerometers are sufficient for spectral ODS measurements - one of them is the reference and is placed in a fixed position and the second one captures the response in each of the DOFs.
2. *Time ODS* - deformation process as a function of time is obtained. This type of ODS is used for transient signals. It is clear that when transient process is observed, it is not possible to measure the individual DOFs successively, but they should be measured all at once. This leads to higher demands on technical equipment - multiple sensors, multi-channel analyzer, software and equipment must be special, software for modal analysis cannot be used. To view the time ODS, signals from accelerometers are integrated to provide speed or displacement.

The procedure for application of ODS is very similar to that for a modal test. It includes following steps:

- preparation
- measurements
- post-processing of the measured data

As for a modal test, a geometrical model should be prepared for measuring operational deflection shapes. It is usually simpler than that for modal test, because ODS measurements are focused on identifying how the machine behaves as a rigid body with respect to the base plate or to other parts of the machine-set, rather than on deformation of the machine itself. A smaller number of measured DOFs is sufficient for this task. However, it is necessary to include points on the supporting structure of the measured structure, on the base plate, etc. because the most relevant information about the nature of the defect often originates from the information about the movement of the structure with respect to the base.

On the geometrical model, degrees-of-freedom should be defined. If triaxial accelerometer is used, all point will be measured in three DOFs (X, Y and Z), with mono-axial accelerometer it should be decided, which directions are to be measured.

Then, reference DOF (position + direction) should be defined. In order to obtained high-quality measurements, it is required for reference DOF to exhibit response of sufficiently high levels at all frequencies that are of interest. A reference accelerometer (rather than a force transducer in modal test) is placed to the reference DOF (see Fig. 5.2).

Using a reference accelerometer, so-called transmissibility, $T(f)$, is measured. It is a function very similar to frequency response function, but it has the signal from a reference accelerometer rather than the signal from a force transducer in the denominator:

$$T(f) = \frac{X_i(f)}{X_{ref}(f)} \left(= \frac{G_{x_i x_i}}{G_{x_i x_{ref}}} = \frac{G_{x_i x_{ref}}}{G_{x_{ref} x_{ref}}} \right) \quad (5.1)$$

The second possibility how to provide the reference signal is to use a phase reference instead of a reference accelerometer. It is the simplest configuration for ODS measurements as possible - single-channel analyzer with the possibility of phase measurements is sufficient. In this case, autospectrum with the assigned phase is measured instead of transmissibility.

Prior to starting complete measurements, it is useful to check if all the components of the measurement chain are set correctly, for example, by checking the transmissibility function in the reference degree-of-freedom. As it is a ration of two identical signals, it should be close to unity in the whole measured frequency range. In Fig. 5.3, transmissibilities measured at the reference point are shown - dark line is for transmissibility in reference DOF, light lines are for transmissibilities in reference point, but in other two directions. A triaxial accelerometer was used for that measurements.

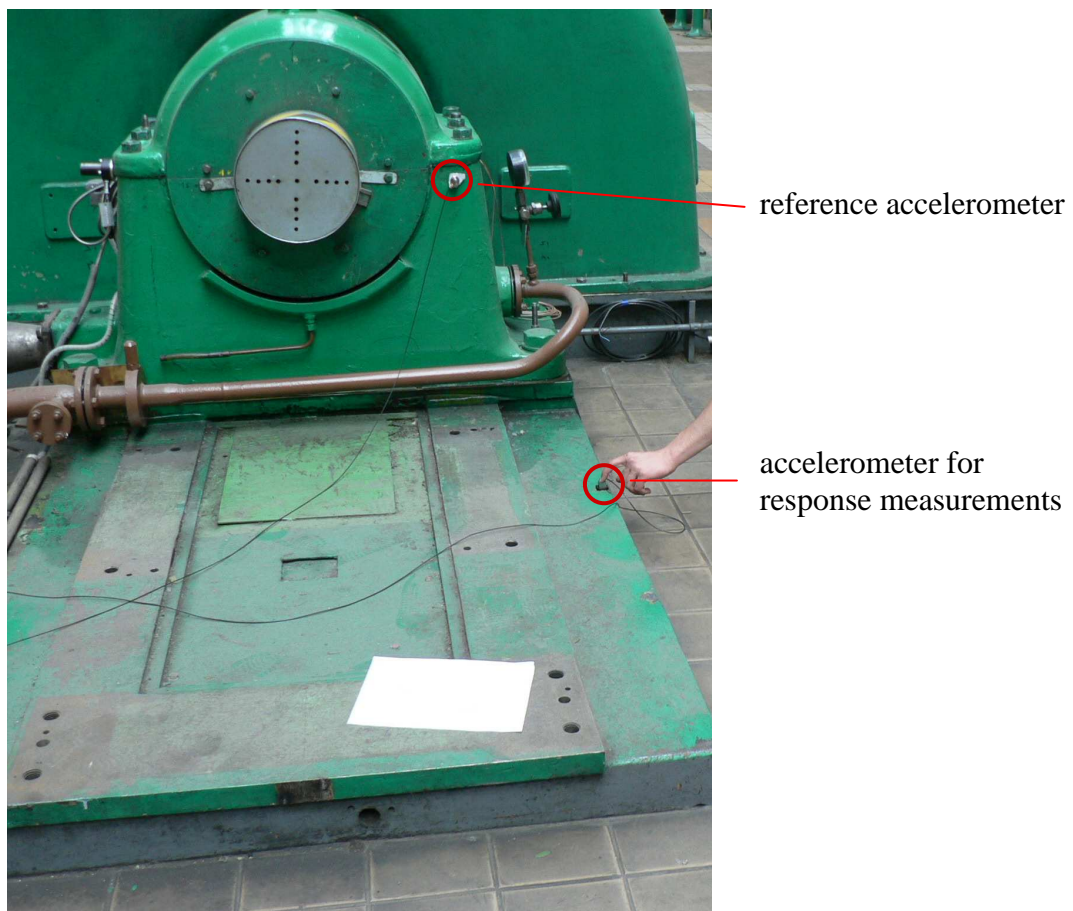


Fig. 5.2 Example of Transmissibility Measurements

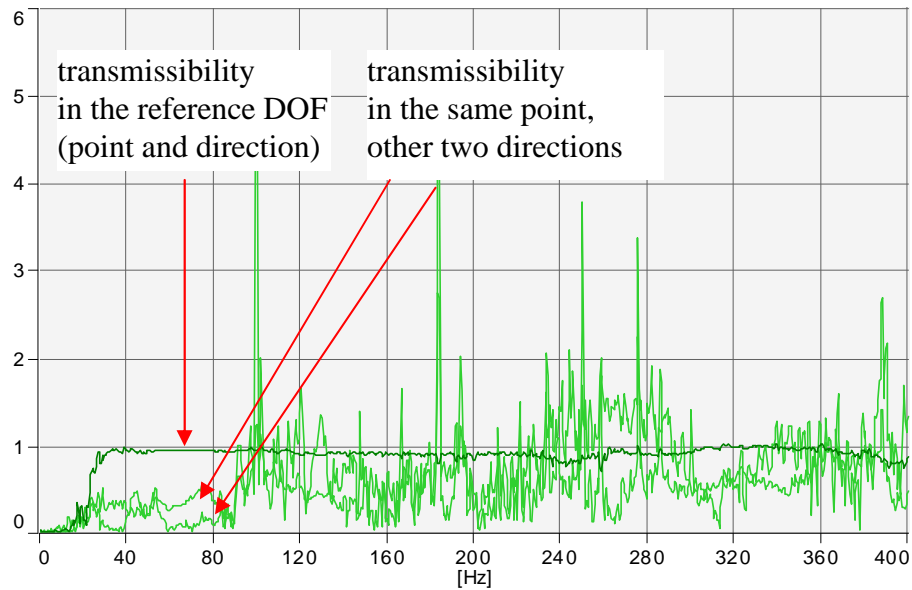


Fig. 5.3 Transmissibility in the Reference Point

After all measurements are done, post-processing of the measured data is performed either in special software for ODS or in modal analysis software. If the latter is used, the peak-peak approximation method is used to obtain operational shapes (see chapter 4.3.2.1). Strictly speaking, no approximation is associated with this method - amplitudes at relevant frequencies are read only. For rotating machinery, the relevant frequency used to be the rotational speed and its harmonics.

Results may be obtained in table form (as in Fig. 4.21), but much more illustrative is to use an animated display of the obtained shape. Operational deflection shapes (similarly to complex mode shapes) cannot be accurately displayed in static position, because different points do not reach the utmost positions at the same time - it can be said that the movement of the structure follows the excitation force.

6. Operational Modal Analysis (OMA)

Operational modal analysis is a method that enables to obtain a modal model based only on response measurements. The measurement procedure is the same as for transmissibility measurements, but the mathematical background behind the operational modal analysis is much more complex. It can be said that only a massive increase in computational capacity of computers in recent years has facilitated the emergence and expansion of this method.

Operational modal analysis, as the name suggests, is performed under actual operating conditions of the measured machine or device, and only the vibration responses are measured, not the input excitation forces. Nevertheless, a valid modal model of the measured system can be obtained by this method, even if unnormalized. This method is particularly suitable for modal tests of large structures, artificial excitation of which is difficult or even impossible. It is successfully used for modal tests of bridges, buildings, off-shore platforms, etc. In these cases, natural excitation from traffic, wind or sea waves is broadband excitation, and this is the main pre-requisite for a successful modal test. Nowadays, OMA is beginning to apply also in engineering applications such as in modal tests of rotating machinery, on-road and in-fly tests, etc. In these cases, the kind of natural excitation constitutes a limitation for the use of this method. For instance, the main excitation force in rotating machinery originates from the rotational speed and excitation on other frequencies is very small. Under these circumstances, reliability of the obtained modal model would be quite unsatisfactory. The situation can be improved by applying an additional broadband excitation that is not measured (see Fig. 6.1).

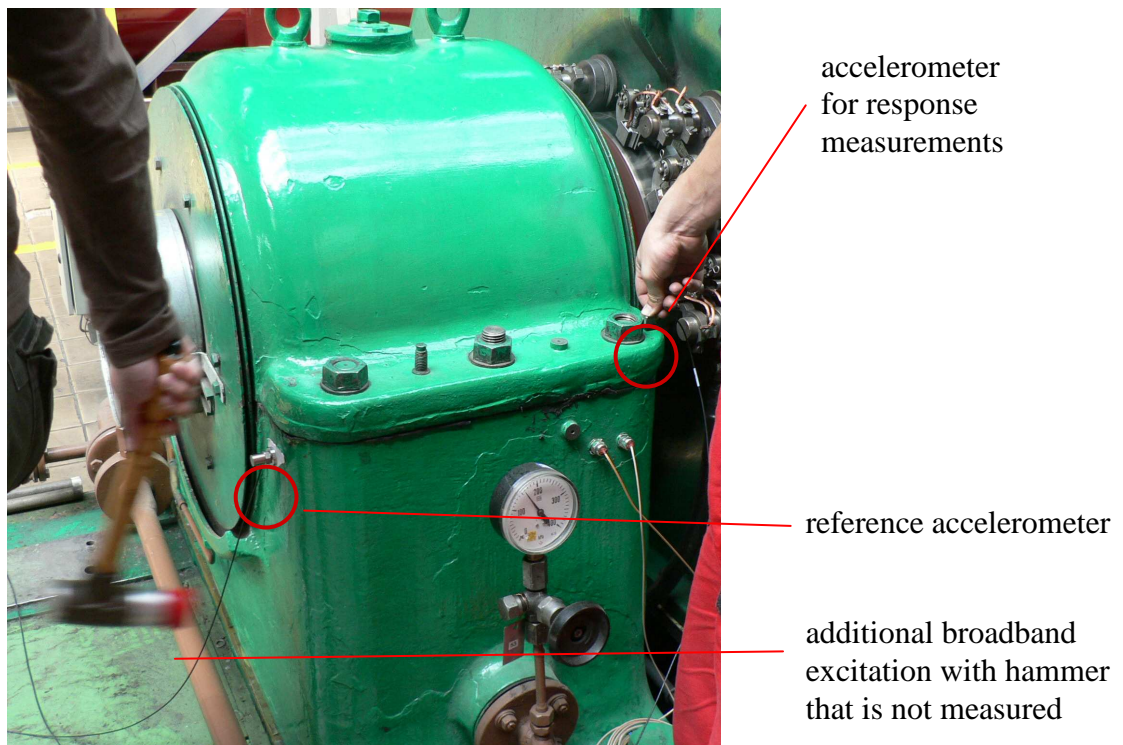


Fig. 6.1 Measurement Setup for Operational Modal Analysis with Additional Excitation

The advantages of the operational modal analysis in comparison to the classical modal test can be summarized as follows:

- No elaborate fixturing of structures, shakers and force transducers:
 - no test rigs needed
 - short setup time
 - no dynamic loading from shakers and stingers
 - no crest factor problems as when using hammers
 - no potential destruction of structure
- Modal model can represent real operating conditions:
 - true boundary conditions
 - actual force and vibration levels
- Only natural random or unmeasured artificial excitation required.
- No interference or interruption of daily use.
- Modal testing can be applied in parallel with other applications.
- OMA is inherently a poly-reference method, as the excitation acts in multiple positions simultaneously. Identification of multiple modes is possible.

Disadvantages of the OMA method should also be mentioned, namely:

- The obtained modal model is unscaled, thus no force response and modification simulations are possible.
- The method requires more operator's skills, pre-analysis is often needed.
- Large time histories might be required:
 - more data handling capacity needed
 - higher computational power needed

In operational modal analysis, some assumptions should be accepted. They may be divided into theoretical (mathematical) and practical.

Theoretical assumptions:

- Stationary input force signals can be approximated by filtered zero mean Gaussian white noise.
 - Signals are completely described by their correlation functions.
 - Synthesized spectral densities and correlation functions are similar to those obtained from experimental data.

Practical assumptions:

- Broadband excitation
- All modes must be excited (as in classical modal test).

And it is the the fact that true broadband excitation is not always achieved that causes problems in data analysis. If the structure is excited by white noise only, then all the peaks in response spectrum indicate modes and the spectrum contains only information about the structure itself (see Fig. 6.2 at the top). However, this is generally not the case in practice. If the spectrum of the excitation force was measured (what is not done in operational modal analysis), it would become evident that it is not flat but it has its spectral distribution. This

fact demonstrates itself in the spectrum as additional modes (see Fig. 6.2 in the middle). But the response spectrum is further contaminated by other factors, such as influence of noise, and also frequencies of rotational speed and its harmonics occur in the spectrum. All these results into the response spectrum shown in Fig. 6.2. at the bottom. It is obvious that the mathematical apparatus, however perfect it could be, is not able to distinguish the true structure modes from the false modes originating from the uneven distribution of the exciting forces. To distinguish them, operator's experience or preliminary knowledge about the real modes of the structure obtained from theoretical model are necessary.

When rotating machinery is examined, it is advisable to know at least the operational deflection shapes prior to starting with the operational modal analysis. OMA would most likely result in a mixture of true structural modes and operational deflection shapes, where the latter would dominate and so it is worth to know about them. If they were not measured in advance, they would be at least expected at the frequencies of rotational speed and its harmonics.

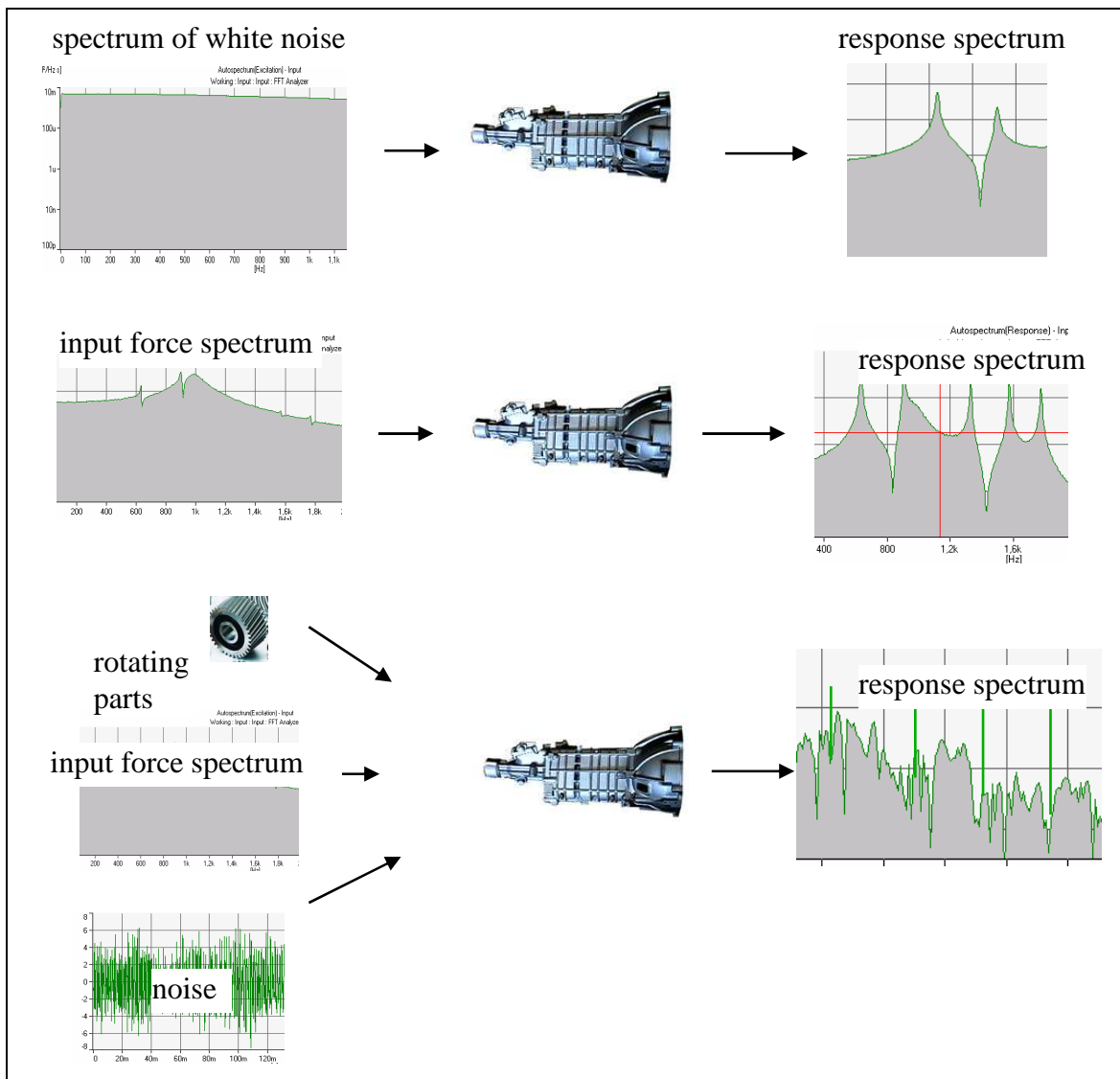


Fig. 6.2 Response Spectrum in Operational Conditions

6.1 Identification Methods

The mathematical apparatus of an operational modal analysis is quite complex and it is beyond the possibilities of the author of this text to describe the theoretical background in detail. Therefore, the methods are introduced here only very briefly. Software package "PULSE Operational Modal Analysis" that is used at the Department of Mechanics has implemented two techniques of modal parameters identification:

- non-parametric - implemented as *frequency domain decomposition* (FDD). Modal parameters are estimated directly from curves, functional relationships or tables.
- parametric - implemented as *stochastic subspace identification* (SSI). Modal parameters are estimated from a parametric model fitted to the signal processed data.

Procedure of the frequency domain decomposition method is as follows:

- power spectral density (PSD) estimation (see Fig. 6.3)
- singular value decomposition (SVD) of PSD
- identification of single degree-of-freedom (SDOF) models from SVD
- modal parameter identification from SDOF models

Singular value decomposition of PSD is described by the expression:

$$G_{yy}(i\omega_j) = \sum_k \frac{d_k}{i\omega_j - \lambda_k} \phi_k \phi_k^T + \frac{d_k^*}{i\omega_j - \lambda_k^*} \phi_k^* \phi_k^{*T} = \sum_k s_k \phi_k \phi_k^T + s_k \phi_k^* \phi_k^{*T} \quad (6.1)$$

where s_k is constant and real for the given frequency. SVD is performed for each frequency.

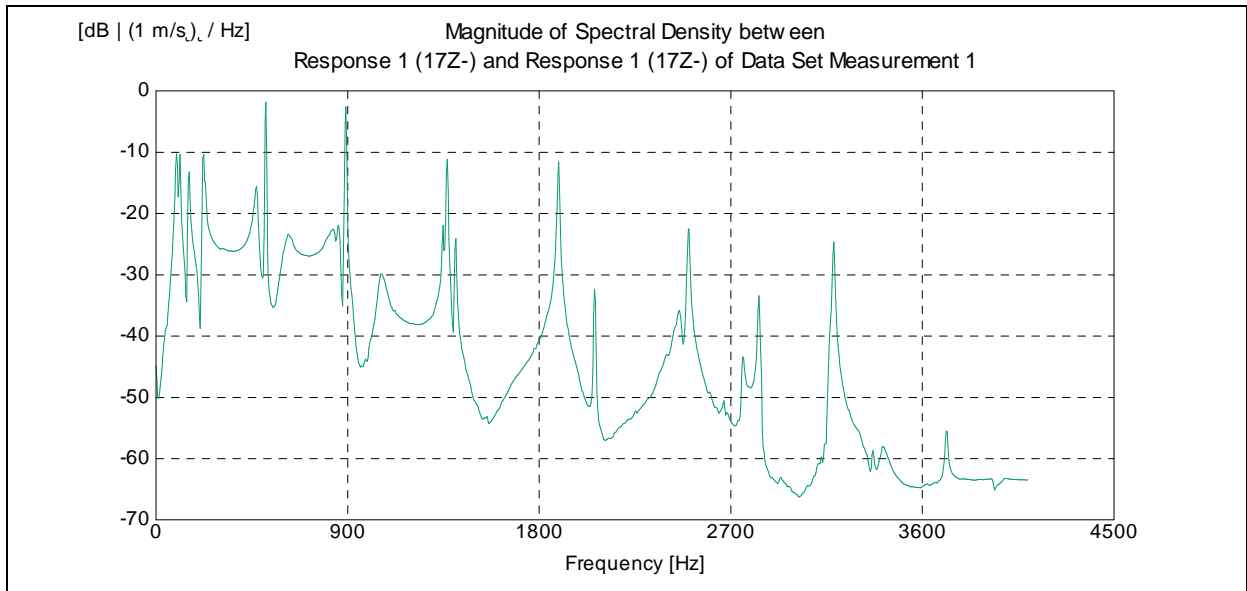


Fig. 6.3 Power Spectral Density Estimate

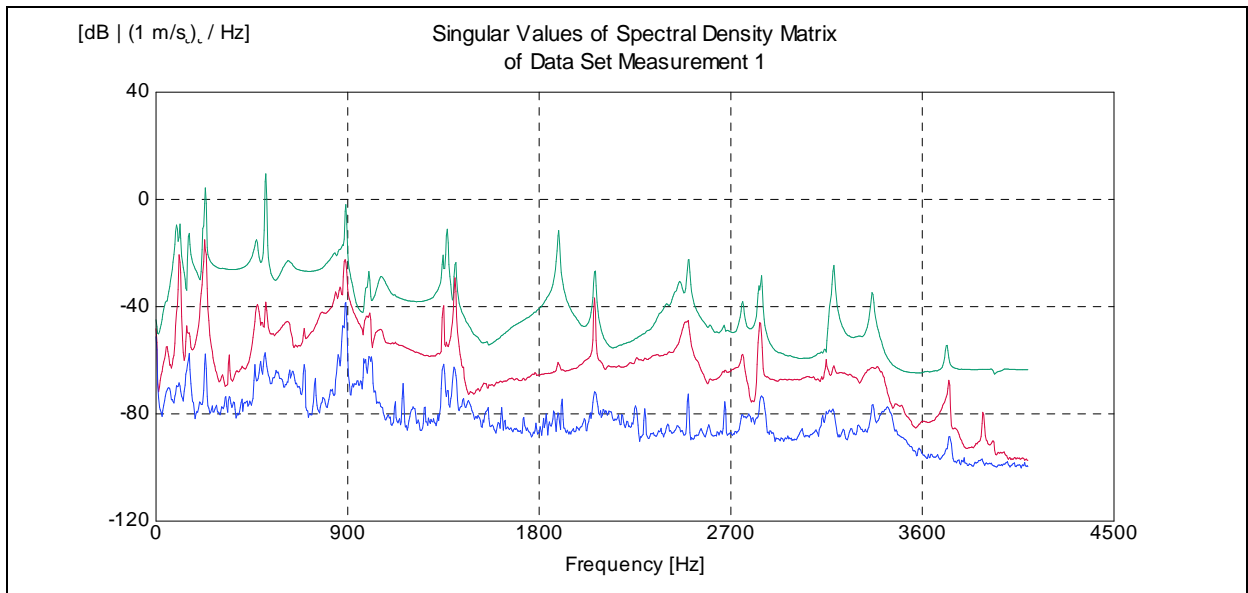


Fig. 6.4 Singular Values

One of the parameters that the operator sets in the OMA software is the number of the required singular values (there are three singular values in Fig. 6.4). The theory says that if there is a peak in the upper line (green), at least one mode exists at that frequency, if there is a peak in the second line (red), at least two mode exist at that frequency, etc. (Author's short experience with OMA has not proved this theory yet.)

6.2 Presentation of Results

As the classical modal analysis, the operational modal analysis leads to a modal model, i.e. modal and spectral matrices are obtained. A modal model can be considered valid only if all false modes and operational deflection shapes are removed from it, as discussed above.

Mode	Frequ...	Std. Fr...	Dam...	Std. ...	Creation Date...
Mode 1	99.62	5.972	3.349	1.129	22-05-2007 12:31:32
Mode 2	112	0.3705	1.989	0.2421	22-05-2007 12:31:38
Mode 3	146.9	14.54	1.885	0.5866	22-05-2007 12:31:42
Mode 4	232	0.01487	0.8545	0.02111	22-05-2007 12:31:47
Mode 5	476.6	10.36	1.249	0.3852	22-05-2007 12:31:52
Mode 6	515.4	0.491	0.4158	0.03736	22-05-2007 12:31:57
Mode 7	891.5	0.6606	0.3261	0.1367	22-05-2007 12:32:05
Mode 8	992.9	8.048	0.2991	0.1439	22-05-2007 12:32:13
Mode 9	997.4	7.178	0.3038	0.1577	22-05-2007 12:32:19
Mode 10	1368	0.6367	0.194	0.01442	22-05-2007 12:34:36
Mode 11	1888	2.718	0.1491	0.04608	22-05-2007 12:34:40
Mode 12	2060	1.83	0.1377	0.01951	22-05-2007 12:34:47
Mode 13	2499	1.933	0.123	0.03253	22-05-2007 12:34:54

Fig. 6.5 Table of Natural Frequencies and Damping Ratios Resulted from OMA

Spectral matrix displays the software PULSE Operational Modal Analysis in the table form where natural frequencies and damping ratios are stated (see Fig. 6.5). As these are statistical estimates, standard deviations of each value are stated as well. Modal matrix, i.e. mode shapes in a numerical format, can be exported in the universal file format (UFF) to various other software. For inspection of mode shapes, an animated display is again the most convenient way.

References

- [1] Ewins, David J.. *Modal Testing - Theory, Practice and Application*, England: Research Studies Press Ltd., 2000, ISBN 0-86380-218-4
- [2] Zaveri, K.. *Modal Analysis of Large Structures - Multiple Exciter Systems*, Denmark: Brüel&Kjær, 1985, ISBN 87-87355-03-5
- [3] Randall, R.B.. *Frequency Analysis*, Denmark: Brüel&Kjær, 1987, ISBN 87-87355-07-8
- [4] Corporate literature, Application notes, presentations and website of Brüel&Kjær company